SISSA ISAS

SCUOLA INTERNAZIONALE SUPERIORE DI STUDI AVANZATI
INTERNATIONAL SCHOOL FOR ADVANCED STUDIES

Superconductivity from strong electron correlation

Thesis submitted for the degree of

Doctor Philosophiæ

Candidate

Matteo Calandra

Supervisor

Prof. Sandro Sorella

October 1999

Abstract

The strong electron electron correlation in the Copper Oxygen layers of the high temperature superconductors has been suggested as a possible explanation for the occurrence of superconductivity in these materials. Under this assumption a proposed model to describe the interplay between antiferromagnetism and superconductivity is the two dimensional $t-J$ model.

In this thesis the ground state properties of this model have been studied using exact diagonalization and quantum Monte Carlo simulations. In fermionic systems quantum Monte Carlo methods are affected by the "minus sign problem" instability that makes simulations prohibitive and even impossible at low enough temperature. In order to overcome this difficulty some approximations are necessary, such as the fixed node approximation or the recently proposed Green function Monte Carlo with stochastic reconfiguration. In this work the first successful application of the latter technique to fermionic system is presented.

It is shown that the two dimensional $t-J$ model, in the physical parameter region, reproduces qualitatively the main experimental features of the high T_c superconductors: $d-$wave superconducting correlations are strongly enhanced upon small doping (δ) and clear evidence of off-diagonal long range order is found at optimal doping. Antiferromagnetic correlations, clearly present for the undoped system, are strongly suppressed at small hole density with clear absence of long range order from $\delta \gtrsim 0.1$.

The possible presence of charge density wave or phase separation instabilities has been investigated. No one of such features has been detected in the physical region, being the homogeneous state the most stable one. Nevertheless the large compressibility suggests that the charge excitations are very close in energy so that small lattice deformations can easily induce the experimentally observed stripes in the system.

The results of this work strongly support the idea of a pairing force driven only by the electron electron correlation that, upon doping, leads the system from an antiferromagnetic Mott insulator to a superconductor.

Contents

Introduction

High temperature superconductivity in the cuprate compounds is certainly one of the most discussed and fascinating issues in modern condensed matter theory. Despite the great efforts spent in trying to understand the remarkable physical properties of these ceramic materials, a microscopic theory is lacking and this fascinating problem remains still unsolved. Nowadays, after more than one decade since the original discovery by Bednordz and Muller [1], the field is still rapidly evolving due to the improvement in the quality of the samples and in the experimental techniques providing a great amount of results which are fundamental clues for a microscopic theory. Moreover the development of new materials has considerably raised the critical temperature (up to $133K$) and, even if the possibility of having superconductors at room temperature seems quite far in time, technological applications (SQUID, Josephson Junction) are increasing.

The differences between these compounds and the conventional BCS superconductors (high critical temperature (T_c), lack of isotope effect on T_c, $d-$wave symmetry of the order parameter, short coherence length, linear behavior of the d. c. resistivity with temperature) led to the belief that the pairing force driving to superconductivity must be of a different nature. As a consequence, the strong electron electron correlation in the copper orbitals has been proposed as a responsible for the pairing. This idea, fascinating and innovative, proposed by several groups [2, 3, 4, 5, 6, 7, 8, 9] and than pursued over the years, relies on the physical similarities between the different high T_c compounds. Indeed all the high T_c superconductors (HTSC) originate from the doping of an antiferromagnetic Mott insulator with non magnetic impurities. The strong antiferromagnetic correlations of the undoped compound quickly disappears by doping leaving room to superconductivity.

The proximity of the Mott Antiferromagnetic insulator state has been considered by several authors [8, 9, 5, 6, 7] as fundamental, meaning that spin fluctuations can be responsible both for the onset of superconductivity and the symmetry of the order parameter. Nevertheless these compounds are also quite close to a phase separation instability (chapter 1), and this physical effect might be important for an accurate theoretical description, as was suggested in ref. [10, 11].

The theoretical approach is complicated by a great number of effects which cooperate in the physics of these materials. A full understanding is practically impossible and as a consequence "simple" theoretical models representative of the main features leading to superconductivity are needed.

In the case strong correlation is the dominant force driving from antiferromagnetism to superconductivity, a proposed lattice model to describe the interplay of these two effects is the two dimensional $t - J$ model [3, 12] (chapter 2). Moreover, since at strong coupling the ground state of the $t - J$ Hamiltonian displays a phase separated state, it is an almost ideal description of the competition between the antiferromagnetic forces and the tendency towards phase separation.

In recent years strongly correlated electrons on a lattice have been a major challenge for numerical simulations [13]. Mean field solution are often misleading due to the quantum fluctuations which are far from being negligible, while perturbative calculations are in practice unfeasible, being the relevant physics in the strong coupling regime.

On the other hand numerical methods allow the evaluation of ground state property of the finite size system. As an example exact diagonalization (Lanczos) in two dimensions is restricted to extremely small lattice sizes, but allows to compute statical and dynamical properties of a model Hamiltonian. This restriction is due to the huge dimension of the Hilbert space increasing exponentially with the lattice size so that in order to numerically investigate larger systems, different approaches are necessary.

A remarkable development from exact diagonalization methods is the density matrix renormalization group [14] which amounts to diagonalize the Hamiltonian in a suitably chosen restricted Hilbert space. This Hilbert subspace is then iteratively improved, adding relevant states and dropping less relevant ones, following the renormalization group idea. This approximation is variational on the ground

state energy and is not restricted to small size systems. Though density matrix renormalization group is "numerically exact" in one dimension, the extension of this method to higher dimensions is highly non trivial and is a current research topic.

Quantum Monte Carlo simulations are stochastic methods which account to generate configurations (samples) distributed as the ground state wavefunction of the Hamiltonian and to compute expectation values of physical observables as weighted averages over a large number of samples. In practice the ground state wavefunction of an Hamiltonian H is projected out by iterative stochastic application of the operator $e^{-H\tau}$ to a trial wavefunction (not orthogonal to the ground state of H).

These techniques allow simulations on large systems and can be safely exported to high dimensions, but suffer, in the case of fermions (or bosonic frustrated systems), from the well known "sign problem" instability. This instability is connected with the sign of the ground state wavefunction which can have regions of positive and negative sign. From the point of view of the simulation this means that the weights in the weighted average over the samples can change sign leading to a well defined mean value but with enormous fluctuations so that in practice no useful informations can be extracted.

To overcome this huge difficulty it is necessary to resort to some kind of approximation. In the framework of the Green function Monte Carlo technique, widely used in this thesis, the fixed node approximation [15] allows to obtain variational estimates of the energy defining an effective Hamiltonian which does not suffer from the sign problem instability. This definition relies on an *ansatz* on the ground state wavefunction (the so called "guiding wavefunction"), chosen on physical grounds. In practice the fixed node approximation does not change the nodes of the guiding wavefunction meaning that if the nodal surface of the true ground state is very far from the original *ansatz* the estimate of the energy is very poor.

The recently proposed Green function Monte Carlo with stochastic reconfiguration [16, 17] allows to systematically improve the fixed node approximation in a controlled way, crossing the nodal surface of the guiding wavefunction and sampling the sign. The results obtained with this technique are less dependent from

the original *ansatz* and the accuracy of the fixed node estimate of the ground state energy and of the local correlation functions is expected to be improved even for large sizes. The Green function Monte Carlo with stochastic reconfiguration has been successfully applied to frustrated quantum spin systems in two dimension [16, 17, 18, 19] and in this thesis the first successful application of the method to a fermionic system on a lattice is presented (chapter 3,4).

The quantum Monte Carlo simulations described in this thesis try to clarify several problems raised in this introduction. Among them the role of phase separation in the physics of the high T_c compounds, the relevance of the neighboring antiferromagnetic Mott insulator state and their relation with superconductivity .

The occurrence of phase separation in the physical region of the two dimensional $t-J$ model is still an open problem. For large coupling strength ($J \gg t$) using variational arguments (chapter 4) it is easy to see that the holes are expelled from the antiferromagnetic background so that the system prefers to phase separate in a hole rich region and in an electron rich one.

Since the physical value of the ratio J/t is at intermediate strength ($J = 0.4t$), where the above arguments are not valid, the issue has been investigated by several numerical techniques. Exact diagonalization [10] has shown that phase separation occurs at all strength in the model, but the size considered are too small for being representative of the thermodynamic limit. On the other hand high temperature expansion [20] found a completely different phase diagram in which phase separation was confined in the strong coupling regime ($J > 1.2t$). High temperature expansion allows to obtain results directly in the infinite volume limit, but suffers from the difficulty of extrapolating to zero temperature an high temperature series.

An even more delicate question regards the occurrence of superconductivity in the $t-J$ model. The results obtained in literature are contradictory.

Using variational Monte Carlo simulation, Gros [21] found enhanced $d-$wave correlation functions, but an improvement of the variational wavefunction with one Lanczos step has led to striking controversial results, confirming[22, 23] or denying [24] the presence of superconductivity.

Recently density matrix renormalization group calculation shows that $d-$wave correlations are depressed due to the presence of stripes. Stripes can be removed adding to the Hamiltonian a next nearest neighbor hopping term which allows the

simulation to recover the uniform solution, and then superconductivity occurs.

All these contradictory results have been obtained by numerical techniques that introduce some approximation in order to deal with the sign problem instability. Moreover these approximations are local and improve only short range quantities such as the energy or the nearest neighbors correlations. Indeed, while these methods allow to obtain less than 1% of accuracy on the ground state energy, the accuracy on the antiferromagnetic or superconducting order parameters is very poor. It is reasonable to believe that any calculation involving long distance operators, as it has been typically done in literature so far, may be not so accurate as an expectation value of a short range operator.

In particular if superconducting long range order occurs a very small order parameter is to be expected (as is shown even from a purely variational estimate, starting from a superconducting *ansatz*) and as a consequence a "great" accuracy is needed in the calculation.

In this thesis a different approach has been considered. It is shown that all the interesting long range properties of a model can be detected adding a suitably chosen *local* perturbation to the Hamiltonian and computing the energy correction due to this perturbation. The results of such a strategy, explained in details in chapter (4), are remarkable. The accuracy achieved is very high and due to the short range character of the perturbation the size effects are very weak.

This approach allowed to obtain a sound description of the ground state properties of the two dimensional $t - J$ model and to address the delicate question of a superconducting phase generated *uniquely* by the strong electron electron correlation .

Chapter 1

The Copper Oxide Superconductors

1.1 General properties of the High T_c materials

In the last two decades, High T_c superconductivity has been discovered in a family of cuprate compounds [1]. Even if several physical details, such as the critical temperature (T_c), change from material to material, there are properties which are common features. These properties involve solid state structure, antiferromagnetism and superconductivity. In order to develop a general theory a good knowledge of these similarities is of great importance.

Starting from the crystalline point of view, all the high temperature superconductors (HTSC) have a similar solid structure, in which every copper atoms is at the center of a tetragonal structure composed by oxygen atoms. Moreover several $\mathrm{CuO_2}$ layers appear in the crystal structure and between these layers are the transition elements (such as La or Ba). A typical example is given by the $\mathrm{La_{2-\delta}Sr_\delta CuO_4}$ ($T_c = 39K$, see fig. 1.1) in which La atoms lies between layers of $\mathrm{CuO_2}$ atoms (one layer per unit cell). A more complex material (the original one examined by Bednorz and Muller [1]) is the $\mathrm{YBa_2Cu_3O_7}$ ($T_c = 92K$) , in which there are two neighboring $\mathrm{CuO_2}$ planes per unit cell (see Fig. 1.1). The presence of $\mathrm{CuO_2}$ layers in all this compounds led to the belief that a lot of the important physics is contained in these two dimensional systems. This is supported by the fact that the $\mathrm{Cu-O}$ in plane bond length is $\sim 1.9\mathring{A}$ while the distance between planes is $\sim 6.6\mathring{A}$ and so the interlayer coupling can be neglected.

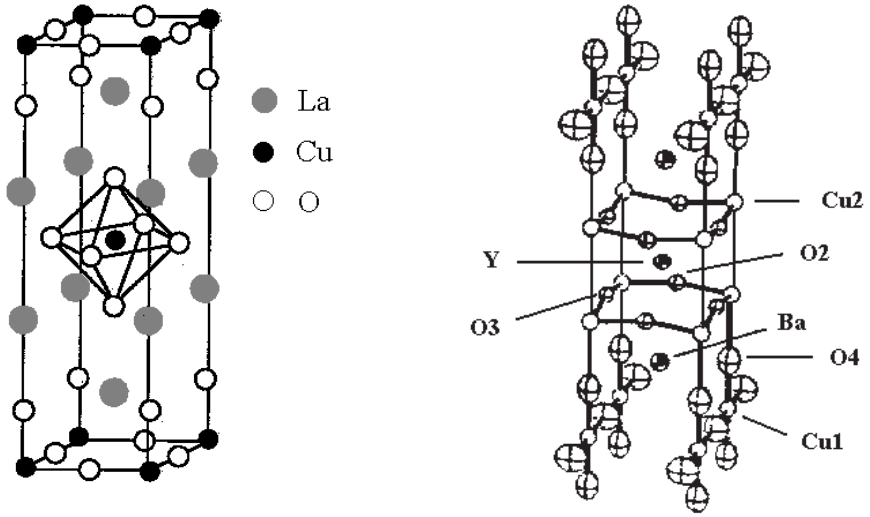

Figure 1.1: Crystal structure of La_2CuO_4 and $YBa_2Cu_3O_{6+x}$

All the High T_c superconductors originate from the doping of an Antiferromagnetic Mott insulator with non magnetic impurities. The antiferromagnetic character of the undoped system is given by the copper which in the solid has a valence Cu^{2+} and has an hole in the $3d$ shell, namely has a net magnetic moment. The oxygen is magnetically neutral and due to his mediation there is a net superexchange coupling between the in plane Cu atoms [25]. Since there is an effective odd number of electrons per copper atom a metallic behavior should be expected, but due to the strong correlations the undoped system is an antiferromagnetic Mott insulator. In the case of La_2CuO_4, doping is achieved in two different ways; substituting La^{3+} with Sr^{2+} or inserting O^{2-}. These two different kind of doping lead to quite different properties in the material. The Sr substitution is equivalent to adding holes in the CuO_2 layers (i.e. extracting electrons) while the oxygen insertion increases the number of electrons. Moreover the additional O^{2-} ions are mobile and are able to screen a charge imbalance, leading to rather different physical features.

An analysis of the phase diagram (see Fig. 1.2) of the considered materials shows that by hole-doping the antiferromagnetic long range order of the ground

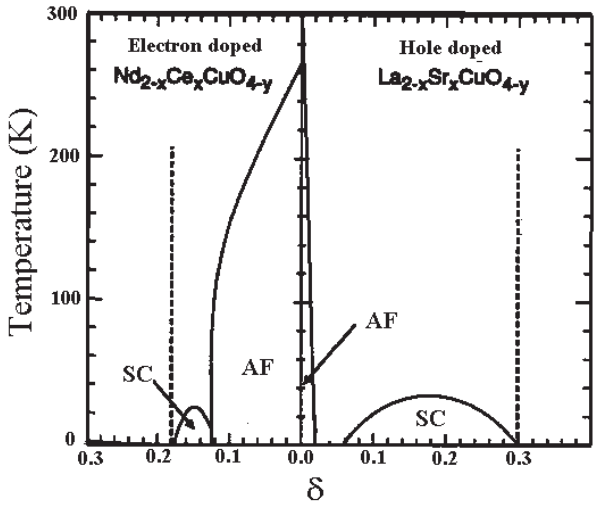

Figure 1.2: Experimental phase diagram of doped $\mathrm{La_2CuO_4}$

state is immediately lost (close to $\delta \sim 0.03$) and superconductivity appears ($\delta \sim 0.08$). T_c reaches its maximum value at $\delta \sim 0.15$ which is usually called optimal doping. When electron doping is considered antiferromagnetic long range order is stable up to $\delta \sim 0.11, 0.12$ and superconductivity occurs immediately after.

A very important similarity between high T_c materials is given by the symmetry of the superconducting gap. In a BCS superconductor the gap has an s-wave symmetry, isotropic in momentum space. There is now a wide consensus that in high T_c superconductors the pairing occurs in a $d_{x^2-y^2}$ symmetry. Experimentally this was detected by SQUID measurements in Josephson junction between BCS and high T_c superconductors [26].

The critical temperature varies a lot, ranging from $24K$ ($\mathrm{Nd_{1.85}Ce_{0.15}CuO_4}$) to $133K$ for the case of $\mathrm{HgBa_2Ca_2Cu_3O_{8+\delta}}$ [27], which represents the compound with the highest T_c discovered up to now. These values must be compared with the critical temperature of a standard BCS superconductor which is typically less than $4K$. So even if their critical temperatures are rather different they share the common properties of being too high for conventional superconductors.

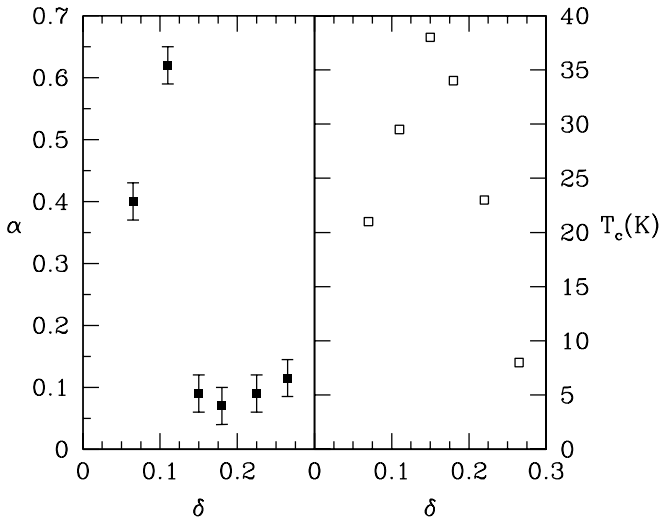

Figure 1.3: α exponent (left) and critical temperature (right) as a function of doping for $La_{2-\delta}Sr_{\delta}CuO_4$ [28]

1.2 Isotope effect

In the BCS type superconductors the pairing between the electron is given by an effective attractive electron electron interaction which originates from the electron phonon interaction. This evidence was experimentally achieved through isotope effect measurements on T_c [29]. In a conventional superconductor the dependence between the critical temperature and the isotope mass is $T_c \propto M^{-\alpha}$ where $\alpha \sim 0.5$. The oxygen isotope measurements in $YBa_2Cu_3O_{6+x}$ showed that the value of the α exponent is less then 0.1 [30]. This value is by far too small to think that the electron-phonon interaction alone can be responsible for the pairing. For $La_{2-\delta}Sr_{\delta}CuO_4$ the behavior of the exponent α is much more complex and depends on doping [28, 31]. In fig. (1.3) T_c and the exponent α are plotted as a function of doping for this material. The α increases up to the large value of $\alpha \sim 0.5$ for doping $\delta = 1/8$ but then decreases by a factor of 5 at optimal doping, reaching the same order of magnitude of the one detected in $YBa_2Cu_3O_{6+\delta}$.

The $1/8$ anomaly is still an open problem. In a parent compound, namely $La_{2-\delta}Ba_{\delta}CuO_4$, it was found [32] that at $\delta = 1/8$ a structural phase transition from a Low Temperature Orthorombic (LTO) phase to a Low Temperature Tetrag-

onal (LTT) phase occurs. This phase transition involves a tilting of the oxygen octahedra and clearly phonons must play an important role. For $La_{2-\delta}Sr_{\delta}CuO_4$ there is no evidence for such a phase transition, but maybe the system is approaching such instability. The $1/8$ anomaly involves even the critical temperature since there is a local minimum of T_c at this doping fraction.

The experimental measurements of the α exponent show that the isotope effect is very small at optimal doping for both the compounds. These results suggested that maybe the pairing could be given by the strong electronic correlations and not only by the electron-phonon interaction.

1.3 Phase Separation

The coexistence between holes and electrons in the CuO_2 layers has been a very discussed issue over the years. Several authors [11, 10] suggested that superconductivity could be connected with the phase separations of electrons and holes in these layers.

Phase separation was observed in the oxygen doped compounds using Neutron Powder Diffraction (NPD) [33] and Nuclear Magnetic Resonance (NMR) [34]. The experimental data showed that the system is separated in an oxygen rich and in an oxygen poor region. The NPD experiments found phase separation at $T < 320K$ and for an oxygen insertion greater than 0.05. Similar results were obtained by NMR[34]. No evidence of phase separation has been found in the hole-doped compounds.

In order to understand the appearance of phase separation in the oxygen doped compounds it is important to recall that the inserted oxygen ions are mobile in the solid. As a consequence these ions are able to screen the long range coulomb repulsion due to the charge imbalance connected with the phase separation instability. This is not the case of the hole doped compounds. The interplay between this effect and superconductivity is still an open question.

1.4 Magnetic properties

Through Neutron Scattering and Nuclear Magnetic Resonance (NMR) experiments it is possible to carefully analyze the change of the magnetic properties of the HTSC materials upon doping. Measurements of the Neutron Scattering cross section provide informations on the spin-spin structure factor of the sample.

As a consequence of the antiferromagnetic long range order, the undoped compound shows a sharp peak in the spin spin structure factor at the antiferromagnetic wavevector, $Q = (\pi, \pi)$. In the case of the $La_{2-\delta}Sr_{\delta}CuO_4$, as the sample is doped with Sr, this peak broadens and at a doping $\delta > 0.05$ disappears and incommensurate spin fluctuations arise close to the Q point [35, 36, 37] at positions $(\pi, \pi \pm 2\epsilon\pi)$ and $(\pi \pm 2\epsilon\pi, \pi)$. The dependence of the incommensurability ϵ with doping [37] is linear for $0.05 < \delta < 0.12$ and after saturates (see fig. 1.4). A striking feature is that the angular coefficient of the linear relation between the incommensurability and the doping fraction is exactly 2π.

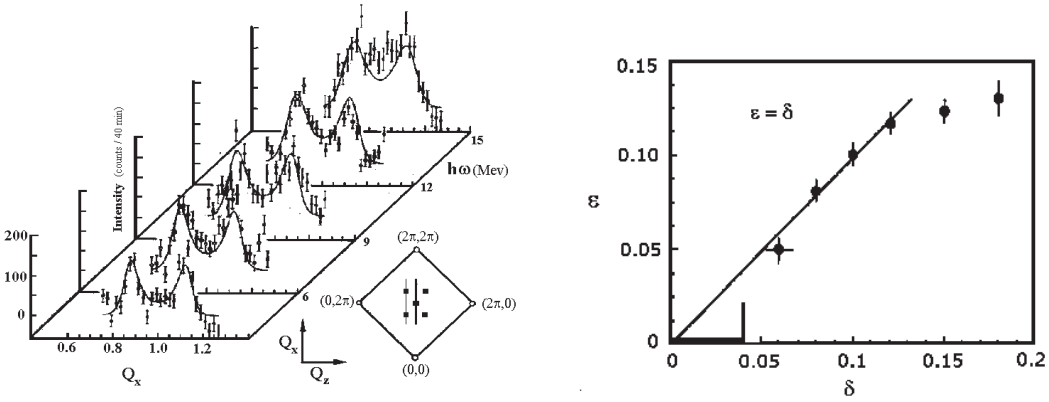

Figure 1.4: Left: Spin fluctuations in the dynamical spin structure factor at $\delta = 0.14$. Right: Linear dependence of the peak position on doping (ϵ being the distance from $Q = (\pi, \pi)$ in units of 2π) [37]

X ray diffraction measurements [38] has shown that similar incommensurate peaks occur in the charge structure factor but close to the $\Gamma = (0, 0)$ point with an incommensurability which is twice the spin structure one. This behavior has been explained by a domain walls ordering of holes in the CuO_2 layers as is shown in Fig. (1.5). The half filled hole stripes separate antiferromagnetic regions which

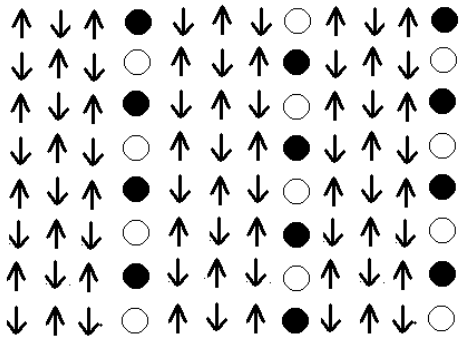

Figure 1.5: Spin and hole structure suggested in [39] at a doping $\delta = 1/8$. The hole stripes are half filled. The antiferromagnetic regions are correlated by a π shift across a domain wall.

are correlated with a π shift across a domain wall. The modulation connected with the charge is then at low momenta, close to the Γ point, while the spin structure presents a spin density wave at incommensurate momentum close to the antiferromagnetic wavevector.

Mook and coworkers [40] showed that even in $YBa_2Cu_3O_{6.6}$ these features are present suggesting that they are a very general property of the HTSC. In $La_{2-\delta}Sr_\delta CuO_4$ the width of the incommensurate spin fluctuations becomes particularly narrow at the doping $\delta = 1/8$. Neutron scattering experiments and T_c measurements at this doping fraction in $La_{1.6-\delta}Nd_{0.4}Sr_\delta CuO_4$ [39] showed that this property occurs together with the anomalous suppression of superconductivity (an effect which was already discovered in $La_{2-\delta}Ba_\delta CuO_4$ [41]).

Nowadays a satisfactory theoretical explanation of the $1/8$ anomaly is not present. Even if several theories involving frustrated phase separation by the repulsive Coulomb interaction [42] and segregation in "stripes" of the charges and spins have been proposed, it is not completely clear their relation with superconductivity, the high value of T_c and the pairing mechanism.

Chapter 2

Theoretical models for the $\mathrm{Cu-O_2}$ layers

The most important step towards an understanding of the cuprate compounds is to derive an effective Hamiltonian describing the low energy physics. Since one of the general features of the HTSC materials is the presence of $\mathrm{CuO_2}$ layers in their solid structure and since the in-plane $\mathrm{Cu-O}$ bonding is very strong it seems reasonable to assume that a two dimensional model of interacting copper and oxygen atoms is able to reproduce common properties of different materials. This assumption is supposed to be correct at least for the zero temperature and low energy behavior. At finite temperature no spontaneous symmetry breaking can occur in two dimensions [43] and as a consequence no magnetic long range order can be detected. The critical temperature (T_c) for the superconducting transition, which is a really material dependent quantity, should require a more complicated model taking into account inter layers coupling.

As was suggested by several experiments, in particular the isotopic effect over T_c, a different kind of pairing is to be expected for the HTSC, maybe related only to the electronic correlations. Since the aim of this work is to understand what is the main physical interaction leading to high temperature superconductivity only models which take into account the electronic correlations will be considered and the role of phonons will be completely neglected. This hypothesis is adopted since the question is: it is possible to have an electron pairing mediated only by

the electron electron repulsive interaction ? In the case that such kind of pairing really occurs, then phonons may enhance this effect.

2.1 Derivation of the models

Due to the crystal field anisotropy, the atomic degeneracy of the copper d levels is broken and the $3d_{x^2-y^2}$ orbital is the highest in energy. Ab initio calculations [44, 45] show that the band crossing the Fermi energy has mainly a $d_{x^2-y^2}$ character. As a consequence it is possible to take into account only one single orbital for each copper atom. In a similar way all the oxygen orbitals apart from the $2p$ lie well below the Fermi energy and need not to be considered. Neglecting hibridization between $2p$ and $3d_{x^2-y^2}$ the situation is that of a completely filled atomic $2p$ orbital and an half filled $3d_{x^2-y^2}$. The state $|3d_{x^2-y^2}1,\ 2p2\rangle$ will be considered as the reference vacuum. On the vacuum state act the operators $d^+_{i\sigma}$, creating a hole of spin σ at site i in the $3d_{x^2-y^2}$, and $p^+_{l\sigma}$, creating a hole of spin σ at site l in the $2p$ orbitals (where i refers to the positions of copper atoms, while l of oxygen). In order to write a full Hamiltonian it is necessary to take into account the Coulomb repulsion U_d and U_p between holes on the same atom (copper and oxygen respectively), the repulsion U_{pd} of holes on different atoms, the strong hybridizations t_{pd} between the $3d_{x^2-y^2}$ and $2p$ orbitals and the hopping amplitude t_{pp} between two near oxygen atoms (see fig. 2.1) :

$$\begin{aligned} H &= \sum_{i,\sigma} \epsilon_d\, d^+_{i\sigma} d_{i\sigma} + \sum_{l,\sigma} \epsilon_p\, p^+_{l\sigma} p_{l\sigma} + \sum_i U_d\, d^+_{i\uparrow} d_{i\uparrow} d^+_{i\downarrow} d_{i\downarrow} + \\ &+ \sum_l U_p\, p^+_{l\uparrow} p_{l\uparrow} p^+_{l\downarrow} p_{l\downarrow} + \sum_{<i,l>,\sigma} t^{i,l}_{pd} \left(d^+_{i\sigma} p_{l\sigma} + p^+_{l\sigma} d_{i\sigma} \right) + \\ &+ \sum_{<l,l'>,\sigma} t^{l,l'}_{pp} \left(p^+_{l,\sigma} p_{l',\sigma} + p_{l,\sigma} p^+_{l',\sigma} \right) + \sum_{<i,l>\sigma,\sigma'} U_{pd}\, d^+_{i\sigma} d_{i\sigma} p^+_{l\sigma'} p_{l\sigma'} \end{aligned} \quad (2.1)$$

where ϵ_p and ϵ_d are the on site energies of the holes on the p and d orbitals respectively. The values of the coupling constants entering in the model Hamiltonian have been obtained from experimental data by several authors [46, 47] or computed from ab-initio band theory calculations [44, 45] and have been reported in table (2.1).

Parameter	[48]	[46]	[49]	[50]	[51]	[52]
$\epsilon_p - \epsilon_d$	3.5	3.6		3.5	4.0	1.5
U_d	9.4	10.5		8.8	10.0	9.0
U_{pd}	0.8	1.5	0.6-1.3	< 1.0	0-1	1.5
t_{pd}	-1.5	-1.3	-1.6	-1.3	-1.38	-1.07
t_{pp}	0.6	0.65	0.65	0.65	0.33	0.53

Table 2.1: Summary of parameters value (in eV) for $\mathrm{La_2CuO_4}$ obtained from ab initio band structure calculations. The numbers between square brackets on the top of the columns label the reference number.

At half filling (the case of the undoped material) there will be one hole for each $\mathrm{CuO_4}$ square (see fig. 2.1). Since $\Delta = \epsilon_p - \epsilon_d > 0$, the hole will occupy the copper orbital. Upon doping, other holes are added to the system and, since U_d is very large compared to Δ, it will be energetically more favorable to occupy the oxygen orbital. In the strong coupling limit $U_d >> \Delta$ there will be only one hole per copper atom.

However the system may also gain energy from the hybridization term and build delocalized hole states over the $\mathrm{CuO_4}$ squares. Starting from this hypothesis Zhang and Rice [12] showed that in second order perturbation theory the singlet state between the two holes is energetically favored ("Zhang and Rice singlet"). As a consequence the creation of an oxygen hole is equivalent to the creation of a Zhang and Rice singlet on the copper atom and the movement of this hole through the lattice can be described by an effective hopping of the singlet state between different copper atoms. In this way the oxygen atoms are eliminated and an effective one band Hamiltonian can be derived, the $t - J$ model Hamiltonian:

$$H = -t \sum_{<ij>} (c_i^+ c_j + c_j^+ c_i) + J \sum_{<ij>} \mathbf{S}_i \cdot \mathbf{S}_j \tag{2.2}$$

where the Heisenberg term describes the superexchange spin interaction between the copper atoms in the strong coupling limit ($U_d >> \Delta$) and the constraint of no double occupancy has to be understood.

In order to achieve consistency with the strong coupling limit of the one band

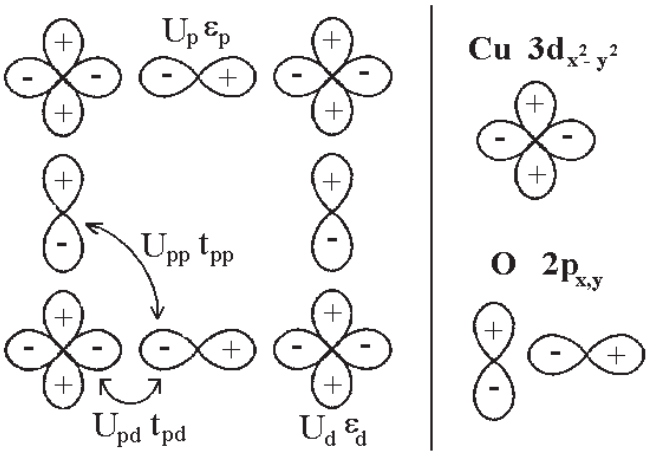

Figure 2.1: $3d_{x^2-y^2}$ orbitals of the Cu atoms and $2p_x$,$2p_y$ orbitals of the O atoms. The three band Hamiltonian parameters (see text) are also shown.

Hubbard model at order t^2/U [53], an attractive nearest neighbor density-density term proportional to J is usually added to the Hamiltonian,

$$H = -t \sum_{<ij>} (c_i^+ c_j + c_j^+ c_i) + J \sum_{<ij>} \left(\mathbf{S}_i \cdot \mathbf{S}_j - \frac{n_i n_j}{4} \right) \tag{2.3}$$

This term is not present in the derivation of the model as presented by Zhang and Rice [12] and its effect is of enhancing the attraction between the holes. We will refer to the $t-J$ model Hamiltonian as the one including the nearest neighbor attractive density-density interaction.

The antiferromagnetic coupling J can be obtained from fourth order perturbation theory as [12, 54]:

$$J = \frac{4t_{pd}^4}{(\Delta + U_{pd})^2} \left[\frac{1}{U_d} + \frac{2}{2\Delta + U_p} \right] \tag{2.4}$$

At half filling the $t-J$ model reduces to the two dimensional Heisenberg antiferromagnet which is known to have a singlet ground state [55], insulating and with antiferromagnetic long range order [56, 57, 58, 59, 60]. This model is supposed to give an accurate description of the undoped parent materials at zero temperature. Due to this relationship, the $t-J$ model describes the doping of an antiferromagnetic insulator with non magnetic impurities, which is the relevant case for the

HTSC compounds.

2.2 Known results and open questions

2.2.1 Phase separation

One of the most important questions raised in the context of high temperature superconductors is if the strong competition between hole propagation and antiferromagnetic order in the $\mathrm{CuO_2}$ planes leads to the segregation of holes in regions without antiferromagnetic order. The $t-J$ model represents a good starting point to clarify this issue because it takes into account spin interaction and hole kinematics. Moreover it is known that at large value of the ratio J/t phase separation of spins and holes occurs. In this limit the kinetic term in the Hamiltonian can be neglected and the energy loss, in units of J, when holes are inserted in an antiferromagnetic background is equal to the energy per bond times the number of antiferromagnetic broken bonds (see section 4.1.1). As a consequence if the holes are all segregated in a region there is a gain in energy if compared to the variational state having the holes far apart. Unfortunately the physical value of the ratio J/t is at intermediate coupling ($J/t \sim 0.4$), very far from this limit.

As a consequence many authors have tried to clarify this issue using numerical techniques. Calculations of exact ground state energies on small lattice sizes [10] show that phase separation occurs at all strength in the model, but the sizes considered are too small to be representative of the thermodynamic limit, where the question is meaningful. In 1992 using high temperature expansion [20] phase separation was found only for large J/t, but this method suffers from the difficulty of extrapolating the zero temperature limit of a series knowing only a few coefficients. Recently [61] Quantum Monte Carlo calculations give similar results to the ones obtained by exact diagonalization, but the most important and delicate low doping region has been studied only with fairly small lattice sizes, so that this result is not surprising. By contrast an improvement of a variational method (the lanczos step method) [62] suggests that no phase separation occurs in the physical region. One of the aim of this thesis is to clarify this controversial issue, as will be shown in section (4.1) in order to detect if the phase separation instability is

really relevant for the physics of the HTSC compounds.

2.2.2 Antiferromagnetism at low doping

At half filling the ground state of the $t-J$ model has antiferromagnetic long range order. Even if an analytical proof of that is still lacking there is a great number of numerical results [56, 57, 58, 59, 60] that strongly support this scenario. Upon doping there is not a general consensus regarding the disappearing of antiferromagnetic long range order. From an experimental point of view, as was discussed in chapter (1), the long range order disappears close to $\delta = 0.03 - 0.05$, but it is not obvious that the $t-J$ model is able to reproduce such feature. Calculations of the spin structure factor by exact diagonalization [63, 64] shows that the antiferromagnetic correlations are resistant up to $\delta = 0.15$, but since the lattice sizes considered are too small to attempt a finite size scaling it is not easy to identify the critical doping for the disappearing of long range order. Moreover the correlation length might be larger than the lattice sizes considered in [63, 64] and antiferromagnetic correlations overestimated. Variational Monte Carlo calculations on larger sizes [65] suggests that the critical doping is $\delta_c = 0.11$. In the framework of the $t-J$ model it is not yet clear if there is coexistence between long range antiferromagnetic order and superconductivity.

2.2.3 Superconductivity

The belief that the pairing mechanism of high temperature superconductors is of pure electronic nature has driven a great interest on strongly correlated fermion models. As a consequence an enormous effort has been devoted to the quest of superconducting long range order in the repulsive Hubbard model and in the $t-J$ model. Nevertheless the results obtained so far on the subject are far from being satisfactory, mainly due to the difficulty of the calculations and to the small value of the order parameter.

Exact diagonalization on small sizes for both the models [63, 64], confirmed the existence of superconducting LRO, but the Quantum Monte Carlo calculations [66, 67] on the Hubbard model suggests that these results were only a finite size effect and the order parameter is zero in the infinite volume limit. In the $t-J$

model a great number of variational calculations [68, 65, 21] show evidence of superconducting long range order. The improvement of the variational wavefunction with one lanczos step iteration has given striking controversial results, confirming [22, 23] or denying [24] the presence of superconductivity.

Since the existence of superconducting long range order remains the main request to be fulfilled by a theoretical model in order to describe the HTSC the main task of this thesis is to understand if the $t - J$ model has this feature.

Chapter 3

Numerical Method

3.1 Green Function Monte Carlo

3.1.1 Single walker formulation

The Green Function Monte Carlo (GFMC)[69] method is a numerical technique that allows to filter out the ground state wavefunction $|0\rangle$ of an Hamiltonian H from a given trial wavefunction $|\psi_T\rangle$, provided that $\langle\psi_T|0\rangle \neq 0$. This is achieved through iterative application of the operator $G = \Lambda - H$ to the trial wavefunction, where Λ is a suitably chosen positive constant to allow for convergence. Namely:

$$G^q|\psi_T\rangle = (\Lambda - E_0)^q \left[C_0|0> + \sum_{n\neq 0} \left(\frac{\Lambda - E_0}{\Lambda - E_n} \right)^q C_n|n\rangle \right] \tag{3.1}$$

where q is the number of times G is applied to $|\psi_T\rangle$, $C_n = \langle n|\psi_T\rangle$, and $|n\rangle$,E_n are the eigenvectors and eigenvalues of the Hamiltonian H respectively. As q goes to infinity, the iteration converges to the ground state wavefunction exponentially in q.

In practice a basis set $|x\rangle$ is chosen (e.g. the spin configuration of the lattice) and the iteration

$$\psi_{q+1}(x') = \sum_x G_{x',x}\psi_q(x) \tag{3.2}$$

is implemented, being $G_{x',x}$ the matrix elements of G in the chosen basis. If the latter recursive equation is evaluated in an exact way it is easy to see that one

obtains, after a few iterations, transitions to a large number of states, so that it is necessary to bookkeep the full Hilbert space. As a consequence the computation becomes cumbersome in terms of memory occupation and only small lattice sizes can be afforded.

A solution to this problem is to sample the matrix-vector product (3.2) in a stochastic way through a Markov process. Since the matrix $G_{x',x}$ is not a stochastic matrix [1], one defines the transition probability between two elements of the Markov chain as

$$p_{x',x} = \frac{G_{x',x}}{b_x s_{x',x}} \tag{3.3}$$

where $b_x = \sum_{x'} G_{x',x}/s_{x',x}$ and $s_{x',x}$ is the sign of the matrix element $G_{x',x}$. In this way the transition probability between two elements of the Markov chain is normalized, being $p_{x',x}$ a stochastic matrix.

The basic element of the stochastic process is the so called "walker" (w, x) which is determined by the configuration x and a weight w. Eq. (3.2) can be seen as a stochastic transition from the state $x \to x'$ and a scaling of the weight of the walker $w \to w' = s_{x',x} b_x w$.

The task of the GFMC approach is to define a Markov process [70], yielding after a large number q of iterations a probability distribution $P_q(w, x)$ for the walker which determines the ground state wavefunction, namely:

$$\int dw\, w\, P_q(w, x) = \langle x|\psi_q\rangle \longmapsto \langle x|\psi_0\rangle \tag{3.4}$$

The evolution of the probability under such process is

$$P_{q+1}(w', x') = \sum_x P_q(w'/b_x s_{x',x}, x) \frac{p_{x',x}}{b_x |s_{x',x}|} \tag{3.5}$$

It is easy to see that the evolution (3.5) correctly reproduces the matrix vector multiplication (3.2) since, rescaling $w'/b_x \to w'$,

$$\begin{aligned} \psi_{q+1}(x') &= \sum_x p_{x',x} \int dw' \frac{w'}{b_x |s_{x',x}|} P(w'/b_x s_{x',x}, x) \\ &= \sum_x G_{x',x} \psi_q(x) \end{aligned}$$

[1] A square matrix $A_{i,j}$ is a stochastic matrix if $\sum_i A_{i,j} = 1$.

As $q \to \infty$ it is possible to evaluate the ground state energy of the Hamiltonian H as

$$E_0 = \frac{\langle \psi_T | H | 0 \rangle}{\langle \psi_T | 0 \rangle} = \frac{\langle w E_x \rangle}{\langle w \rangle} \tag{3.6}$$

where E_x is the so called "local energy" , $(E_x = \sum_{x'} H_{x',x})$ and the brackets $\langle\ \rangle$ are for the stochastic average, namely averaging over the independent configurations. The so called "mixed average" of the observables O^k are also easily obtained:

$$O^k_x = \frac{\langle \psi_T | O^k | 0 \rangle}{\langle \psi_T | 0 \rangle} = \frac{\langle w O^k_x \rangle}{\langle w \rangle} \tag{3.7}$$

where $O^k_x = \sum_{x'} O^k_{x',x}$. The configurations generated in the Markov chain will be distributed, as q goes to infinity, as the right eigenvector of the matrix $p_{x',x}$, which is in general different from $|0\rangle$. We can consider the right eigenvector as a trial state for the initial iteration of the power method and compute the weight of the walker assuming that L iterations before it was equal to 1. In this way it is simple to compute the ground state energy as:

$$E_0 = \frac{\sum_n E_{x_n} G^L_n}{\sum_n G^L_n} \tag{3.8}$$

where

$$G^L_n = \prod_{j=1}^{L} b_{x_{n-j}} s_{x_{n-j+1}, x_{n-j}} \tag{3.9}$$

In principle this procedure concludes the GFMC scheme. However several technical problems arises.

Since the weight of the walker is the results of L independent products, it grows exponentially with L and can assume very large (or very small) values, implying a diverging variance in the above averages. In the case the weight of the walker is always positive this instability can be solved introducing a set of M walkers and defining a reconfiguration process [60] that introduces a small but controlled bias in the simulation as will be shown in the next section (3.1.2) .

Moreover when $G_{x,x'}$ is applied to $|\psi_q >$ it is possible to collect negative sign contributions to w since the trial wavefunction might have a negative value

on the configuration $|x' >$. This case is of great importance when dealing with fermions due to the antisymmetric character of the ground state wavefunctions. In practice the weight of the walker collects negative and positive contributes so that the average sign after q iterations is:

$$\langle s_q \rangle = \frac{\sum_x \int dw w P_q(w,x)}{\sum_x \int dw |w| P_q(w,x)} \sim \left(\frac{\Lambda - E_0}{\Lambda - E_0^{bos}} \right)^q \tag{3.10}$$

where E_0^{bos} is the "bosonic" ground state energy of the Hamiltonian $|H|$ (obtained by changing sign to the positive off-diagonal matrix elements of the Hamiltonian H), which is obviously below E_0. The latter result shows that the average sign decreases exponentially to zero as the number of iterations is increased, leaving a small quantity which is very difficult to sample. The so called "sign problem" instability [71] limits in a severe way the application of the GFMC technique to fermionic systems unless some kind of approximations is used (Fixed Node Approximation, Green Function Monte Carlo with Stochastic Reconfiguration).

3.1.2 Reconfiguration process in the absence of sign problem

Consider M walkers and label the corresponding configurations and weights with a couple of vectors $(\underline{w}, \underline{x})$, with each vector component (w_i, x_i) $i = 1, \cdots, M$, corresponding to the i^{th} walker. Suppose that all the weights of the walker are positive in the stochastic process, $s_{x',x} = \delta_{x',x}$. It is then easy to generalize Eq. (3.5) to many independent walkers:

$$P_{q+1}(\underline{w}, \underline{x}') = \sum_{x_1, x_2, \ldots, x_M} P_q(w_1/b_{x_1}, w_2/b_{x_2}, \cdots w_M/b_{x_M}, x_1, x_2, \cdots x_M) \left(p_{x'_1,x_1} p_{x'_2,x_2} \cdots p_{x'_M,x_M} \right) / (b_{x_1} b_{x_2} \cdots b_{x_M}) \tag{3.11}$$

If the evolution of P is done without further restriction each walker is uncorrelated from any other one and :

$$P(w_1, w_2, \cdots, w_M, x_1, x_2, \cdots x_M) = P(w_1, x_1) P(w_2, x_2) \cdots P(w_M, x_M) \tag{3.12}$$

The moment of order k over the weight variable can be defined as:

$$X_{k,q}(x) = \int dw_1 \int dw_2 \cdots \int dw_M \tag{3.13}$$

$$\sum_{\underline{x}} \left(\frac{w_1^k \delta_{x,x_1} + w_2^k \delta_{x,x_2} + \cdots w_M^k \delta_{x,x_M}}{M} \right) P_q(\underline{w}, \underline{x})$$

Since we are interested only in the first moment of P we can define a reconfiguration process that changes the probability distribution P_q without changing its first moment, and in this we follow [72]:

$$P'_q(\underline{w}', \underline{x}') = \int \sum_{\underline{x}} K(\underline{w}', \underline{x}'; \underline{w}, \underline{x}) P_q(\underline{w}, \underline{x}) \, [d\underline{w}] \tag{3.14}$$

$$K(\underline{w}', \underline{x}'; \underline{w}, \underline{x}) = \prod_{i=1}^{M} \left(\frac{\sum_j w_j \delta_{x'_i, x_j}}{\sum_j w_j} \right) \delta(w'_i - \frac{\sum_j w_j}{M}) \tag{3.15}$$

Hereafter the multiple integrals over all the w_j variables are conventionally shorthand for $\int [d\underline{w}]$. Note that the defined kernel K is normalized:

$$\int [d\underline{w}'] \sum_{\underline{x}'} K = 1$$

In practice this reconfiguration process amounts to generate a new set of M walkers (w'_j, x'_j) in terms of the given M walkers (w_j, x_j) in the following way. Each new walker w'_j, x'_j will have the same weight $\bar{w} = \frac{\sum_j w_j}{M}$ and an arbitrary configuration x'_j among the possible old ones $\{x_k\}_{k=1,\cdots,M}$, chosen with a probability $p_k = w_k / \sum_j w_j$. It is clear that after this reconfiguration the new M walkers have by definition the same weights and most of the irrelevant walkers with small weights are dropped out (see fig. 3.1). This is just the desired reconfiguration which plays the same stabilization effect of the conventional branching scheme.[69, 58]

It is well known that the control of the population size M introduces some bias in the simulation simply because some kind of correlation between the walkers is introduced. However for high accuracy calculations this bias often becomes the most difficult part to control. It is possible to prove that the reconfiguration of the M walkers defined in (3.15) does a better job. Though this reconfiguration clearly introduces some kind of correlation among the walkers, it can be rigorously proven (see A.1) that the first momentum $X_{1,q}(x)$ of the distribution of P_q is exactly equal to the one $X'_{1,q}(x)$ of P'_q, obtained after the reconfiguration. This

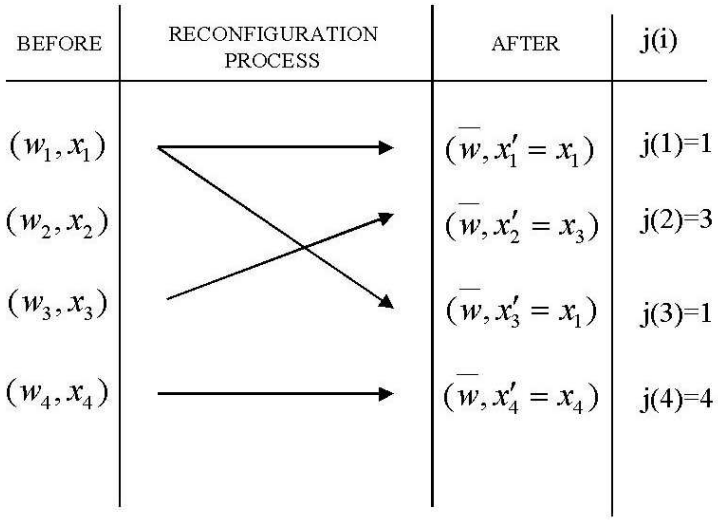

Figure 3.1: Example of reconfiguration process in the absence of sign problem for a population of 4 walkers. The new walkers after the reconfiguration have the same weight $\bar{w}$ but different configurations from the walkers before the reconfiguration. $j(i)$ is the mapping between the new and the old population. This mapping must be saved in order to perform the forward walking technique (section 3.1.7)

means that there is no loss of information in the described reconfiguration process and

$$X'_{1,q}(x) = X_{1,q}(x) \tag{3.16}$$

3.1.3 From power method to exact imaginary time propagation

In order to have non negative diagonal matrix elements in $G_{x',x} = \Lambda\delta_{x',x} - G_{x',x}$ it is necessary to choose the constant Λ in eq. (3.1) large enough. However an exceedingly large value of Λ -which is often the case especially for fermions- determines a slowing down of the algorithm, since there is a very small probability $\sim 1/\Lambda$ to accept a new configuration x' and the algorithm remains almost always stacked in the old one x. Thus one needs much more power iterations (3.2) to generate statistically independent configurations and the auto correlation time be-

comes very large. In order to overcome this difficulty, following [69], it is better to determine *a priori* the number of diagonal moves before an off diagonal is accepted. Thus one can generate each time a new configuration without caring of a very large value of Λ. The probability p_d to remain in the same configuration can be written as

$$p_d = \frac{\Lambda - H_{x,x}}{\Lambda - E_x} \tag{3.17}$$

where E_x is the local energy. Given p_d, the probability $t(k)$ to make k diagonal moves before the first acceptance of a new configuration ($x' \neq x$) is $t(k) = p_d^k(1 - p_d)$ if k is less than the number of trials n_T that are left before approaching the successive reconfiguration process, and $t(n_T) = p_d^{n_T}$. In practice the algorithm after each reconfiguration proceeds as follow:

1. Set $n_T = k_p$, where k_p is the number of power iteration between two different reconfigurations.

2. Extract a random number ξ ($0 < \xi < 1$) and choose k as,

$$k = \min\left(n_T, \left[\frac{\ln \xi}{\ln p_d}\right]\right) \tag{3.18}$$

   where the square brackets denote the integer part.

3. if $k \geq n_T$ go to number 7.

4. update the weight of the walker in a way consistent with k diagonal moves.

5. Perform an off diagonal move.

6. Rescale n_T in $n_T - k - 1$ and go to number 2.

7. Perform the new reconfiguration and then restart the procedure from number 1.

In this way it is possible to choose even an infinite value of the constant Λ so that the power method (3.1) can be cast in an exponential form. In fact choosing $k_p = \Lambda\Delta\tau$, with $\Delta\tau$ fixed, the usual propagator can be written in exponential form, $\Lambda^{k_p}(1 - H/\Lambda)^{k_p} \propto e^{-H\Delta\tau}$ as $\Lambda \to \infty$. Thus Δ_τ represents the imaginary time difference between two successive reconfiguration schemes.

3.1.4 Importance Sampling

One of the most important advantages of the Green function Monte Carlo technique is the possibility to reduce the variance of the energy by exploiting some information of the ground state wavefunction, sometimes known a priori on physical grounds [71]. In order to understand how to reduce this variance, we just note that the power method, as described in the previous sections, is not restricted to symmetric matrices, simply because we never used this property of the Hamiltonian matrices. Following [71] we consider not the original matrix , but the non symmetric one:

$$\bar{G}_{x',\,x} = \psi_G(x') G_{x',\,x} / \psi_G(x)$$

where ψ_G is the so called **guiding wavefunction** , that has to be as simple as possible to be efficiently implemented in the calculation of the matrix elements and , as we will see, as close as possible to the ground state of G.

In order to evaluate the maximum eigenvalue of G', corresponding obviously to the ground state of H, the local energy E_x is now given by:

$$E_{x_n} = \sum_{x'} \psi_G(x') H_{x',x_n} / \psi_G(x_n) = \sum_{x'} \bar{H}_{x',x} \tag{3.19}$$

where, for simplicity of notations, the bar over an operator represents the same operator after the importance sampling transformation. Thus if ψ_G is exactly equal to the ground state of H then, by definition, $E_{x_n} = E_0$, independent of x_n. This is the so called **zero variance property** satisfied by the method. Namely if the guiding wavefunction approaches an exact eigenstate of H , the method is free of statistical fluctuations. Of course one is never in such a fortunate situation, but by improving the guiding wavefunction one is able to considerably decrease the error bars on the energy. This property is very important and non trivial.

As a consequence of the importance sampling transformation, in order to compute the mixed average estimator (3.19) for general operators it suffices to introduce the quantity

$$\bar{O}^k_{x,x'} = \psi_G(x') O^k_x \psi_G(x) \tag{3.20}$$

and substitute $O^k_{x,x'}$ with $\bar{O}^k_{x,x'}$ in equation (3.7).

3.1.5 Fixed Node approximation

As we have seen when the weights of the walkers are not all positive it is always possible to define the transition probability for the stochastic process but even if the Markov process converges to a probability distribution which determines the ground state wavefunction, calculations are unfeasible due to the large fluctuations of the weights due to the "pathological" cancelation between positive and negative weights. It is then necessary to revert to some kind of approximation. The most popular one is the Fixed Node (FN) approximation[15]. In this approach an effective Hamiltonian $\bar{H}^{eff}$ is defined, starting from $\bar{H}$, and setting to zero the positive off diagonal elements of $\bar{H}$

$$\bar{H}^{eff}_{x',x} = \begin{cases} \bar{H}_{x',x} & \text{if} \quad \bar{H}_{x',x} \leq 0 \\ 0 & \text{if} \quad \bar{H}_{x',x} > 0 \end{cases} \tag{3.21}$$

as a consequence the diagonal term has an additional $sign - flip$ contribute:

$$\bar{H}^{eff}_{x,x} = \bar{H}_{x,x} + \mathcal{V}_{sf}(x) \tag{3.22}$$

$$\mathcal{V}_{sf}(x) = \sum_{\bar{H}_{x',x}>0 \, and \, x' \neq x} \bar{H}_{x',x} \tag{3.23}$$

It is possible to prove (see A.2) that the ground state of the effective Hamiltonian $\bar{H}^{eff}$ is a variational upper bound for the ground state energy of the Hamiltonian $\bar{H}$.

A slight generalization of the fixed node approximation can be obtained defining the effective Hamiltonian in a different way. Indeed reversing the sign of the positive off-diagonal matrix elements of $\bar{H}$ and multiplying them by a constant $\gamma > 0$ one obtains:

$$\bar{H}^{eff}_{x',x} = \begin{cases} \bar{H}_{x',x} & \text{if} \quad \bar{H}_{x',x} \leq 0 \\ -\gamma \bar{H}_{x',x} & \text{if} \quad \bar{H}_{x',x} > 0 \end{cases} \tag{3.24}$$

As a consequence the diagonal term must be changed as

$$\bar{H}^{eff}_{x,x} = \bar{H}_{x,x} + (1+\gamma)\mathcal{V}_{sf}(x) \tag{3.25}$$

where $\mathcal{V}_{sf}(x)$ is defined in (3.23). Note that the standard Fixed Node dynamic is recovered with the parameter choice $\gamma = 0$, while the case with $\gamma = -1$ is the opposite limit in which $\bar{H}^{eff} = \bar{H}$, the so called "nodal release". In appendix (A.2)

it is proved that even this case gives a variational estimate for the ground state energy. The dependency on γ of the ground state energy is shown if Fig. (3.2). The energy only slightly depends on γ and the lowest value can be obtained in the

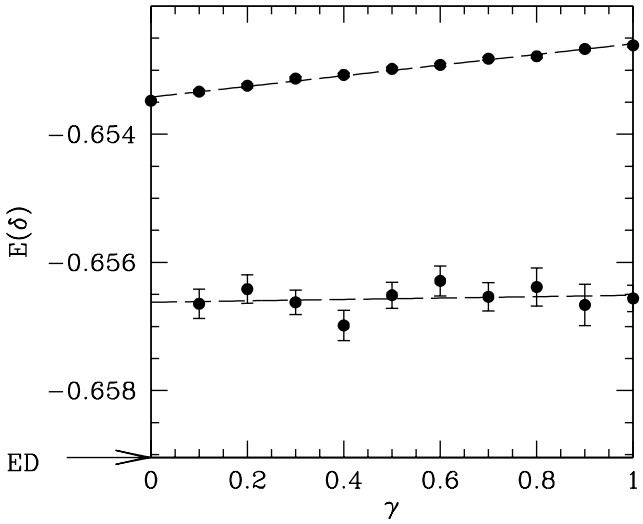

Figure 3.2: Fixed node (empty dots) and stochastic reconfiguration (full dots) energy dependence on γ.

standard fixed node framework ($\gamma = 0$). Nevertheless the introduction of γ allows transition to states on different nodal regions. This feature will be extensively used in the framework of the Green Function with Stochastic Reconfiguration.

3.1.6 Green Function Monte Carlo with Stochastic Reconfiguration

The Green Function Monte Carlo with stochastic reconfiguration (GFMCSR) [16, 17] is a systematic improvement of the FN dynamic that allows to sample the sign crossing the nodal surface of the guiding wavefunctions. The Green function $\bar{G}_{x',x}$ is connected to the FN one $\bar{G}^{eff}_{x',x}$ by a pre-factor $s_{x',x}$:

$$\bar{G}_{x',x} = s_{x',x}\bar{G}^{eff}_{x',x} \tag{3.26}$$

where the pre-factor $s_{x',x}$ is given by

$$s_{x',x} = \begin{cases} 1 & \text{if} \quad \bar{G}_{x',x} \geq 0 \\ -1/\gamma & \text{if} \quad \bar{G}_{x',x} < 0 \\ \frac{\Lambda - H_{x,x}}{\Lambda - H_{x,x} - (1+\gamma)\mathcal{V}_{sf}(x)} & \text{if} \quad x = x' \end{cases} \tag{3.27}$$

In the simulation both the dynamics are present at the same time. Similarly to what was done in eq. (3.3) one defines

$$b_x = \sum_{x'} \bar{G}^{eff}_{x',x} \tag{3.28}$$

and then develops a stochastic process with the following form:

1. Given the walker (w, x), change the weight by scaling it with b_x:

$$w \to b_x w \ .$$

2. Generate randomly a new configuration x' according to the stochastic matrix $p_{x',x}$.

3. Finally multiply the weight of the walker by $s_{x',x}$:

$$w' \to w s_{x',x} \ .$$

Without the latter step the Hamiltonian $\bar{H}^{eff}$ is sampled. The walker can be characterized by the triad (w, w^{eff}, x) where w^{eff} are the FN weights. If $P_q(w, w^{eff}, x)$ is the probability of having a walker with weight w, w^{eff} in a configuration x after q iterations, the propagated wavefunctions of the two dynamics will be represented by:

$$\psi_q(x) = \int dw^{eff} \int dw w P_q(w, w^{eff}, x) \tag{3.29}$$

$$\psi^{eff}_q(x) = \int dw^{eff} \int dw w^{eff} P_q(w, w^{eff}, x) \tag{3.30}$$

and it is straightforward to check that the evolution of the probability in the Markovian process is

$$P_q(w', w'^{eff}, x') = \sum_x \frac{p_{x',x}}{b_x^2 \, |s_{x',x}|} \, P_q(w, w^{eff}, x). \tag{3.31}$$

Given M walkers

$$(\underline{w},\underline{x}) \equiv \left\{(w_j, w_j^{eff}, x_j)\right\}_{j=1,2,\ldots,M} \tag{3.32}$$

the generalization of (3.29) to the many walkers case is given by:

$$\psi_q(x) = \int [d\underline{w}] \sum_{\underline{x}} \frac{\sum_j w_j \delta_{x,x_j}}{M} P_q(\underline{w},\underline{x}) \tag{3.33}$$

$$\psi_q^{eff}(x) = \int [d\underline{w}] \sum_{\underline{x}} \frac{\sum_j w_j^{eff} \delta_{x,x_j}}{M} P_q(\underline{w},\underline{x}) \tag{3.34}$$

and the symbol $\int [d\underline{w}]$ is a shorthand for the $2M$ dimensional integral.

The two equations (3.33) show that the states $\psi_q^{eff}(x)$ and $\psi_q(x)$ are not uniquely determined by the distribution probability $P_q(\underline{w},\underline{x})$ but, as was done in the case where no sign problem occurs (3.1.2) [60], it is possible to change the probability distribution without losing information of the quantum mechanical state. It suffices to define a new probability through a linear transformation

$$P'_q(\underline{w}',\underline{x}') = \int [d\underline{w}] \sum_{\underline{x}} K(\underline{w}',\underline{x}';\underline{w},\underline{x}) P_q(\underline{w},\underline{x}) \tag{3.35}$$

where now the kernel of the integral equation is defined as

$$K(\underline{w}',\underline{x}';\underline{w},\underline{x}) = \prod_{i=1}^{M} \left(\frac{\sum_j |g_{x_j}| \delta_{x_i',x_j}}{\sum_j |g_{x_j}|} \right) \delta(w_i' - \beta^{-1} \frac{\sum_j w_j}{M} \mathrm{sgn}\, g_{x_i'})\, \delta(w_i^{eff\,\prime} - |w_i'|) \tag{3.36}$$

and $\beta = \frac{\sum_j g_{x_j}}{\sum_j |g_{x_j}|}$ is the average sign after the reconfiguration.

In Eq. (3.36) the only thing which is left to define are the g_{x_j}. If no sign problem occurs it is easy to see that the choice $g_{x_j} = w_j = w_j^{eff}$ leads directly to the results of section (3.1.2). If the simulation suffers for the sign problem instability the latter choice is unfeasible and better choices are necessary for the g_{x_j}.

If the quantum state of the system is conserved before and after the reconfiguration the following relation must hold, namely

$$\psi'_q(x) = \psi_q(x) \tag{3.37}$$

In practice this relation cannot be satisfied with a simple choice of g_{x_j}. Then a less strict constraint is required. Let $\left\{O^k\right\}_{k=1,2,..,p}$ be a number of suitably chosen observables and impose the following constraint,

$$\sum_x \psi_q(x) = \sum_x \psi'_q(x) \tag{3.38}$$

$$\sum_{x,x'} O^k_{x',x}\psi_q(x) = \sum_{x,x'} O^k_{x',x}\psi'_q(x) \tag{3.39}$$

It is possible to prove [16, 17] that in order to fulfill the conditions (3.38) it is *sufficient* that the following holds:

$$\frac{\sum_{j,x'} g_{x_j} O_{x',x_j}}{\sum_j g_{x_j}} = \frac{\sum_{j,x'} w_j O_{x',x_j}}{\sum_j w_j} \tag{3.40}$$

meaning that the the mixed average of the chosen observables are conserved in the reconfiguration process. A possible choice for the g_{x_j} is

$$g_{x_j} = w_j^{eff}\left[1 + \sum_k \alpha_k \left(O^k_{x_j} - \bar{O}^{k,eff}_j\right)\right] \tag{3.41}$$

where $O^k_{x_j} = \frac{\langle\psi_G|O^k|x_k\rangle}{\langle\psi_g|x_j\rangle}$ and $\bar{O}^{k,eff} = \frac{\sum_j w_j^{eff} O^k_j}{\sum_j w_j^{eff}}$. The coefficients α_k are to be obtained requiring that Eq. (3.38) hold. This requirement involves the solution of the following linear system for α_k [17]:

$$\sum_{k'} \alpha_k \left[\frac{\sum_j w_j^{eff}\left(O^k_{x_j} - \bar{O}^{k,eff}\right)\left(O^{k'}_{x_j} - \bar{O}^{k',eff}\right)}{\sum_j w_j^{eff}}\right] = \frac{\sum_j w_j (O^k_{x_j} - \bar{O}^{k,eff})}{\sum_j w_j} \tag{3.42}$$

Once the α_k coefficients are completely determined then the new weights after the reconfigurations are determined by Eq. (3.35,3.36),

$$w'_j = \beta^{-1}\frac{\sum_j w_j}{M}\mathrm{sign} g_{x_j} \tag{3.43}$$

3.1.7 Forward walking

The Green function Monte Carlo method can be used with success to compute also correlation functions on the ground state of H. In fact it is simple to compute

expectation values of operators that are diagonal in the chosen basis, so that to a given element x of the basis corresponds a well defined value $O(x) = \langle x|O|x\rangle$ of the operator. By the Green Function Monte Carlo technique, as we have seen, configurations w, x are distributed according to the desired wavefunction $\psi_0(x)$, or $\psi_0(x)\psi_G(x)$ if importance sampling is implemented. However in order to compute $< O >= \langle\psi_0|O|\psi_0\rangle$ a little further work is necessary as the square of the wavefunction is required to perform the quantum average. To this purpose the desired expectation value is written in the following form:

$$\langle O\rangle = \lim_{N',N\to\infty} \frac{\langle\psi_G|G^N O G^{N'}|\psi_G\rangle}{\langle\psi_G|G^{(N'+N)}|\psi_G\rangle} \tag{3.44}$$

From the statistical point of view Eq.(3.44) amounts first to sample a configuration x after N' reconfigurations , then to measure the quantity $\langle x|O|x\rangle$ and finally to let the walker propagate forward for further N reconfigurations.

If all the weights of the walkers are positive definite (or in the framework of the fixed node technique) in order to evaluate the stochastic average an approach similar to what was done for the energy is clearly possible. The only change to expression (3.8) is to replace E_{x_j} with the average measured quantity $O_{\underline{x}_N} = \frac{1}{M}\sum_j O_j^n$ at the generation n and change the corresponding weight factors in (3.9) as:

$$G_n^L = \prod_{j=-N}^{L-1} \bar{w}n - j \tag{3.45}$$

where we denote with O_j^n the value of the diagonal operator O on the configuration x_j of the j^{th} walker, at the iteration n. Indeed these new factors (3.45) contain a further propagation of N reconfiguration processes as compared to the previous expression Eq. (3.9). It is important that both L, correcting the bias, and N, correcting the quantum average of the operator are finite, due to the exponential growths of the fluctuations as N and L increase. On the other hand, these fluctuations can be controlled by enlarging the population size M, and the method for M large enough remains stable. A further condition is however necessary in order to control the bias in the forward walking technique. The set of measured values O_i^n with weight factors (3.45) has to be modified after each reconfiguration process occurring in the forward direction. In practice after each reconfiguration it is important to bookkeep only the values O_i of the observables that survive after

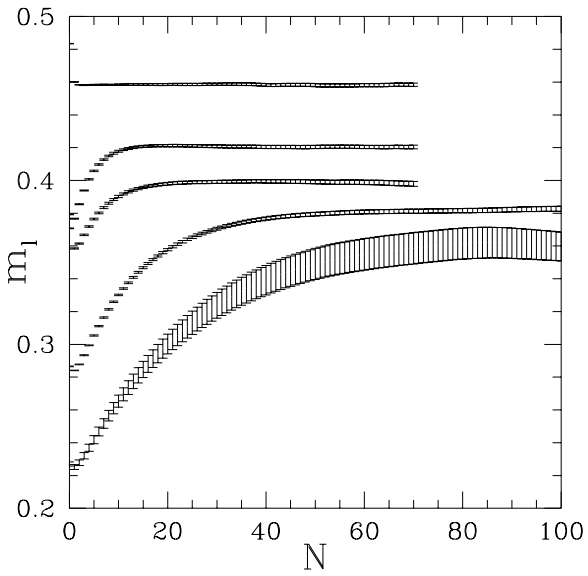

Figure 3.3: Staggered magnetization m_l for the $2D$, $S = 1/2$ Heisenberg model [60] for increasing lattice sizes (from top curve to bottom curve) as a function of the forward walking iteration number N computed with the forward walking technique. The number of walkers for each lattice size and is $M = 1000$, 2000, 3000, 3000, 3000 and $L = 36$, 64, 100, 144, 256 respectively.

the reconfiguration (we omit in the following the superscript n for simplicity). In other words after each reconfiguration $O'_i = O_{j(i)}$ for $i = 1, \cdots M$ with the integer function $j(i)$ describing the reconfiguration process in our scheme (after any reconfiguration the walker with index i assumes the configuration with index $j(i)$ before the reconfiguration, see Fig. 3.1).

In order to implement recursively the forward walking it is useful to store at each reconfiguration process the integer function $j_n(i)$ for each reconfiguration n and the values O_i of the operator O for each walker. Then it is possible to compute the relevant configurations contributing to the operator O after N reconfiguration process by a recursive application of the integer functions j_n, namely $O'_i = O_{j_N(j_{N-1} \cdots j_1(i) \cdots))}$. An example on how this scheme works is shown in Fig.(3.3). As it is seen it is simple to reach the exact ground state average.

In appendix (A.3) it is proved that the bias control property (3.16) is satisfied even in the framework of the forward walking technique.

3.1.8 Hellmann-Feynman theorem

The calculations of observables in the framework of the GFMC technique can also be done using the Hellmann - Feynman theorem. Consider the Hamiltonian H, having ground state energy E_0 and let be O the observable that has to be computed. If the following perturbation is added to the Hamiltonian

$$H(h) = H + hO \tag{3.46}$$

the first order correction to the energy can be computed as:

$$E(h) = E(0) + h\langle 0|O|0\rangle \tag{3.47}$$

where $|0\rangle$ is the unperturbed ground state. As a consequence it is possible to evaluate the expectation value $\langle O\rangle$ as

$$\langle O\rangle = \lim_{h\to 0} \frac{E(h) - E(0)}{h} \tag{3.48}$$

In practice it suffices to make several runs for several values of h (including $h = 0$),compute the difference in Eq. (3.48) and extrapolate to $h \to 0$.

If the matrix elements $\bar{O}_{x',x}$ are not all negative then the addition of such an operator to the Hamiltonian involves a change in the nodal surface of the guiding wavefunction which implies a break down of Eq. (3.48). For example in the framework of the FN approximation, this means that there will be an additional term in the sign-flip potential since it is possible that $\bar{O}_{x',x} > 0$. To overcome this difficulty it suffices to define the following operators

$$\begin{aligned} \bar{O}^{+}_{x',x} &= \begin{cases} \bar{O}_{x',x} & \text{if} \quad \bar{O}_{x',x} \leq 0 \\ 0 & \text{if} \quad \bar{O}_{x',x} > 0 \end{cases} \\ \bar{O}^{-}_{x',x} &= \begin{cases} -\bar{O}_{x',x} & \text{if} \quad \bar{O}_{x',x} > 0 \\ 0 & \text{if} \quad \bar{O}_{x',x} < 0 \end{cases} \end{aligned} \tag{3.49}$$

and compute the ground states eigenvalues $E^{+}(h)$,$E^{-}(h)$ of the perturbed Hamiltonian obtained adding $\bar{O}^{+}_{x',x}$ and $\bar{O}^{-}_{x',x}$ respectively. Then the expectation value of the operator can be written in terms of

$$\langle O\rangle = \lim_{h\to 0} \frac{E^{+}(h) - E^{-}(h)}{h} \tag{3.50}$$

3.2 Application to the $t-J$ model

3.2.1 Action of the Green Function

In this section we present the application of the numerical methods introduced in the preceding sections to a fermionic Hamiltonian, namely the two dimensional $t-J$ model (2.3). The basis set chosen in the simulation is the spin configuration of the lattice, $\{|x\rangle\} = \{|S_1^z, ..., S_L^z\rangle\}$, where S_i^z is the z component of the spin of the electron on site i and $S_i^z = 0$ in the case when on site i a hole is found (e.g. no electrons are present). Following equation (3.2) $G_{x,x'}$ must be computed which is, a part from a constant, equivalent to compute the action of the Hamiltonian on a general state of the basis set. For a better understanding of the processes involved in the application of H_{t-J} it is useful to rewrite the $t-J$ Hamiltonian (2.3) as:

$$H_{t-J} = K + V^{flip} + V^{diag}$$

where

$$V^{diag} = J \sum_{<i,j>} \left(S_i^z S_j^z - \frac{n_i n_j}{4} \right) \tag{3.51}$$

$$K = -t \sum_{<i,j>} K_{ij} = -t \sum_{<i,j>} (c_i^+ c_j + c_j^+ c_i) \tag{3.52}$$

$$V^{flip} = \frac{J}{2} \sum_{<i,j>} V_{ij}^{flip} = \frac{J}{2} \sum_{<i,j>} \left(S_i^+ S_j^- + S_i^- S_j^+ \right) \tag{3.53}$$

$$\tag{3.54}$$

are the diagonal part of the Hamiltonian, the kinetic energy term and the spin-flip interaction respectively and the constraint of no double occupancy is to be understood. Since V^{diag} is diagonal in the chosen basis set its action over a vector $|x\rangle$ does not change the spin configuration of the lattice. It is more interesting to understand what transitions between states $|x\rangle \rightarrow |x'\rangle$ are involved when the off-diagonal part of H_{t-J} is applied to a vector of the basis set. The kinetic energy term K_{ij} gives a non zero contribution to the energy only when acting on an empty j (i) site and on an occupied i (j) site causing the electron to hop from site i to site j (j to i) (see Fig. 3.4). Since energy is gained in making an hopping this term tend to delocalise the holes and to avoid a segregation of holes in one region.

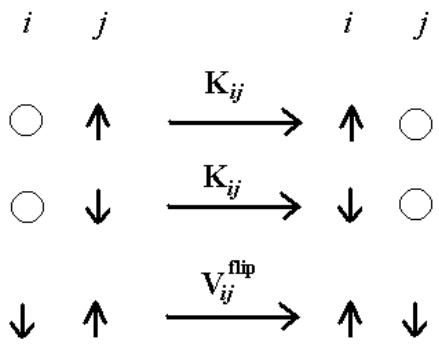

Figure 3.4: Action of the different off diagonal interactions in the Hamiltonian. K_{ij} hops the electron from an occupied site to an empty one, while V_{ij}^{flip} acts on two anti parallel neighboring spins flipping them. The moves obtained exchanging $i \rightleftarrows j$ are also allowed.

On the contrary the spin-flip potential V_{ij}^{flip} gives a non zero contribution only when acting on states in which both sites i and j are occupied but with different component of the two spins along the z axis. As is clear from Fig. (3.4) this potential exchanges two spins and generates a spin-flip. Due to the fact that the super-exchange coupling constant J is greater than zero (antiferromagnetic coupling between the spins) this term gains energy expelling the holes from an antiferromagnetic background and segregating them in one region (as can be also noticed considering the strong coupling limit, $J \gg t$, and comparing the energies of the variational state with holes far apart with that of holes segregated in one region).

The physics of the $t - J$ model Hamiltonian lies in the competition between these two terms, the hole repulsion of the kinetic energy and the spin attraction of the super-exchange interaction. This competition is crucial since the physical value of the ratio J/t is at intermediate coupling [45], ($J/t \approx 0.4$).

3.2.2 Importance Sampling

A fundamental ingredient in the GFMC is the choice of the guiding wavefunction $\psi_G(x)$ in order to perform importance sampling, as described in section (3.1.4). An ideal guiding wavefunction must satisfy some important requirements.

First of all it must be a good approximation of the ground state wavefunction $\psi_0(x)$. A variational calculation is always good starting point to detect how accurate this ansatz is.

It is then important that the same approximation that is made on small systems (where the result can be checked using exact diagonalization) can be safely exported to larger ones, without losing accuracy in the calculation. This means that the guiding wave function must satisfy the **"size consistency"** condition. Suppose that if A and B are two weakly interacting subsystems of the larger $A+B$ system then:

$$\psi_G(A+B) \approx \psi_G(A)\psi_G(B) \tag{3.55}$$

namely as the interaction between A and B becomes negligible, the wavefunction of the larger system must factorize in the product of the wavefunctions of the two subsystems. If this property is satisfied then the Energy (and any observable not involving long range correlations) of the large system is additive respect to the energies of the subsystems and if a reliable estimate of this quantity is available for A or B the same accuracy is preserved in $A+B$.

Finally an ideal guiding wavefunction should also be easily computable, not involving more then order L^3 operation to detect the value of ψ_G over the configuration x from scratch and not more than L^2 to update its value in the transition from $|x\rangle \to |x'\rangle$ for a local move like the ones displayed in fig. (3.4).

In this thesis a Bardeen, Cooper and Schriffer (BCS) wavefunction (see appendix B) has been used [21] by adding a density-density Jastrow factor [73], namely:

$$|\psi_G\rangle = \mathcal{P}_N \mathcal{P}_G \exp\left\{\sum_{i,j} v(i-j) n_i n_j\right\} \exp\left\{\sum_k w_k c^+_{k\uparrow} c^+_{-k\downarrow}\right\} |0\rangle \tag{3.56}$$

where $\mathcal{P}_G$ and $\mathcal{P}_N$ are the Gutzwiller projector (which forbids double occupancy on each site) and the projector at fixed number of particles N respectively.

The long range potential of the Jastrow factor $v(i-j)$ behaves as $1/|i-j|$ as $|i-j| \to \infty$ [73] and is translational invariant:

$$v(R) = \frac{2}{L}\sum_{q\neq 0} e^{iqR}\left[1 - \sqrt{\frac{1+(\cos q_x + \cos q_y)/2}{1-(\cos q_x + \cos q_y)/2}}\right] \tag{3.57}$$

Concerning the BCS part of the guiding wavefunction, the Fourier transform of the pairing function w_k, can be obtained from the mean field theory applied to the BCS Hamiltonian allowing for a superconducting order parameter Δ_k as is shown in appendix (B). Its form is given by the following equation:

$$w_k = \frac{\Delta_k}{\epsilon_k + \sqrt{\epsilon_k^2 + \Delta_k^2}} \tag{3.58}$$

and $\epsilon_k = -2t(\cos(k_x) + \cos(k_y)) - \mu$, being μ the chemical potential, which is a variational parameter in the wavefunction.

In order to perform importance sampling it is important to compute the value of the guiding wavefunction over a configuration of the basis set, $\psi_G(x) = \langle x|\psi_G\rangle$. Here we consider the action of the BCS part over a configuration.

$$\langle x|BCS\rangle = \langle 0|c_{R_1\downarrow}\dots c_{R_N\downarrow}c_{R'_1\uparrow}\dots c_{R'_N\uparrow}\exp\{\sum_{lm} w_{R'_l,R_m}c^+_{R'_l\uparrow}c^+_{R_m\downarrow}\}|0\rangle \tag{3.59}$$

where a Fourier transform has been performed in the BCS wavefunction and N is half the number of the electrons. The $\{R_1 \dots R_N\}$ coordinates refer to the positions of the spin down electrons while $\{R'_1 \dots R'_N\}$ to the positions of the spin up electrons. Consider the following operators equalities:

$$\begin{aligned}
\exp\left\{-\sum_{lm} w_{R'_l,R_m}c^+_{R'_l\uparrow}c^+_{R_m\downarrow}\right\} c_{R'_i\uparrow} \exp\left\{\sum_{lm} w_{R'_l,R_m}c^+_{R'_l\uparrow}c^+_{R_m\downarrow}\right\} = \\
= c_{R'_i\uparrow} + \sum_m w_{R'_i,R_m}c^+_{R_m\downarrow} \\
\exp\left\{-\sum_{lm} w_{R'_l,R_m}c^+_{R'_l\uparrow}c^+_{R_m\downarrow}\right\} c_{R_i\downarrow} \exp\left\{\sum_{lm} w_{R'_l,R_m}c^+_{R'_l\uparrow}c^+_{R_m\downarrow}\right\} = \\
= c_{R_i\downarrow} - \sum_l w_{R'_l,R_i}c^+_{R'_l\uparrow}
\end{aligned} \tag{3.60}$$

Inserting between every two destruction operators the product of the exponential of the BCS wavefunction and its inverse and computing the commutators one obtains:

$$\langle x|BCS\rangle = \langle 0|\prod_{i=1}^{N}[c_{R_i\downarrow} - \sum_j w_{R'_j,R_i}c^+_{R'_j\uparrow}]\prod_{i=1}^{N}[c_{R'_i\uparrow} + \sum_j w_{R'_i,R_j}c^+_{R_j\downarrow}]|0\rangle \quad (3.61)$$

Then left carrying the creation operators in the first of the two products and right carrying the destruction operators in the second:

$$\langle x|BCS\rangle = \sum_{\underline{R}_1\dots\underline{R}_N} w_{R'_1,\underline{R}_1}\dots w_{R'_N,\underline{R}_N}\langle 0|c_{R_1\downarrow}\dots c_{R_N\downarrow}c^+_{\underline{R}_1\downarrow}\dots c^+_{\underline{R}_N\downarrow}|0\rangle \quad (3.62)$$

where $\{\underline{R}_1\dots\underline{R}_N\}$ is a set of dummy indices of spin down sites involved in the summations. Then it follows that [74]:

$$\langle x|\psi_G\rangle = \det W(R_i^\uparrow, R_j^\downarrow) \quad (3.63)$$

and $W(R_i^\sigma, R_j^{\sigma'})$ is an $N\times N$ matrix whose elements are the same of the $(L\times L)$ w matrix, the row being determined by position of the i^{th} σ electron and the column by the position of the j^{th} σ' electron, e.g. $W(R_i^\uparrow, R_j^\downarrow) = w_{R_i,R_j}$.

The computation of the value of the BCS wavefunction over a configuration involves a determinant, an operation demanding L^3 operations, which is by far too expensive. The solution to this problem can be found noticing that it is not necessary to compute this determinant from scratch for any matrix element $G_{x',x}$ (thus would involve $N^3\times L$ operation as there are $\sim L$ non zero matrix elements in $G_{x',x}$ for a given x)), but it suffices to know how it changes under the two process of (3.53,3.52). In this way it is possible to update the value of the determinant in only order N^2 operations.

The hopping of an up spin electron from site R_k to an empty site R_l produces the following changes in $\psi_G(x)\to\psi_G(x')$:

$$\langle x'|\psi_G\rangle = \langle x|c^+_{R_k\uparrow}c_{R_l\uparrow}|\psi_G\rangle \quad (3.64)$$

Carrying out the calculation in a similar way as was done before, it is straightforward to obtain that, a part from an overall minus sign, which can be neglected choosing a proper ordering for the sites,

$$\psi_G(x') = \det W'(R_i^\uparrow, R_j^\downarrow) \quad (3.65)$$

and the array $W'(R_i^{\uparrow}, R_j^{\downarrow})$ differs from $W(R_i^{\uparrow}, R_j^{\downarrow})$ by properly modifying only one row, namely

$$W'(R_i^{\uparrow}, R_j^{\downarrow}) = W(R_i^{\uparrow}, R_j^{\downarrow}) + \delta_{ik}[W(R_l^{\uparrow}, R_j^{\downarrow}) - W(R_k^{\uparrow}, R_j^{\downarrow})] \tag{3.66}$$

This determinant update is a well known rank 1 operation in linear algebra, it suffices to define a vector v_q,

$$v_q = W(R_l^{\uparrow}, R_q^{\downarrow}) - W(R_k^{\uparrow}, R_q^{\downarrow}) \tag{3.67}$$

so that

$$\det W'(R_i^{\uparrow}, R_j^{\downarrow}) = \det W(R_i^{\uparrow}, R_j^{\downarrow}) \left[1 + \sum_q W^{-1}(R_q^{\uparrow}, R_k^{\downarrow}) v_q\right] \tag{3.68}$$

In practice this means that it is necessary to store not only the matrix w but even the inverse one. Obviously the inverse matrix need to be updated after a hopping too,

$$W'^{-1}(R_i^{\uparrow}, R_j^{\downarrow}) = W^{-1}(R_i^{\uparrow}, R_j^{\downarrow}) + g W^{-1}(R_i^{\uparrow}, R_k^{\downarrow}) \sum_q W^{-1}(R_q^{\uparrow}, R_j^{\downarrow}) v_q \tag{3.69}$$

where

$$g = -\frac{1}{1 + \sum_q W^{-1}(R_q^{\uparrow}, R_k^{\downarrow}) v_q} \tag{3.70}$$

This rank 1 operation on the W matrix and its inverse is an operation of order N^2 since it involves a matrix-vector product. As was stressed before the calculation of a determinant from scratch involves order N^3 operations, so this updating represents a speed up in term of computation, at the price of memory, since it is necessary to bookkeep also the inverse matrix W^{-1}.

A similar optimization can be done for the spin-flip case. As an example consider the following spin flip:

$$|R_k \uparrow; R_l \downarrow\rangle \longmapsto |R_k \downarrow; R_l \uparrow\rangle \tag{3.71}$$

This process involves the calculation of

$$\langle x | c^+_{R_k\downarrow} c_{R_k\uparrow} c^+_{R_l\uparrow} c_{R_l\downarrow} | \psi_G \rangle \tag{3.72}$$

which leads to the determinant $\psi_G(x) = \det W'(R_i^{\uparrow}, R_j^{\downarrow})$ where the new matrix W' differ from the old one by the changing of one row and one column,namely:

$$\begin{aligned} W'(R_i^{\uparrow}, R_j^{\downarrow}) &= W(R_i^{\uparrow}, R_j^{\downarrow}) + \\ &+ \delta_{ik}(1-\delta_{jl})[W(R_l^{\downarrow}, R_j^{\uparrow}) - W(R_k^{\uparrow}, R_j^{\downarrow})] + \\ &+ \delta_{jl}(1-\delta_{jk})[W(R_i^{\uparrow}, R_k^{\uparrow}) - W(R_i^{\uparrow}, R_l^{\downarrow})] + \\ &+ \delta_{ik}\delta_{jl}[W(R_l^{\uparrow}, R_k^{\downarrow}) - W(R_k^{\uparrow}, R_l^{\downarrow})] \end{aligned} \tag{3.73}$$

This operation involves a rank 2 updating, as can be seen introducing:

$$b_i^k = b(R_i^{\uparrow}, R_k) = W(R_i^{\uparrow}, R_k) \tag{3.74}$$

$$u_i = (1-\delta_{ik})[b_i^k - W(R_i^{\uparrow}, R_l^{\downarrow})] \tag{3.75}$$

$$\begin{aligned} v_j &= (1-\delta_{jl})[W(R_l^{\downarrow}, R_j^{\uparrow}) - W(R_k^{\uparrow}, R_j^{\downarrow})] + \\ &+ \delta_{jl}[W(R_l^{\uparrow}, R_k^{\downarrow}) - w(R_k^{\uparrow}, R_l^{\downarrow})] \end{aligned} \tag{3.76}$$

where b_i^k is a $N \times L$ matrix having as columns the value of the BCS potential over the lattice respect to the position of the i^{th} up electron. Eq. (3.73) takes the form:

$$w'(R_i^{\uparrow}, R_j^{\downarrow}) = w(R_i^{\uparrow}, R_j^{\downarrow}) + \delta_{ik}v_j + \delta_{jl}u_i \tag{3.77}$$

and represents a change of one row and one column from the initial matrix. In this case it is not only necessary to bookkeep and update w and its inverse, but also the quantity $\bar{b}_i^k$ (where from now on the bar over vectors indicate the matrix vector product $\bar{u} = W^{-1} \cdot u$). Obviously even the hopping of an up electron has consequences on $\bar{b}_i^k$, but it's quite easy to see that it is a rank 1 update.

Even in the spin flip process it is possible to update the determinant $L \times N$ operations so that the whole algorithm remains of order $L \times N$.

The updating of the density-density Jastrow term can be performed in a very efficient way noting that it only changes under an hopping process. So considering the hopping of an electron from site k to site l, the local electrons density becomes

$$n_i \longmapsto n_i + \delta_{il} - \delta_{ik} \tag{3.78}$$

and as a consequence the Jastrow term changes as:

$$\exp\{\sum_{ij} v(i,j)n_i n_j\} \longmapsto \exp\{\sum_{ij} v(i,j)n_i n_j\} \cdot$$

$$\cdot \quad \exp\{ \quad 2\sum_i (v(i,l) - v(i,k))n_i + 2v(1,1) - 2v(l,k)\} \tag{3.79}$$

where translational invariance and symmetry of the potential have been used. This update only involves order L operations which is by far negligible as compared to the $L \times N$ scaling of the algorithm. In practice it suffices to store a vector (for each walker) of size L holding the following product ($i = 1, \ldots, L$):

$$v(i) = \exp\{2\sum_l v(l,i)n_l\} \tag{3.80}$$

and to update the vector for any local move (hopping) involving a change in the on site occupation number. The quantity $\exp\{2v(1,1) - 2v(l,k)\}$ does not depend on the single walker and can be stored in a simple $L \times L$ matrix.

Chapter 4

Results on the 2D t-J model

4.1 Phase Separation

Consider a physical system at zero temperature composed by two components, A and B, having density of particle ρ_A and ρ_B and total energies $\mathcal{E}_A$ and $\mathcal{E}_B$ respectively. If the Hamiltonian of the system can be written as

$$H = H_A + H_B + V_{SR} \tag{4.1}$$

where H_A (H_B) is the Hamiltonian of the A (B) subsystem and V_{SR} is a short range interaction between the two subsystems, then the choice of a variational wavefunction which is the product of the two non-interacting ground states of A and B leads directly to

$$\mathcal{E}_{A+B} \leq \mathcal{E}_A + \mathcal{E}_B + \mathcal{E}_{SR} \tag{4.2}$$

where $\mathcal{E}$ is the total energy of the system ($A+B$) and $\mathcal{E}_{SR}$ is the expectation value of V_{SR} over the chosen variational state. For short range models (such as the $t-J$ model considered in this thesis) $\mathcal{E}_{SR}$ is proportional to the surface interface $\mathcal{S}$ between the two subsystems and is negligible in the thermodynamic limit, since $\mathcal{E}_A$ and $\mathcal{E}_B$ are proportional to their respective volumes, L_A and L_B. On the contrary, if the lattice sizes considered are very small, the surface can be a significant portion of the volume and the term $\mathcal{E}_{SR}$ is far from being negligible. The density ρ of the large system ($A+B$) can be expressed as:

$$\rho = p\rho_A + (1-p)\rho_B \tag{4.3}$$

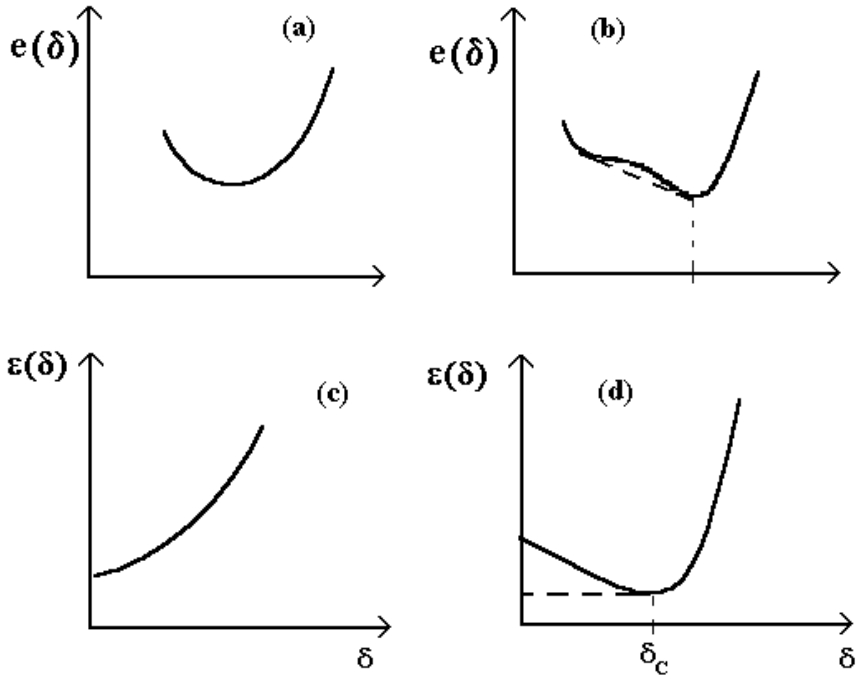

Figure 4.1: Energy per site landscape versus doping for a stable system (a) and for a phase separated one (b). Energy per hole versus doping for (c) a stable and (d) an unstable system. The dashed line in (b) and (d) is the Maxwell construction

where $p = L_A/L$, being L the total volume. Therefore the energy per site $E(\rho)$ at a given density (4.2), takes the form

$$E(\rho) \leq pE(\rho_A) + (1-p)E(\rho_B) \tag{4.4}$$

and the total volume is assumed to be large enough so that $\mathcal{E}_{SR}$ can be neglected. If the system phase separates, for all density $\rho_a < \rho < \rho_b$ the Maxwell state is exact and the equality equation (4.4) holds in the thermodynamic limit, namely

$$E(\rho_A) = \frac{E(\rho) - E(\rho_B)(1-p)}{p} \tag{4.5}$$

In the application considered the system is always composed by electrons and holes. The number of holes per volume is the doping fraction δ. Emery et al. [10] pointed out that the occurrence of phase separation is better understood in terms

of the energy per hole,

$$e_h(\delta) = \frac{E(\delta) - E_0}{\delta} \tag{4.6}$$

where $E(\delta)$ is energy per site at a given doping fraction and $E_0 = E(\delta = 0)$. The stability condition in terms of the energy per hole can be written as:

$$\frac{\partial e_h(\delta)}{\partial \delta} > 0 \tag{4.7}$$

If the system becomes unstable a minimum in the energy per hole occurs on finite size and in the infinite volume limit the system follows the Maxwell construction which is the dashed line in fig. 4.1(d).

The Maxwell construction in an unstable system is satisfied *only in the thermodynamic limit* . Since on finite size $\mathcal{E}_{\mathcal{SR}}$ is not always negligible, an exact calculation displays a minimum and fails to recover the Maxwell construction (see fig. 4.1). The position of this minimum may be weakly size dependent. In the case of the two dimensional $t - J$ model, we notice that when phase separation really occurs, large sizes are required to recover the Maxwell construction ($E_{SR} \sim 1/\mathcal{S}$ implying that the energy per site converges as $E(\delta) \sim 1/L$).

4.1.1 Strong Coupling limit

To gain insight on the coexistence of holes and spin in the $2D$ $t - J$ model it is instructive to study the strong coupling limit of the theory, namely $J/t >> 1$.

If the kinetic term can be neglected then one can evaluate the energy of the variational state having two holes far apart in a classical AF background (see Fig. 4.2). The energy loss respect to the energy of the uniform AF background is given by the number of broken AF bonds times the energy per bond (B) times J, namely $\Delta E = 8BJ$. The situation is quite different if the holes tend to form a pair, since they only break 7 AF bonds ($\Delta E = 7BJ$). This variational calculation suggests that for large J the state with all the holes segregated in one region is much more favorite as compared to the uniform solution.

The energy necessary to extract an electron from an AF background is $2BJ$. When the kinetic energy joins the game it can cause the electrons to hop, leading to a gain in energy which is $4t$. Then if $J/t > 2/B$ it is not favorable to extract

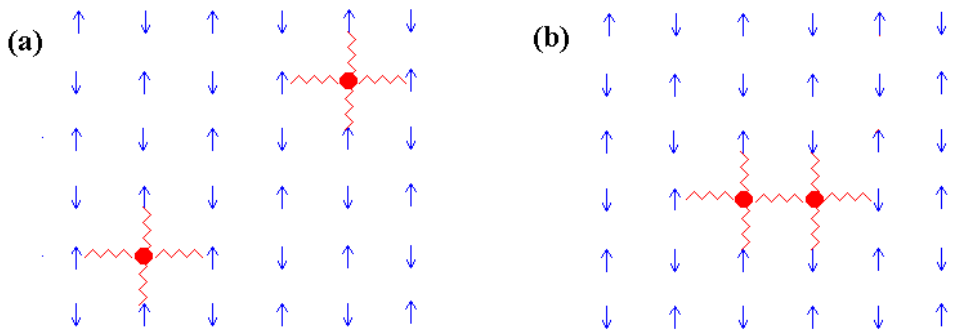

Figure 4.2: At strong coupling $(J >> t)$ the energy loss from the antiferromagnetic background is given by the number of broken bonds. If the holes are far apart (a) the energy loss is $8BJ$ while if they form a cluster (b) it is $7BJ$.

an electron from the AF background. As a consequence the fully phase separated state is unstable to the transfer of single electrons when $J/t < 3.42$ (according to the estimate of the ground state energy given in [60]). Hellberg and Manousakis [75] considered the low electrons density limit of the model and showed that two electrons form a bound state for $2 < J/t < 3.4367$. The binding of two electrons is not enough for the occurrence of phase separation, since a gas of free pairs is not a phase separated state.

The interesting region for the high T_c compounds is at intermediate coupling ($J/t \sim 0.4$) and low doping ($0 < \delta \lesssim 0.3$) and in order to clarify the phase separation problem it is necessary to revert to some numerical approximation.

4.1.2 Weak coupling limit

Emery et al. [10] suggested that phase separation could occur at all strength in the $2d$ $t-J$ model. Their claim was supported by exact diagonalizations on small clusters (Fig. 4.7) and by a variational calculation in the weak coupling limit ($J/t << 1$). Starting from the assumption that for $J \to 0$ the N_h holes behave as spinless fermion with the dispersion,

$$\epsilon_k = -2t(\cos(k_x) + \cos(k_y)) \approx -4t + tk^2$$

the energy per site can be computed as:

$$\begin{aligned} E(\delta) &= -4t\delta + \frac{t}{2\pi}\int_0^{k_F} dk\, k^3 \\ &= -4t\delta + 2\pi t\delta^2 \end{aligned} \tag{4.8}$$

where $k_F = \sqrt{4\pi\delta}$ is the Fermi momentum. The energy per hole is obtained subtracting the energy per site from the energy of the uniform background and then dividing by the doping fraction, namely from the contribute of the uniform AF background

$$e_h(\delta) = \frac{2BJ}{\delta} - 4t + 2\pi t\delta \tag{4.9}$$

From this approach it follows that, even at weak coupling, the energy per hole has a minimum and phase separation occurs at the critical doping $\delta_c = \sqrt{BJ/\pi t}$.

This variational estimate (4.8) for the energy recovers the Nagaoka [76] energy for the single hole case. This argument is only variational and needs to be checked by numerical calculations since a not enough accurate wavefunction could overestimate the tendency of the system towards phase separation.

4.1.3 Quantum Monte Carlo calculations of $e_h(\delta)$

The calculation of the energy per hole as a function of the doping fraction has been performed with the numerical methods explained in chapter (3). A common feature of these methods is that they rely on a guess of the ground state properties of the system by the choice of the guiding wave function. At finite doping a pure d-wave BCS guiding wave function has been used [21, 65] with in addiction a long range density-density Jastrow factor [73], as was shown in section (3.2.2). At half filling the guiding function described in [60] allows to obtain the exact answer for e_0, as there is no sign problem at zero doping for this particular guiding function. In what follows the energy per hole is computed inserting the exact e_0 at the given size L for all VMC, FN and GFMCSR calculations. Several authors [62, 61] used the infinite volume limit for e_0 even for the finite L evaluation of $e_h(\delta)$. On the contrary the exact e_0 for each lattice size has been used in this thesis and it has been checked that for the largest size calculations both choices of e_0 lead to the

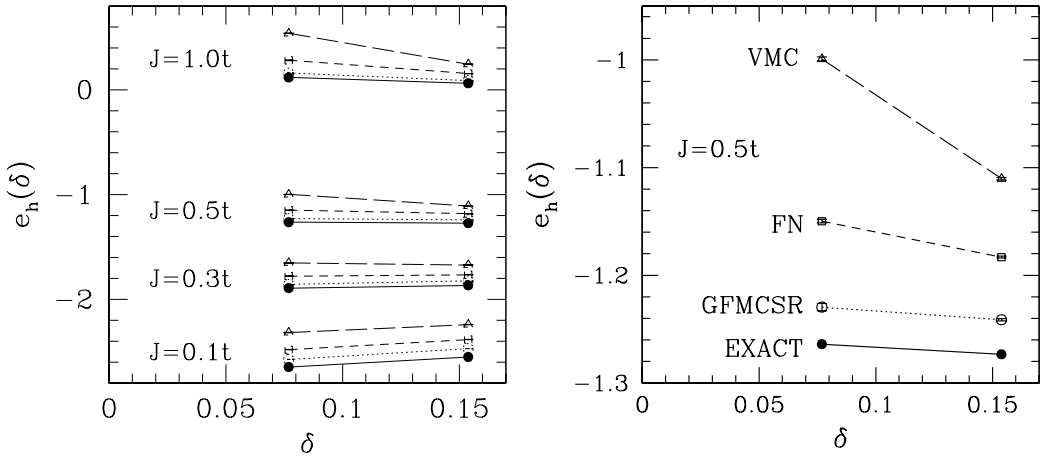

Figure 4.3: Left:$e_h(\delta)$ computed with VMC (long dashed line), FN (short dashed line),GFMCSR (dotted line) compared with the exact results [64, 77] (continuous lines) for a 26 lattice size. Error bars are much smaller than the size of the symbols. Lines (guides to the eye) connect the two and four hole results. Right: Energy per hole for $J = 0.5t$,$L = 26$,2 and 4 holes.

same $e_h(\delta)$. Indeed the small lattice size results are very sensitive at low doping to the particular choice of e_0 and this may explain the contradictory results presented in the literature so far.

In Fig. (4.3) the Monte Carlo calculations are compared with the exact Lanczos results for the largest size ($L = 26$) available in literature[64, 77]. As can be seen the VMC calculations over estimate the tendency toward phase separation of the system. The slope of the energy per hole as a function of δ obtained with this approach is very different from the exact one meaning that the accuracy of a variational calculation is not enough to solve the problem. This difference is particularly relevant at $J = 0.5t$ close to the physical region (see Fig. 4.3), where both the VMC and the FN fails in reproducing the correct slope for the energy per hole while the GFMCSR succeeds in obtaining the right one.

The FN approximation improves the ground state energy of the best starting variational (and guiding) wavefunction by a factor of three (Fig. 4.3) and the GFMCSR by another similar factor, yielding finally an accuracy of less than 100K on the energy per hole, which is physically acceptable if compared with the low

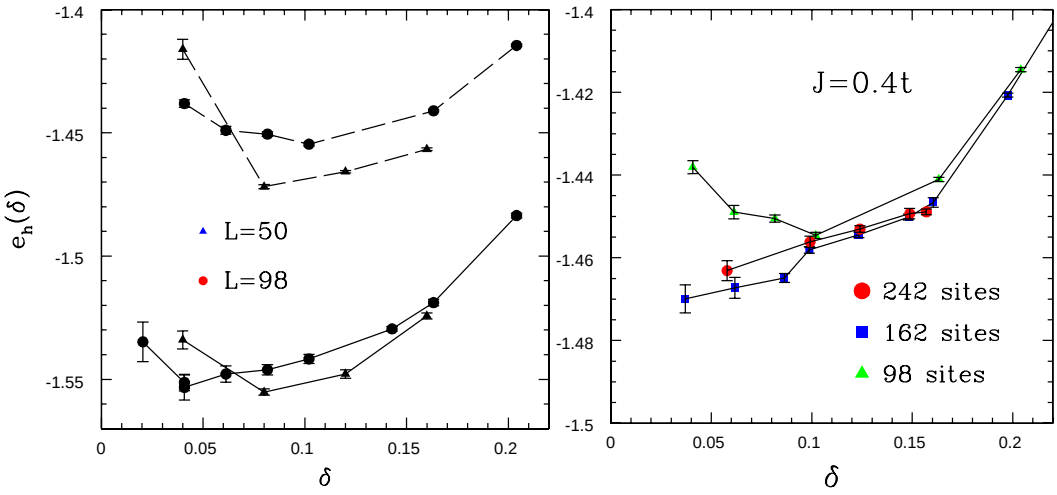

Figure 4.4: Left: $e_h(\delta)$ computed with FN (dashed lines) and with GFMCSR (continuous lines) for $L = 50$ (triangles) and $L = 98$ (circles) at $J = 0.4t$. Right:$e_h(\delta)$ computed with FN for several lattice sizes.

energy coupling of the model $J \sim 1500K$. As shown in Fig. (4.3) this kind of accuracy depends weakly on the number of holes and on the strength of the coupling constant. However, for small lattices, the main difficulty to detect phase separation is the resolution in doping. By increasing the system size (see Fig.4.4), the difference between the FN calculation and the GFMCSR one remains of the same order, and much below the VMC energies. Thus the accuracy of the calculation is not very much size dependent, even for large systems where no exact solution is available. All the approximations employed are indeed "size consistent" (see section 3.2.2) and it is reasonable to expect that the same accuracy obtained on small systems can be also achieved on larger ones.

By improving the approximation from FN to GFMCSR, the minimum in the hole energy disappears for the largest size in Fig. (4.4). Moreover the slope in the energy per hole obtained for the 242 system size with the FN is very close to the largest system size GFMCSR calculation, meaning that, at this coupling strength, the energy per hole is probably converged to the thermodynamic limit. This suggests that the occurrence of phase separation at $J/t = 0.4$ and $L = 98$ is an artifact of the FN approximation that acts mainly on the kinetic energy term thus implying a tendency to localize the holes. Nonetheless, as shown in Fig. 4.4,

even within the FN framework it is possible to obtain the stability of the uniform phase in the thermodynamic limit at $J/t = 0.4$. Phase Separation at this J/t value is only *a finite size effect*.

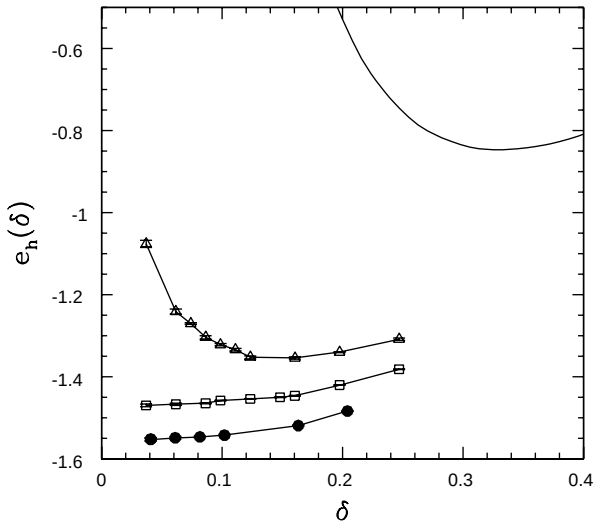

Figure 4.5: Energy per hole versus doping computed with spinless fermion variational approach (continuous line), VMC (triangles), FN (empty squares) and GFMCSR (full dots).

Since this calculation strongly disagrees with the variational prediction in [10], it is instructive to compare this ansatz with our calculations . As is shown in fig. (4.5), where the largest size calculations (supposed to be representative of the thermodynamic limit) with all the methods are displayed, the variational approach in [10] gives a very poor estimate of the energy per hole. Even VMC is able to obtain an energy per hole that at low doping is more than a factor of 2 lower than the variational ansatz.

To clarify the role of the phase separation instability in the $t-J$ model and in the physics of the high T_c compounds, it is of great importance to determine if it occurs close to the physical region, as was suggested by several authors [10, 11]. It is then necessary to perform extensive calculation at different values of the coupling strength J/t to obtain the phase separation diagram of the model. The calculation at larger J/t were performed on $L = 50, 98$ using only GFMCSR, since it is the most reliable method for energy calculations on large lattice sizes

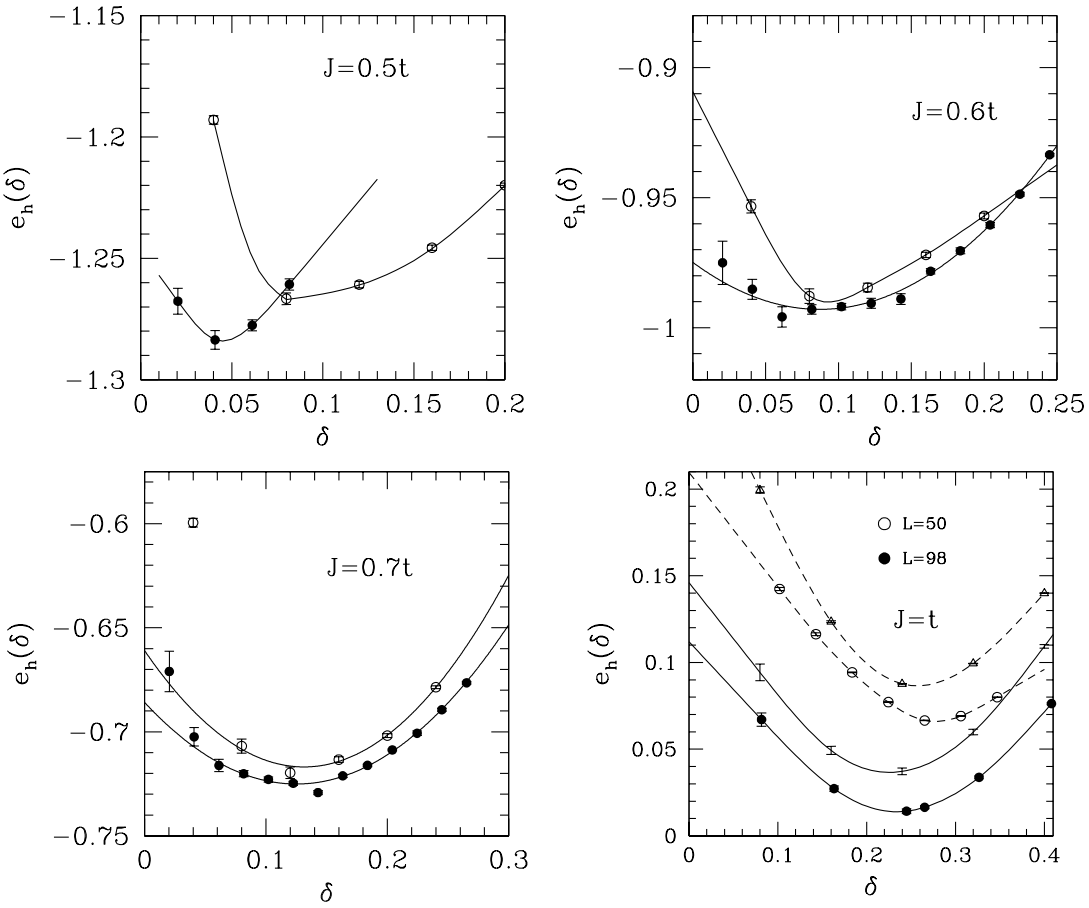

Figure 4.6: Energy per hole for $J = 0.5t, 0.6t, 0.7t, 1.0t$, $L = 50$(empty dots),$L = 98$ (full dots) computed with GFMCSR (continuous lines) and FN (dashed lines). Lines are guides to the eyes

(Fig. 4.6).

At $J = 0.5t$ and $L = 50$ the energy per hole shows a minimum at the doping corresponding to 4 holes. This would suggest that phase separation occurs at this doping fraction ($\delta = 0.08$) but as the calculation is extended to the larger size the minimum almost disappears and only 2 holes binds. It is safe to conclude that no phase separation occurs at this coupling strength.

The $J = 0.6t$ is a bit more controversial since in this case the 50 sites lattice calculation of the energy per hole displays a minimum which moves to lower doping as the system is enlarged (98 sites). Probably the $J = 0.6t$ is very close to the critical strength for the phase separation instability. In this case size effects are expected to be large so that even $L = 98$ might not be an enough large system size. From the data shown in fig. (4.6) the onset of phase separation has been found at $\delta_c = 0.08t$. Indeed clear evidence of phase separation occurs for $J = 0.7t$ and $J = t$ where both the lattice sizes considered display a very evident minimum whose position slightly moves to lower (higher) doping for $J = 0.7t$ ($J = t$).

As summarized in the phase separation diagram picture (Fig. 4.7) we find no evidence of PS for $J \leq 0.5t$, and a transition to the phase separated regime at a critical J_c very close to $0.5 - 0.6$. These results are in acceptable quantitative agreement with Ref. [62, 23, 22] but we believe that this calculation represents a much better attempt to control the finite size effects, which are very important, especially at small doping. Instead, in the large doping region, the best agreement is found with the exact diagonalization data[10] on small clusters.

On the contrary this results are in evident disagreement with the recently published calculation by Hellberg and Manousakis [61] which states that phase separation occurs at all strength in the 2D $t - J$ model. The main difference concerns the most important and delicate low doping region where the question is meaningful at $J = 0.4t$ which in [61] is studied only with fairly small lattice sizes. As was shown in several examples in this chapter the energy per hole in this region suffers from huge size effects and a small size calculation, even if very accurate, gives misleading results which are not at all representative of the thermodynamic limit.

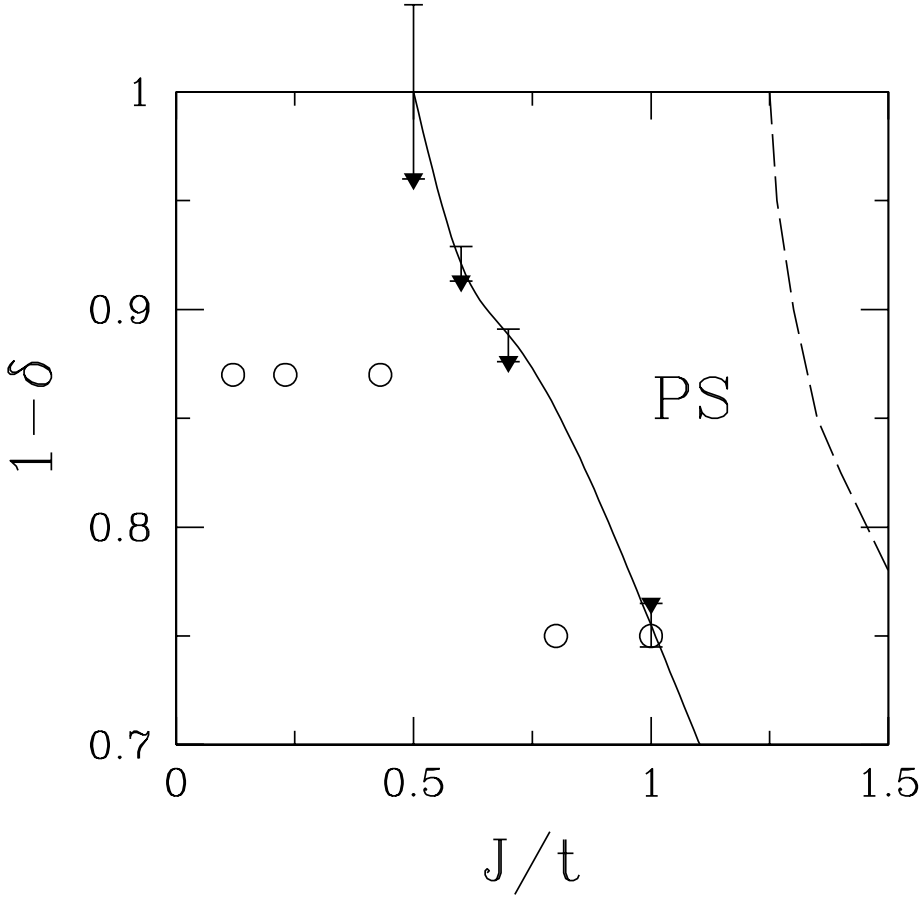

Figure 4.7: Phase separation diagram of the 2 dimensional $t-J$ model computed with FN (full dots) and GFMCSR (triangles). Empty dots are from [10], the dashed line from [20], triangles are GFMCSR calculation ($L = 98$) (this work).Errors are estimates of finite size effect and correspond to twice the difference between the 98 and 50 site critical doping [78]. Continuous line is a guide to the eye.

4.2 Hole-hole correlations

The behavior of the hole-hole correlation function $N(q)$ allows to gain information on the charge behavior in the $2D\ t-J$ model,

$$N(q) = \frac{1}{L}\sum_{i,j} e^{iq(R_i-R_j)}\,(1-n_i)(1-\,n_j) \tag{4.10}$$

where L is the number of lattice sites. A divergence at low momenta (close to the Γ point) of the hole-hole correlation function represents a more evident and reliable mark of the phase separation instability than the calculation of the energy per hole. Moreover if the ground state displays a charge density wave behavior (stripes [79]) it should be revealed by diverging peaks at incommensurate momenta. As a consequence an accurate calculation of the $N(q)$ provides a considerable insight on the ground state properties of the model.

In order to compute the ground state correlation functions $N(q)$ two different methods have been used: the "forward walking technique" (FW) [60] (3.1.7) which allows the direct evaluation of the ground state expectation value, at the expense of very large error bars when the convergence to the ground state is particularly slow, as shown in [60]; the second technique is based on Hellmann-Feynman theorem (3.1.8), and amounts to compute the ground state energy $E(h)$ of the Hamiltonian in presence of a small perturbation $H_{t-J} \rightarrow H_{t-J} - hN(q)$. By Hellman-Feynman theorem the first derivative, estimated numerically by a few runs for different h's, gives ($N(q) = \frac{d}{dh}E(h)\ |_{h=0}$). The latter technique is much more stable, especially for large size, but each q value requires several simulations, whereas a single one is sufficient for the FW technique for all q's. Thus we have used the more expensive method for the small q values where the FW convergence is more difficult, and we have checked the consistency of both methods in the remaining momentum region.

For the 26 site cluster the FN results for $N(q)$ are accurate within 3%, as compared with the exact diagonalization data in tab. (4.1). In Fig.(4.8,4.9) the $N(q)$ is plotted for several doping, lattice sizes and coupling strength. Well inside the phase separated region, at $J = t$ (Fig. 4.8), $N(q)$ shows a divergent peak at small q close to the Γ point, as can be expected when phase separation occurs. No features at incommensurate momenta are present and the hole-hole correlations

$(q_x, q_y)\frac{2\pi}{26}$	Fixed Node	Fixed Node + Lanczos Step	Exact[64, 77]
$(5, 1)$	0.1295(5)	0.1264(3)	0.1253
$(4, 6)$	0.1436(3)	0.1418(3)	0.1393
$(3, 11)$	0.1235(2)	0.1257(2)	0.1223
$(10, 2)$	0.1211(3)	0.1220(4)	0.1283
$(9, 7)$	0.1452(3)	0.1458(2)	0.1446
$(8, 12)$	0.1456(2)	0.1468(2)	0.1487
$(13, 13)$	0.1502(3)	0.1503(3)	0.1508

Table 4.1: Hole-Hole correlations computed in the Fixed Node approximation and applying one lanczos step to the guiding wavefunction of (3.56). Exact results are from [64, 77]

far from the Γ point display a rather flat behavior. On the contrary, for $J = 0.4t$ (Fig. 4.9), the charge correlations approach zero as $q \to 0$, confirming the absence of PS even at the lowest doping considered. Moreover enhanced fluctuations are clearly evident along the $(1, 1)$ and $(1, 0)$ directions. These incommensurate peaks are a genuine feature of the ground state of the model, since they do not appear for instance at the VMC level, and it is extremely important to use many power iterations to eliminate the bias due to the VMC guiding wavefunction. The $N(q)$ at this J/t value is very weakly size dependent, much less than the energy per hole, so that the overall shape of this function in the thermodynamic limit should not differ too much from the one shown in Fig. (4.9) (a). Thus $N(q)$ should be always finite even for small q, ruling out PS and charge density wave instability. Even though some peaks at incommensurate wavevectors were found, that maybe reminiscent of some dynamical stripe order, they are not consistent with a static stripe structure (the peaks should diverge).

Remarkably, as δ is increased the peak at finite momentum moves far from the Γ point at a distance that scales linearly with the doping with a coefficient which is surprisingly close to 4π. This is exactly the coefficient obtained experimentally in $La_{2-x-\delta}Nd_xSr_\delta CuO_4$ [37]. We have also found that this peak position does not depend on J/t, implying that the $4\pi\delta$ slope could be a general feature of the $t-J$ model in the region without PS. It is reasonable to expect that the interaction of

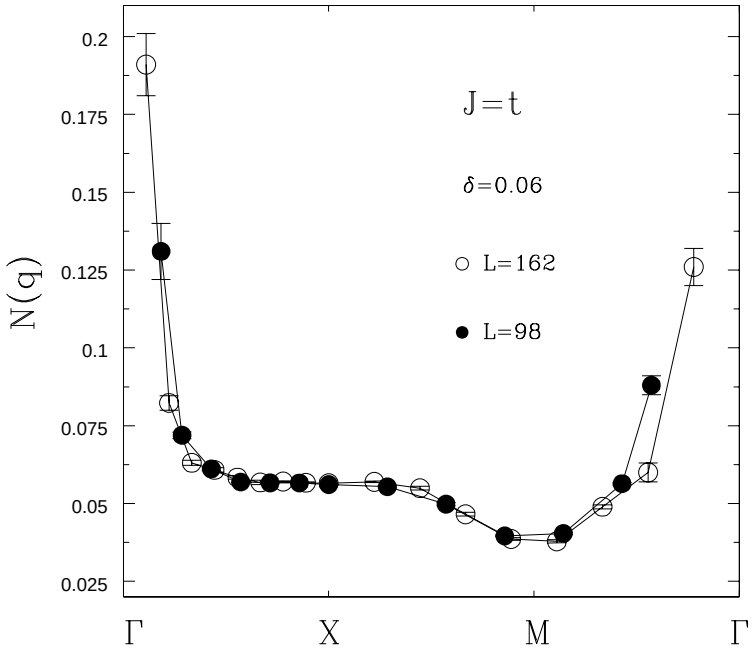

Figure 4.8: $N(q)$ for $\delta = 0.06$ and $L = 162$ (empty dots), $L = 98$ (full dots) and $J = t$

electrons with the ions could further enhance the intensity of this incommensurate peaks, leading not only to a qualitative but also to a quantitative agreement with experiments[39, 37].

The position of these peaks approaches the Γ point linearly with the doping, a property which cannot be explained within a simple spinless fermion model for the holes, contrary to what was proposed by [80] to explain the shape of $N(q)$ using high temperature expansion. In this case in fact the characteristic incommensurate wavevector $2k_F$ approaches the Γ point in a much more singular fashion $2k_F \sim \sqrt{\delta}$. On the other hand the hard-core boson model is unable to produce any feature at momenta different from Γ.

Recently S. White and D.J. Scalapino [79] proposed that the ground state of the two dimensional $t-J$ model has charge density wave order, for a wide range of doping. Their statement was supported by density matrix renormalization group calculations (DMRG). It was claimed that this kind of stripe order suppress superconductivity and only adding a next nearest neighbor hopping term to the Hamiltonian an homogeneous state with $d-$wave long range order is recovered. In our

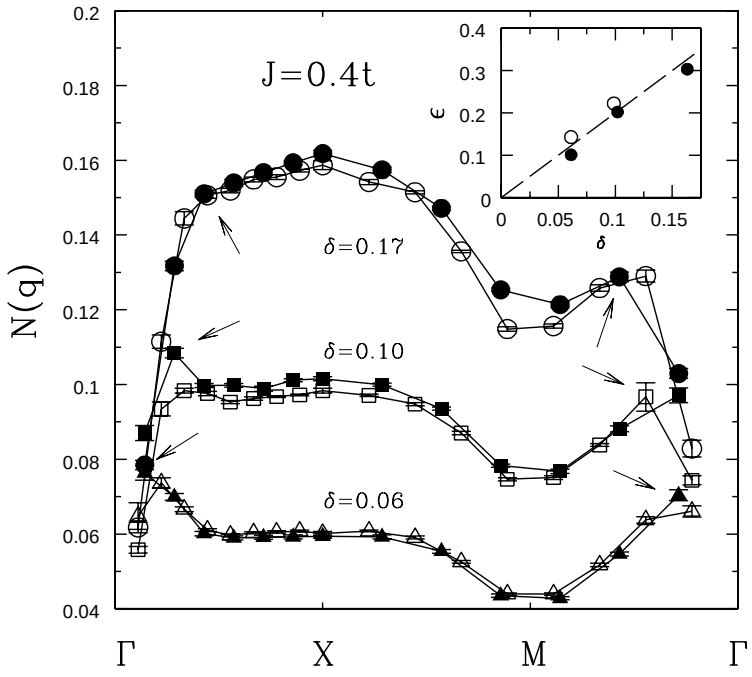

Figure 4.9: $N(q)$ for several doping $\delta = 0.06$ (triangles), $\delta = 0.10$ (squares), $\delta = 0.17$ (circles) for different sizes, $L = 98$ (full symbols) and $L = 162$ (empty symbols). Incommensurate peaks are shown by the arrows. $\Gamma = (0,0)$, $X = (\pi,\pi)$, $M = (\pi,0)$. Inset: empty dots (full dots) represent peak positions along the $(1,0)$ direction in q space (diagonal direction). The dashed line displays the 4π slope.

approach the homogeneous state is always the most stable one (at least for J/t in the physical region) and no charge density waves instabilities were found. In order to detect if the ground state of the $2D$ $t-J$ model really has any kind of "stripe order" we compare our results with DMRG calculations [81] on a 12×6 system and 8 holes, $J = 0.4t$, with open boundary conditions in the x (long) direction and periodic in the y (short) direction with DMRG.

Open boundary conditions are certainly unphysical and may introduce uncontrolled finite size effects but, unfortunately, these are the only boundary conditions where DMRG works reasonably well in two dimensions and a comparison with our results is possible.

Starting from a variational $d-$wave BCS wavefunction with energy per site $-0.6043(1)t$, the FN (variational) approximation over the guiding wavefunction

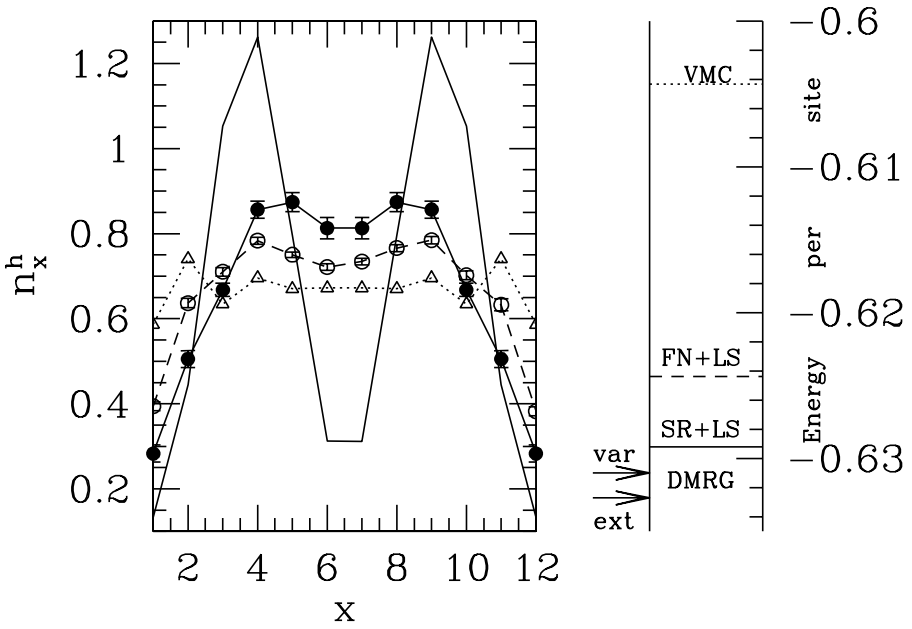

Figure 4.10: Left: Density on a rung n_x for a 12×6 lattice, 8 holes, $J = 0.4t$ with open boundary condition in the x (long) direction and periodic on the y (short) direction computed with VMC(empty triangles), FN+LS(empty dots), GFM-CSR+LS(full dots), DMRG (continuous line with no dots). Right: Energy calculation with several variational methods, VMC(dotted line),FN+LS, fixed note with one lanczos step applied to the guiding wavefunction (dashed line), GFM-CSR+LS (labeled SR+LS, continuous line). The arrows shows the DMRG results (variational and extrapolated to infinite number of states).

obtained applying one lanczos step to the original BCS one leads to a variational estimate energy $-0.6244(1)$. Using GFMCSR over the latter guiding function the most accurate ground state energy per site is $-0.6292(2)t$.

These data have been compared with the most accurate estimate for the ground state energy available by DMRG [81]. Using 2100 states, DMRG obtains a better variational energy than the GFMCSR with one lanczos step guiding wavefunction, $-0.6310(1)t$, and the extrapolated value at infinite number of states for the energy is $-0.6327(3)t$ (not variational). DMRG is able to obtain better energies (of order $0.004t$) on rectangular size with open boundary conditions. This is probably connected also with the fact that the gap in these systems is smaller since the translational symmetry in the x direction is broken (and the momentum is not definite on the finite lattice).

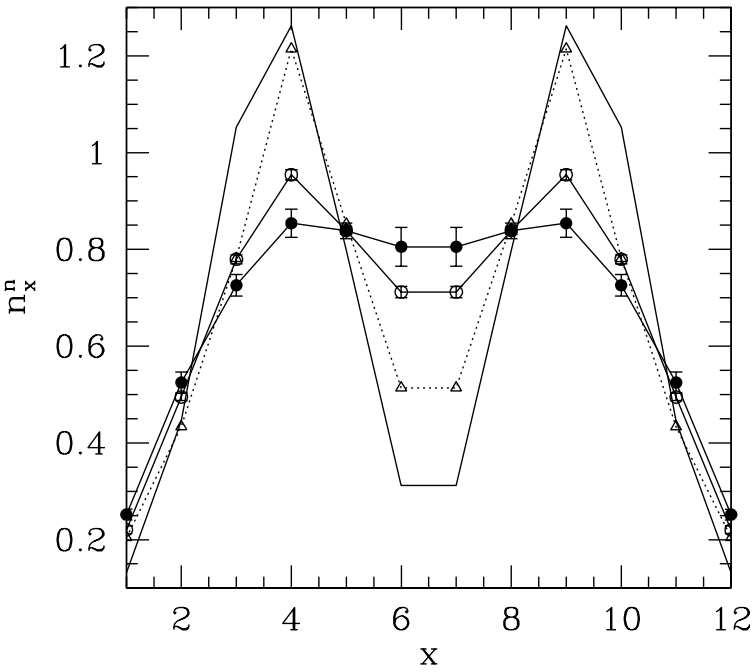

Figure 4.11: Density on a rung n_x for a 12×6 lattice with open boundary condition in the x (long) direction and periodic on the y (short) direction, starting from a non uniform variational wavefunction. n_c^h has been computed with VMC(empty triangles), FN+LS(empty dots), GFMCSR+LS(full dots), DMRG (continuous line with no dots).

On periodic boundary condition the results are different. Indeed in these systems DMRG has a very poor accuracy. On 6×6 lattice with periodic boundary condition and 32 electrons, the best energy obtained in the framework of DMRG is $-0.7231(6)t$ (extrapolated to infinite number of states, the best variational estimate with 2600 states being $-0.7212t$). Using GFMCSR and a BCS guiding wavefunction (with no Lanczos step) the estimate for the energy is $-0.7301(1)t$ (being $-0.7261(2)$ the best variational estimate obtained using FN with a guiding wavefunction with one lanczos step), leading to a gain in energy which is roughly $0.007t$, compared with the DMRG results.

In the case of rectangular lattices and open boundary condition the charge distribution over the lattice can be easily detected computing the number of holes

per rung

$$n_x^h = \sum_{y=1}^{N_r} (1 - n_{x,y}) \tag{4.11}$$

for each of the 12 lattice rungs, being $n_{x,y}$ the local electron density at site (x, y) and N_r the number of sites in the rung. Starting from the optimal energy variational ansatz we compute n_x^h. As can be seen from fig. (4.10) as the accuracy is increased the number of holes close to the open boundaries is sharply reduced while it is raised in the central region ($4 \leq x \leq 9$). This can be easily understood because when the holes are on the open boundaries the system loses kinetic energy since the allowed hopping are less than in the bulk. This results is in agreement with the DMRG calculations [81]. On the contrary the density of holes in the bulk ($x = 6, 7$) is quite different in the two cases. Indeed the DMRG finds total absence of holes in the central region (even if the extrapolation to infinite number of states gives results in the direction of a uniform solution) while the GFMCSR gives an almost uniform profile.

In order to check if the bias was given by the homogeneous guiding wavefunction a site dependent chemical potential was added to the BCS Hamiltonian tuning it in such a way that the variational calculation of n_x^h gives similar results to the DMRG findings. At a variational level this changing implies a small energy loss ($0.0025t$). This new guiding wavefunction is not homogeneous and has a different nodal surface than the uniform one. As can be seen in fig. (4.11) using the guiding wavefunction with one lanczos step applied the charge density wave behavior of n_x^h disappears and the simulation recovers the homogeneous ground state. Even by starting with a VMC wavefunction with big variation of the hole density along the x-direction, a solution with almost uniform hole density in the middle of the lattice is recovered, as opposed to the DMRG findings. This suggests, at least, that there exist low energy states very close in energy , with completely different hole density profile. This is not inconsistent with the stripe scenario, but is more plausibly explained by the anomalously large compressibility (also confirmed by DMRG [82]), found in the t-J model- to strong variations of the hole density correspond very small changes in the energy per site.

4.3 Short range versus long range operators

In order to determine if the ground state of the model has some kind of long range order it is necessary to simulate large systems and to perform a finite size scaling. This is in practice unfeasible by exact diagonalization since it only allows small size calculations. On the other hand the quantum Monte Carlo (QMC) methods allow simulations on larger systems but suffer from the well known "minus sign problem" instability, which makes the simulation difficult or even impossible at low enough temperatures.

At present, this instability can be controlled up to zero temperature, only at the price of introducing some approximation, such as the fixed node approximation [15], which is strictly variational on the ground state energy, the constrained path quantum Monte Carlo [83, 66, 67] and the Green function Monte Carlo with stochastic Reconfiguration [16, 17], which has been developed to improve the accuracy of the FN. Both the FN and GFMCSR techniques will be extensively used in this work. Similar approximations on the ground state wavefunction can be obtained by applying one (or more) lanczos step (LS) to the variational wavefunction [22, 62], or also using the Density matrix renormalization group (DMRG) [14], which in 2D is also affected by a sizable error, and is not "numerically exact" as in 1D.

All these approximations allow to obtain typically a rather accurate value of the ground state energy of the model, with an error typically less than 1% on the correlation energy even for relatively large lattice sizes. However this kind of accuracy for the energy certainly does not allow to draw reasonable conclusions on the interesting long range AF or SC properties of the model, see e.g. [84].
On the other hand it is reasonable to expect that a similar good accuracy can be obtained on the GS expectation value of short range operators (SRO) like the kinetic energy and the exchange energies in Eq.2.3. These class of SRO, represented by suitable chosen operator O acting only on nearest neighbors sites, has the important property that, if added to the Hamiltonian $H_h \rightarrow H - hO$ does not change its local character, H_h remaining a SRO. Moreover such perturbation of H with SRO typically leads to a sizable change of the ground state energy per site E_h even in the linear regime $E_h = E_0 - h < O > /L + o(h)$, providing a very reliable

estimate of the ground state expectation value $< O >$, once the energy $E(h)$ can be accurately determined for few values of the field h.

It is reasonable to believe that the calculation of the AF or SC order parameter, involving long distance operators O, as is typically done in the literature so far [24], maybe not so accurate and well controlled as the GS expectation values of SRO. For instance in the LS method a clear improvement of the variational energy is obtained by applying a generalized Lanczos operator $1 + \alpha H$ to the variational wavefunction ψ_G. However the long range correlation functions are clearly insensitive to this remarkable improvement of the energy, at least for large system size, as for the long distance behavior order of the volume powers of the Hamiltonian are required to converge to the ground state.

In the following subsections it will be shown how it is possible to compute long range quantities adding only local perturbations to the Hamiltonian for the antiferromagnetic and superconducting long range order.

4.4 Antiferromagnetism

4.4.1 Susceptibility and staggered magnetization

The response function to an external staggered magnetic field can be computed adding a local perturbation to the Hamiltonian,

$$H(h) = H - h\sum_R (-1)^R S^z_R$$

and then computing the ground state energy with and without the local perturbation. In a QMC simulation the expectation value of the staggered magnetization along the z axis,$m^z = \sum_R (-1)^R S^z_R$, on the unperturbed ground state is zero on every finite size (provided that the guiding wavefunction is a spin singlet). As a consequence the susceptibility can be computed as:

$$\chi = \lim_{h\to 0} \frac{1}{2}\frac{E(h) - E(0)}{h^2} \tag{4.12}$$

The calculation of the AF susceptibility as an energy difference is very accurate since it involves expectation values of operators which are short range. Moreover the accuracy on the ground state energy is very high in a QMC simulation, much more accurate that any long range operator. This is clearly seen in fig. (4.12) where χ_h is computed with lanczos and with the FN approximation for 2 holes on a 18 sites lattice. As can be seen even at a FN level, the agreement with the exact result is quite satisfactory.

In order to see if AF long range order exists it is necessary to extend the calculation to larger sizes and to extrapolate to the infinite volume limit. It is instructive to see what happens when true AF long range order exists, namely the $2D$ Heisenberg model. In Fig. (4.12) the behavior of the energy difference $(E(h) - E(0))/2h^2$ is shown for several lattice sizes ($J = 1$). The results show a clear divergence in the susceptibility as the volume is increased meaning that the response of the system to the external magnetic field is very strong. Moving to finite doping it is interesting to see that a similar divergence persists even at a doping $\delta = 0.08$. Indeed the susceptibility on the 98 sites lattice at this doping fraction is still divergent (fig. 4.13), while at $\delta = 0.12$ χ shows no size dependence with a rather flat behavior.

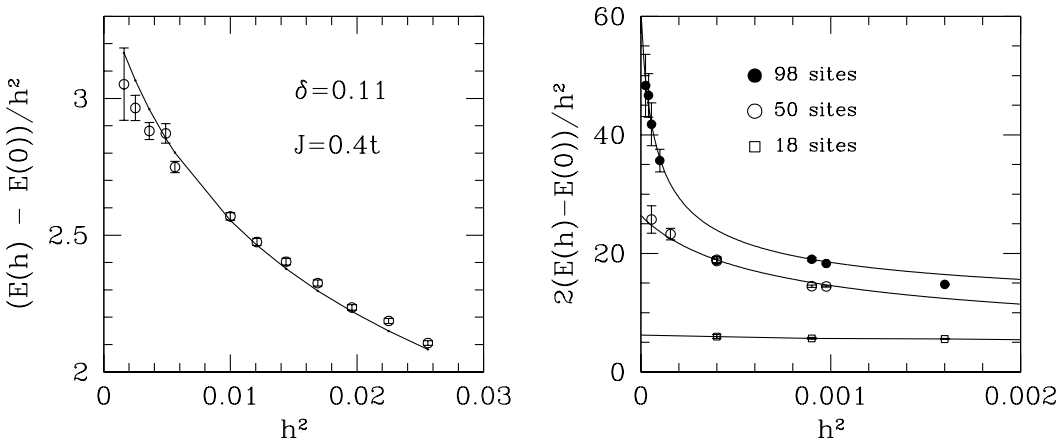

Figure 4.12: Left: AF susceptibility for $L = 18$ computed with FN(empty dots) and ED(continuous line). Right: AF susceptibility for the $2D$ Heisenberg model at J=1.0t

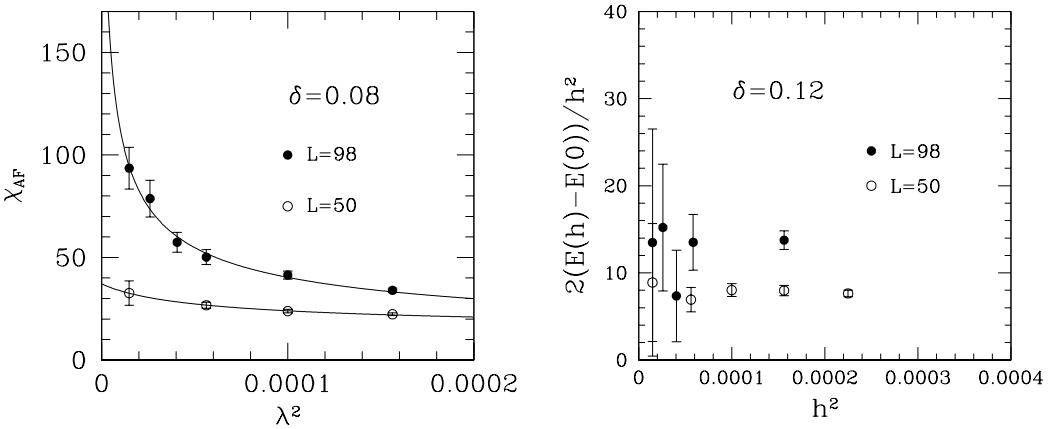

Figure 4.13: Antiferromagnetic susceptibility for the doped system for $\delta = 0.08$ (left) and $\delta = 0.12$ (right).

Since it is quite difficult to extract the zero field value of the susceptibility, being the divergence in a region of order $1/L$ as the system is enlarged, the order parameter in presence of a staggered magnetic field has been computed too.

The staggered magnetization in the presence of the magnetic field can be computed as:

$$m_h = -\frac{1}{2}\frac{dE}{dh} \tag{4.13}$$

This derivative can be evaluated exactly using forward walking which in the case of a SRO is very accurate and stable.

For the Heisenberg antiferromagnet, where broken symmetry occurs, the magnetization as a function of the rescaled field $h \to h \cdot L \cdot J$ lies on a universal curve [85] which depends only weakly on the system size. This weak size dependence has to be compared with similar calculations performed for the squared order parameter [60, 59] which shows much larger size effects (Fig. 4.14 b, horizontal dotted line).

This feature strengthen the validity of our results that are *all* based upon GS expectation values of SRO in presence of a field. This approach for computing the magnetic order parameter[86] can be readily extended to the doped system. Indeed choosing a suitable field $\bar{h}$ and computing the staggered magnetization for the doped system in the presence of the field $\bar{h}$, a result in agreement with the one obtained by the susceptibility calculation was found implying a clear absence of antiferromagnetic long range order for $\delta > 0.1$.

In the optimal doping region the staggered magnetization is vanishingly small even in presence of a sizable magnetic field, meaning that AF order has already disappeared.

4.5 Superconductivity

4.5.1 Superconducting susceptibility

In order to detect SC long range order with a more controlled approximation, we perform simulations in the grand canonical ensemble and add a short range

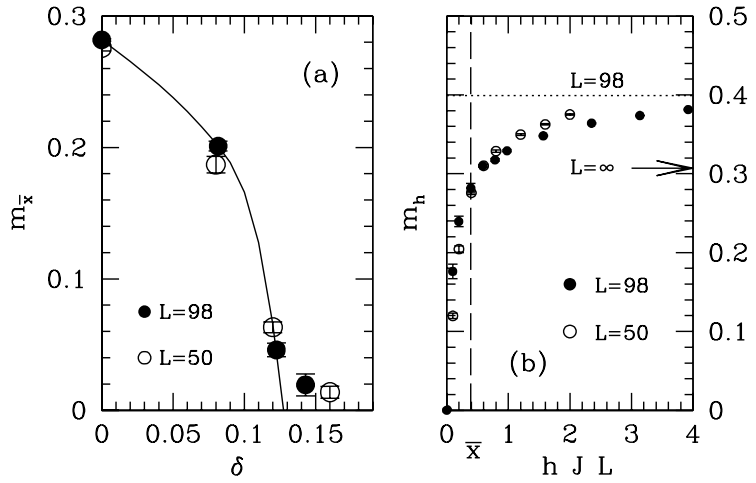

Figure 4.14: Staggered magnetization m_x for $x = \bar{h}JL = 0.392$ (a). m_h for $\delta = 0$ (b). Lines are guides to the eye.

perturbation which creates a $d-$wave symmetry Cooper pair in a singlet state, namely:

$$H(h) = H - h\left(\Delta^+ + \Delta\right) - \mu N \tag{4.14}$$

where $\Delta^+ = \sum_{<i,j>} M_{ij}(c^+_{i\uparrow}c^+_{j\downarrow} + c^+_{j\uparrow}c^+_{i\downarrow})$ and $M_{ij} = 1$ or -1 if the bond $< i, j >$ is in the x or y direction respectively, while μ is the chemical potential.

By studying how the ground state energy per site $E(h)$ behaves as a function of h it is easy to understand the superconducting ground state properties of the model. Indeed since the unperturbed Hamiltonian conserves the total number of particles, the first non zero correction to the ground state energy of the N particle system E_N is proportional to the susceptibility χ_d,

$$E(h) = E_N(0) - \frac{h^2}{2}\,\chi_d \tag{4.15}$$

By the Hellmann-Feynman theorem, the d-wave order parameter $m^d_h =< \Delta^+ >_h /L$, under the action of the perturbation, can be easily computed by

$$m^d_h = -\frac{1}{2}\,dE(h)/dh \tag{4.16}$$

.

In a finite system the fluctuations of the number of particles become always negligible for $h \to 0$, but by employing first the thermodynamic limit ($L \to \infty$)

one can obtain true long range order ($m_h^d \neq 0$) for $h \to 0$. In this case, to be consistent with this singular behavior, the linear coefficient $\chi_d = m_h^d/h$ defined for $h \to 0$ has to diverge for $L \to \infty$. This coefficient χ_d can be thought as a generalized susceptibility, in analogy to the more conventional magnetic case, and can be computed by extrapolating to zero field the finite size energy difference

$$\chi^d = \lim_{h\to 0} \frac{2(E_N - E(h))}{h^2} \tag{4.17}$$

The chemical potential μ is chosen in such a way that the average number of particles as $h \to 0$ converges to N,

$$\mu = \frac{[E_{N+2} - E_{N-2}]L}{4} \tag{4.18}$$

where E_N is the unperturbed energy per site for a N particle system.

In practice one reduces the problem of the calculation of a long range operator to the calculation of the energy of an Hamiltonian perturbed by a short range term. The latter energy can be accurately computed by the techniques described in chapter (3) at least if a good trial wavefunction is provided.

The BCS guiding wave function (3.56) can be generalized by introducing a proper weight f_N to each sector of fixed number of particles N, namely

$$|\psi_G\rangle = \sum_N f_N P_N \mathcal{P}_G |BCS\rangle \tag{4.19}$$

where $\mathcal{P}_G$ projects out doubly occupied sites and P_N selects the $N-$particle component of the wavefunction. In Fig. (4.5.2 b), it has been shown that the $|BCS\rangle$ wavefunction has long range superconducting order even after applying to it the projectors P_G and P_N.

The following step is the choice of the weights f_N. For $h \neq 0$, the variational parameters f_N are chosen by allowing only the smallest deviation of the particle number around the desired one N_0. In particular only the subspaces with $N = N_0, N_0 \pm 2$ particles are important for the correct estimate of χ_d, as easily follows from perturbation theory. In order to minimize the statistical errors, $f_{N_0} = 1$, and $f_{N_0 \pm 2}$ must be optimized with the variational Monte Carlo (VMC) for each value of h. This allows also an estimate of $E(h)$ and χ_d at the variational level.

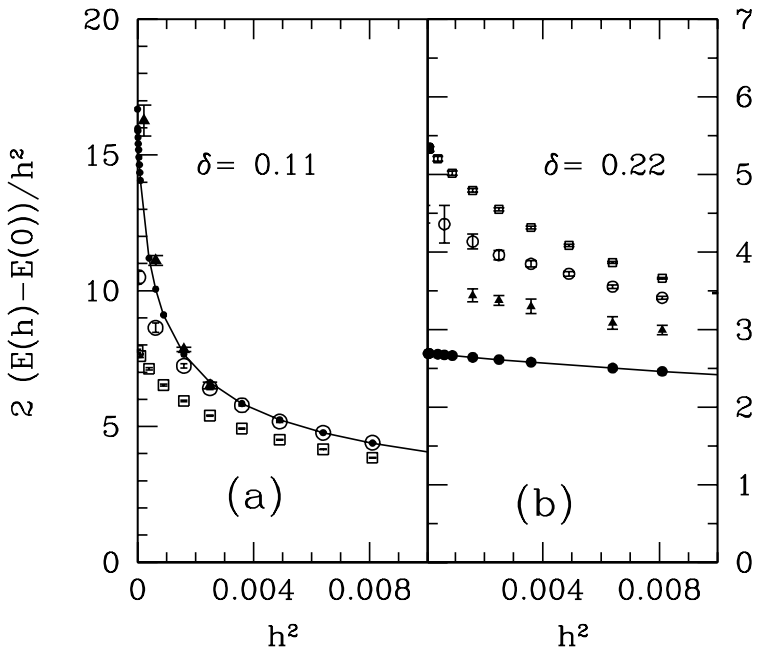

Figure 4.15: χ for $L = 18$ with 2 (a) and 4 (b) holes , $J = 0.4t$ computed with VMC (empty squares), FN (empty dots), GFMCSR (full triangles), ED (full dots connected by continuous line)

As can be seen from Fig. 4.5.1, where the results for a $L = 18$ lattice with 2 and 4 holes and $J = 0.4t$ are shown, this choice of the guiding functions gives a very accurate estimate of the susceptibility as compared to the exact diagonalization results. For the 2 hole case ($\delta = 0.11$) it is crucial to notice that the exact results give a much more enhanced value for χ_d than the VMC calculation, which has true long range order indeed. The FN is successful in reproducing this behavior and the GFMCSR is very close to the exact result.

As the system is over-doped the situation is quite different. For the 4 hole case ($\delta = 0.22$) the susceptibility is strongly suppressed and while the FN node only slightly depress the tendency of the VMC calculation towards long range order, the GFMCSR is successful in reproducing the qualitative correct behavior.

Moving to larger sizes $L = 50, 98$ (Fig. 4.5.1) the calculation of χ_d in the FN approach gives a very large value suggesting that χ_d should eventually diverge in the thermodynamic limit meaning that the response of the system to the pertur-

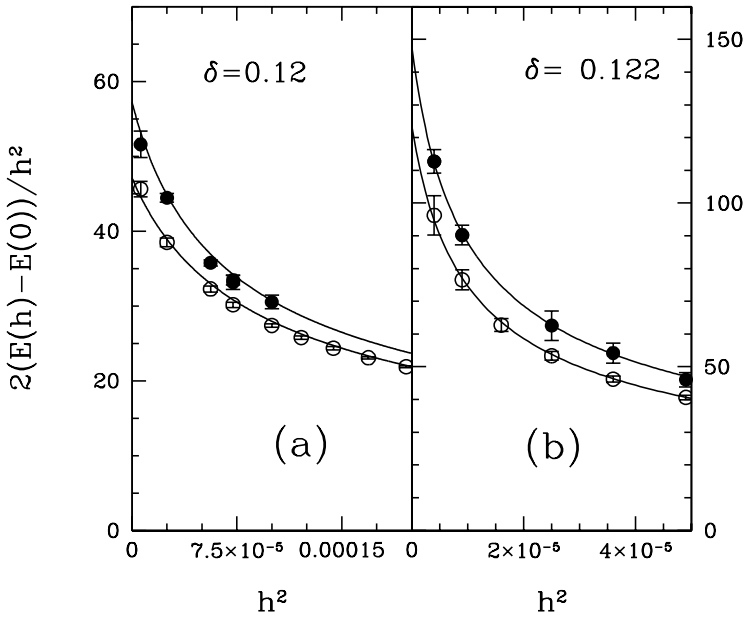

Figure 4.16: χ for $L = 50$ (a) and $L = 98$ (b), computed with VMC (empty dots) and FN full dots

bation is very strong. Moreover the FN calculation always tend to enhance the susceptibility computed using VMC. These results suggest that the ground state of the model has d-wave superconducting LRO.

4.5.2 Anomalous average of the order parameter

To confirm the prediction of the susceptibility calculation the anomalous average of the order parameter p_d has been computed, $p_d = |\langle N+2|\Delta^+|N\rangle|/L$, where $|N\rangle$ and $|N+2\rangle$ are the N and $N+2$ particles ground states respectively. p_d can be non zero even on a finite size and zero external field. Moreover if superconducting long range order occurs p_d is finite in the thermodynamic limit.

In the variational approach the calculation of p_d can be done using as a variational ansatz the BCS wavefunction projected at fixed number of particles (3.56). If the simulation is performed with the N particle projected BCS wavefunction then the quantity $\frac{\langle N+2|\Delta^+|N\rangle}{\langle N|N\rangle}$ can be easily computed in the VMC approach. Unfortunately this expectation value is not normalized, since $\frac{\langle N+2|\Delta|N\rangle}{\sqrt{\langle N|N\rangle\langle N+2|N+2\rangle}}$ should be needed. In order to overcome this difficulty it suffices to perform a second run

with the variational BCS wavefunction (3.56) projected at $N+2$ particles so that $\frac{\langle N|\Delta|N+2\rangle}{\langle N+2|N+2\rangle}$ is computed. The product of the two VMC calculation clearly yields the square of the desired quantity.

A simple strategy is possible to compute directly the finite size zero field anomalous average with FN and GFMCSR too. Choosing the chemical potential μ in such a way that the ground state energies for the N and $N+2$ particles are degenerate, the first order correction to the energy due to the perturbation (4.14) is given by the eigenvalues of the secular matrix:

$$\begin{vmatrix} E_N & hp_d \\ hp_d & E_{N+2} \end{vmatrix} \tag{4.20}$$

which gives $E(h) = E_N \pm hp_d$, meaning that the anomalous average of the order parameter can be computed as an energy difference $(E_N - E(h))/h$ for $h \to 0$. The numerical measurement of a long range property of the model can be done studying the ground state energy change under the effect of a local perturbation. This is clearly a much more convenient and controlled way to characterize the long range properties of a model, with an approximate numerical technique.

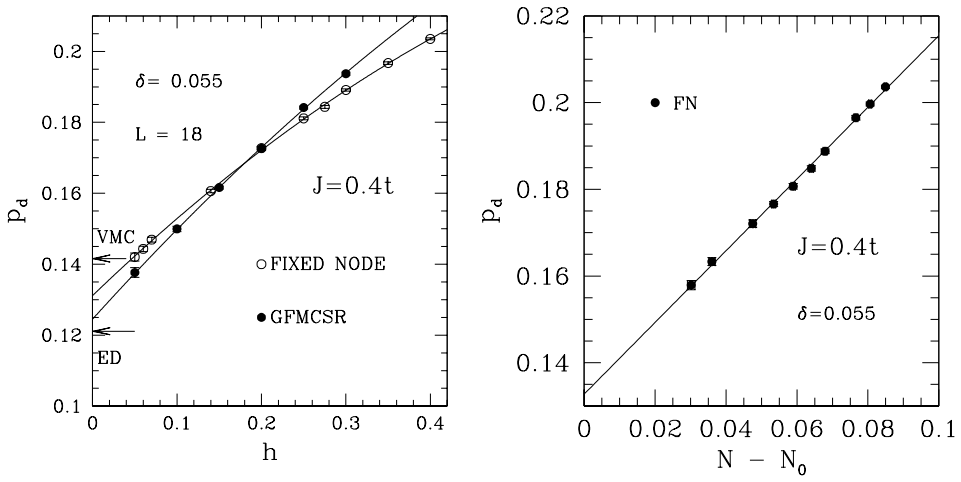

Figure 4.17: p_d for $L = 18$,$J = 0.4t$,$\delta = 0.055$ as a function of h (left) and as a function of the deviation from the unperturbed mean value of particle $N_0 = 17$ (right).

In order to reduce the statistical error on the ground state energy, we optimize the variational parameters f_N by restricting ourselves to the subspaces of N and

$N+2$ particles relevant for the matrix element p_d, f_N being zero otherwise. In the guiding function f_N and f_{N+2} are then determined by requiring that the average particle number $< \psi_G|N|\psi_G >$ is equal to $N+1$.

As can be seen in fig. (4.5.2 b) for the $L = 18$ and $N + 1 = 17$ case, by performing runs for several values of h and extrapolating to zero field, the number of electrons converges to the unperturbed value linearly with the perturbation. Even if a small error ϵ is done in the determination of the chemical potential, the corrections to the energy are of order ϵ^2, as can be seen from first order perturbation theory for degenerate levels (eq . 4.20)

The comparison with the exact result in the 18 site lattice with 2 holes shows that the VMC highly overestimates the order parameter. The FN reduces this value.

In order to perform the same calculation with the GFMCSR the energy of the two subspaces at N and $N+2$ particles were reconfigured in an independent way. In practice in the simulations the walkers are divided in two groups, some of them sample the $N+2$ particle subspace $\{(\underline{w}^{(N+2)}, \underline{x})\}$, while the other ones the N particle state $\{(\underline{w}^{(N)}, \underline{x})\}$. All the other subspaces of the Hilbert space are not sampled due to the choice of the $\{f_j\}$ coefficients in eq. (4.19). The stochastic reconfiguration for the energy was then done keeping the two subspaces separate, namely defining (see eq. 3.41)

$$\begin{aligned} g_{x_i}^{(N)} &= w_i^{eff,(N)}[1+\alpha^{(N)}(E_{x_i}^{(N)} - \bar{E}_{eff}^{(N)})] & i = 1, \dots M^{(N)} \\ g_{x_j}^{(N+2)} &= w_j^{eff,(N+2)}[1+\alpha^{(N+2)}(E_{x_j}^{(N+2)} - \bar{E}_{eff}^{(N+2)})] & j = 1, \dots M^{(N+2)} \end{aligned}$$

being $M^{(N+2)}$ ($M^{(N)}$) the number of walkers sampling the $N+2$ (N) particle Hilbert space sectors so that $M = M^{(N+2)} + M^{(N)}$ (Notation is consistent with the one given in chapter (3). In the calculation of p_d in Fig. (4.5.2), $M = 2000$ and for larger sizes the number of walkers was increased with the volume up to 5400 for the $L = 98$ case.

As can be seen from the $L = 18$ case with 2 holes, (fig. 4.5.2), the GFMCSR is very accurate extrapolating to a value very close to the exact lanczos result. In order to attempt a finite size scaling for the SC order parameter we compute $\langle N+2|\Delta^+|N\rangle$ on the $L = 50$ and $L = 98$ lattice sizes at doping $\delta = 0.14$ and $\delta = 0.133$ respectively, (Fig. 4.18). As can be seen in the $L = 50$ lattice case the

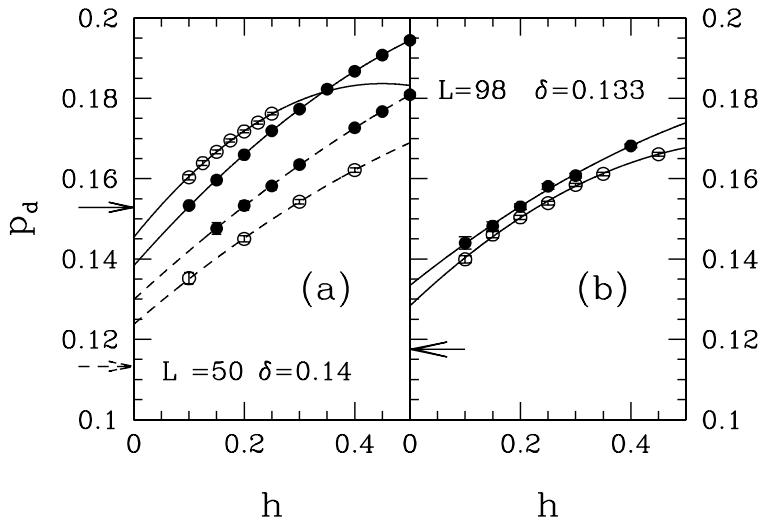

Figure 4.18: p_d for $L = 50$ (left), $L = 98$ (right). Empty dots are FN calculations, full dots are GFMCSR. Arrows label the variational estimate for p_d. Continuous lines label the calculations performed with optimal energy variational parameters ($\Delta_{DW} = 0.65$), dashed lines with $\Delta_{DW} = 0.3$.

FN and the GFMCSR reduces the variational value but still gives a finite estimate of the order parameter.

In this case, in order to test the accuracy of the calculation and the dependency of the result from the chosen guiding wavefunction, we reduce the optimal energy variational parameter $\Delta_{DW} = 0.65$ to the value of $\Delta_{DW} = 0.3$. This implies a reduction of the quantity p_d of roughly one third at a variational level, as shown in Fig. (4.18). The FN is unable to obtain the same value of the calculation at a different Δ_{DW}, even if it produces a correction which goes in the right direction suggesting that the real value of the order parameter should lie between the two different fixed node results. The GFMCSR correct in a very efficient way the change in the guiding wavefunction extrapolating at a value very close to the preceding calculation, being the difference for the two GFMCSR results a conservative estimate of the possible error in the determination of the p_d. GFMCSR improves the FN estimate of p_d by roughly three times, both for the 18 sites (fig. 4.5.2) and 50 sites (fig. 4.18), and this improvement is expected to remain even for larger sizes, being GFMCSR, as well as FN, a size consistent approximation.

From this very strict test we conclude that our result does non depend very

much from the choice of the parameters in the guiding wavefunction and the criterion of optimizing the variational parameters on the energy remains the most reliable one, in contradiction to what was suggested in Ref. [24, 22].

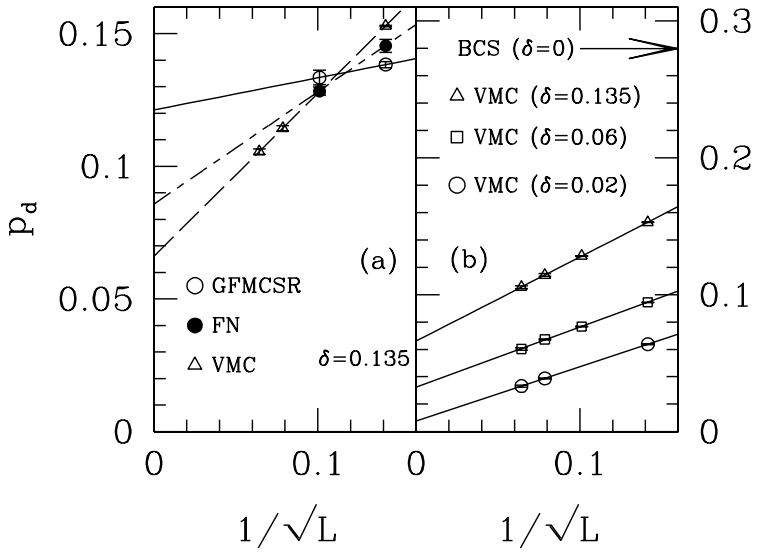

Figure 4.19: Size scaling of p_d. Lines connecting FN and GFMCSR in (a) are guides to the eye. In (b) the expectation value of the $d-$wave order parameter over the BCS wavefunction before Gutzwiller projection is shown by the arrow.

The 98 sites calculation shows that the VMC value of p_d is enhanced both by the FN and GFMCSR calculation and remarkably the computed value is very close to the one obtained in the 50 lattice site. This result, alone, is very much suggestive and represents one of the most clear numerical evidence of d-wave superconductivity in a 2D strongly correlated model. However the limited number of lattice sizes considered does not allow us to perform a more robust finite size scaling, since as shown in fig.(4.5.2), size effects are present also at the variational level and the true order parameter maybe well below the value ~ 0.12 reported in fig. (4.5.2). However we expect that the finite size effects for SRO are well behaved and the enhanced superconducting correlations found for the 98 sites should be a genuine feature of the model at this doping and J/t value.

4.5.3 Effect of a nearest neighbor repulsive interaction

In real materials such as the high T_c compounds the Coulomb repulsion between electrons on different sites is a very important interaction which can suppress the pairing force driving to superconductivity. Another important feature of these materials is that they possess a very high compressibility, a feature present even in the two dimensional $t-J$ model whose compressibility at optimal doping is almost 20 times the compressibility of a gas of spinless fermions.

In two dimensions the Fourier transform of the screened coulomb potential $V(r) = (e^2/r)e^{-r/\xi}$ is given by

$$V(q) = \frac{2\pi e^2}{|q| + \xi} \tag{4.21}$$

where ξ is the screening length. The screening length can be written as a function of the derivative of the chemical potential respect to the density of the number of particles [87], namely

$$\xi \;=\; \frac{1}{2\pi e^2}\frac{\partial \mu}{\partial n} \tag{4.22}$$

As a consequence when the compressibility is large the screening length decreases. Moreover in two dimension this is even more effective than in three, since in the latter case $\xi^2 = (1/4\pi e^2)\frac{\partial \mu}{\partial n}$. [87].

When the compressibility is very large the system very easily screens a charge imbalance so that even if there is a coulomb repulsion acting on the valence electrons on different lattice sites the effect is very short ranged. It is then reasonable to assume that the effect of the coulomb repulsion could not be so drastic on superconductivity.

This prediction can be tested with numerical simulation. Under the assumption that the screening length is around one lattice spacing a nearest neighbor coulomb repulsion is added to the Hamiltonian of the two dimensional $t-J$ model, namely:

$$H = -t\sum_{<ij>}(c_i^+ c_j + c_j^+ c_i) + J\sum_{<ij>}\left(\mathbf{S}_i \cdot \mathbf{S}_j - \frac{n_i n_j}{4}\right) + V\sum_{<i,j>} n_i n_j \tag{4.23}$$

where the coulomb repulsion coupling constant V is positive.

The $d-$wave susceptibility has been computed in the presence of this Coulomb field on small lattice size by exact diagonalization. As can be seen the results are

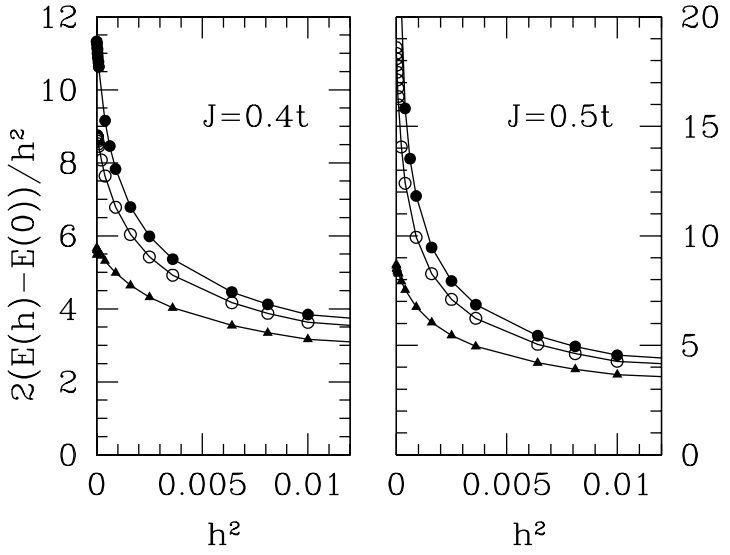

Figure 4.20: $d-$wave susceptibility in presence of a coulomb repulsion $V = 0.25J$ (full dots), $V = 0.5J$ (empty dots), $V = 1.1J$ (full triangles).

weakly affected by the coulomb repulsion and the susceptibility is still showing a diverging behavior even at values of the coulomb repulsion which are far beyond the estimated physical value for this parameter ($V \equiv 0.2t - 0.3t$). This result strengthen the validity of the belief that the electronic correlation is the main responsible for the pairing in the cuprate compound. Moreover this means also that the presence of superconductivity in the $t - J$ is very robust since the pairing is not destroyed even by the coulomb repulsion.

4.6 Drude weight

As was shown in section (4.4) there is clear absence of AF long range order only from $\delta > 0.1$. It is an important issue to understand what are the conducting property of the model for low doping, close to half filling. In real materials the system is an insulator until the AF long range order is lost and superconductivity occurs. A good criterion [88] to detect if a system is a metal or an insulator is the calculation of the Drude weight. The kinetic energy in the presence of a vector

potential $A_x(l)$ in the x direction takes the form:

$$K_A = \sum_{l,\sigma}(c^+_{l\sigma}c_{l+y\sigma} + c^+_{l+y\sigma}c_{l\sigma}) + \sum_{l,\sigma}(e^{i\phi_x(l)}c^+_{l\sigma}c_{l+x\sigma} + c^+_{l+x\sigma}c_{l\sigma}e^{-i\phi_x(l)}) \quad (4.24)$$

where $e^{\pm i\phi_x(l)}$ are the Peierls [89] phase factors and $\phi_x(l) = eA_x(l)/\hbar c$. Expanding in $\phi_x(l)$ it is easy to see that the kinetic energy terms becomes:

$$K_A = K - \sum_l \left[\phi_x(l)j^p_x(l) + \frac{1}{2}\phi_x(l)^2 k_x(l)\right] \quad (4.25)$$

being K the usual kinetic energy term and

$$k_x(l) = -t\sum_\sigma(c^+_{l\sigma}c_{l+x\sigma} + c^+_{l+x\sigma}c_{l\sigma}) \quad (4.26)$$

$$j^p_x(l) = it\sum_\sigma(c^+_{l\sigma}c_{l+x\sigma} + c^+_{l+x\sigma}c_{l\sigma}) \quad (4.27)$$

As a consequence the energy per site of the full Hamiltonian in the presence of the vector potential $A_x(l)$ is given by

$$E(\phi) = E_0 + \frac{D}{2\pi}\sum_l \phi_x(l)^2 \quad (4.28)$$

where the paramagnetic current $j^p_x(l)$ in the ground state without external fields is supposed to vanish and D is the Drude weight, which can be obtained from second order perturbation theory in $\phi_x(l)$:

$$\frac{D}{2\pi} = -\frac{1}{2}\left[\langle 0|k_x|0\rangle + \sum_\nu \frac{|\langle 0|j^p_x|0\rangle|^2}{E_\nu - E_0}\right] \quad (4.29)$$

In order to compute with QMC the Drude weight we consider the analytic continuation of eq. (4.24) and introduce the exponential $e^{\pm\eta_0(l)}$ with $\eta_0(l)$ real,

$$K_A = \sum_{l,\sigma}(c^+_{l\sigma}c_{l+x\sigma} + c^+_{l+x\sigma}c_{l\sigma}) + \sum_{l,\sigma}(e^{\eta_0(l)}c^+_{l\sigma}c_{l+x\sigma} + c^+_{l+x\sigma}c_{l\sigma}e^{-\eta_0(l)}) \quad (4.30)$$

It is easy to see that in second order perturbation theory this analytic continuation gives eq. (4.28), a part from a minus sign due to the definition of $\phi \to i\eta$. The resulting Hamiltonian is no longer symmetric, but this is not a problem for the

QMC methods used in this thesis since in this case the simulation converges to the right lowest eigenvector of the Hamiltonian.

The Drude weight can be easily computed as:

$$D = \lim_{\eta_0 \to 0} \frac{2\pi[E_0 - E(\eta_0)]}{\eta_0^2} \tag{4.31}$$

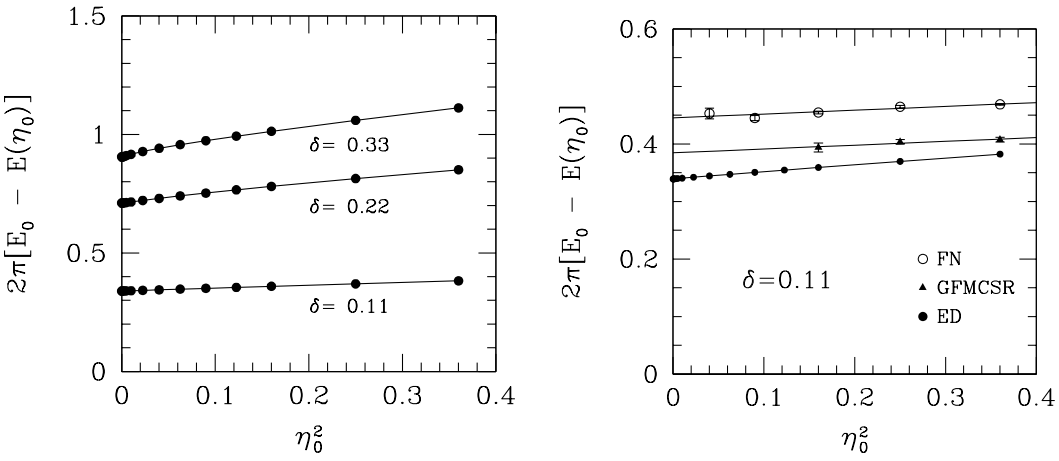

Figure 4.21: Left: Drude weight for $L = 18$ and several doping by exact diagonalization. Right: Comparison between FN (empty dots), GFMCSR (triangles), ED(full dots) for the $L = 18$,2 holes case.

In practice it is necessary to perform several runs at different η_0 and then extrapolate the zero energy difference 4.31.

In Fig. (4.6 b) the Drude weight has been computed with lanczos using the analytic continuation suggested before. As can be seen the extrapolation to zero perturbation is linear even at large value of the perturbation, where the energy difference is sizable. As the doping is increased the value of the Drude weight on small lattice size has an increasing metallic character as the system is doped.

The linear behavior obtained with exact diagonalization is confirmed by the FN and GFMCSR calculations on the same size. The FN approximation overestimates the Drude weight. The GFMCSR improves more than a factor of 2 the accuracy of the starting FN approximation converging to a value which only slightly overestimates the exact result computed with lanczos. The accuracy of the GFMCSR calculation on the Drude weight is around the 10%, which represent a remarkable achievement for the calculation of a dynamical property of the system.

The FN calculation on larger size ($L = 50, 98$) gives a Drude weight different

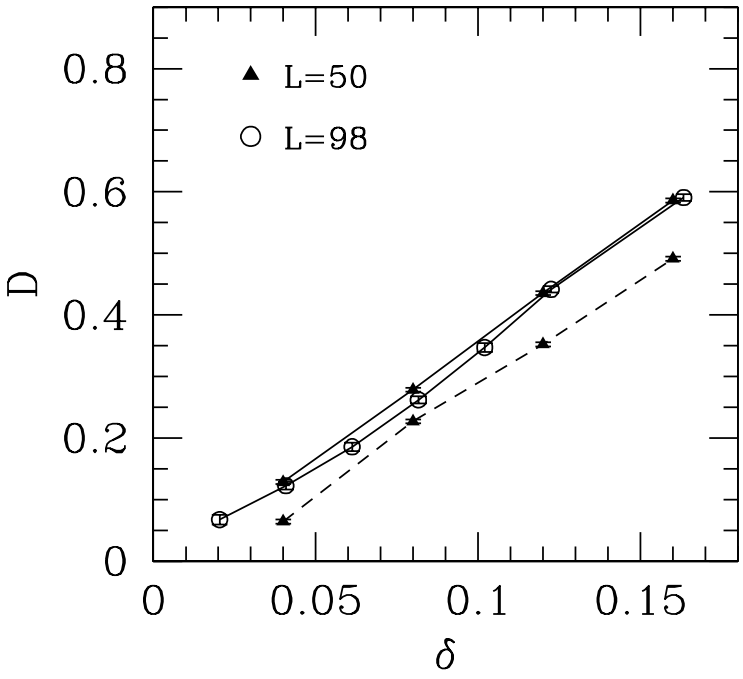

Figure 4.22: Drude weight calculation for $L = 50, 98$ as a function of the doping fraction. FN results are connected by continuous line, GFMCSR by dashed line.

from zero as soon as the Mott insulator state is doped (see fig. 4.6). Moreover it looks that the 50 and 98 site results lie on the same curve, meaning that the size effects are almost absent. In the 98 site lattice a curvature term (missing in the 50 site case probably due to the low resolution in doping) occurs suggesting that the Drude weight approach zero as δ^2. This is consistent with the hyperscaling scenario proposed by Imada [90] for metal-insulator transition in two dimensions in which the Drude weight dependency on the doping should behave in this way.

Since from the small size case it is known that the FN overestimates the Drude weight we compute the same quantity with GFMCSR and as can be seen in fig. 4.6 the FN conclusions are confirmed even if the value of Drude weight is slightly reduced (as happens in the 18 sites lattice). This calculation seems to suggest that the insulating state of the undoped system is quickly lost with doping (at least for $\delta > 0.04$) and in the case of the $t - J$ model one is left with a metal with long range antiferromagnetic correlations before superconductivity takes place.

Conclusions

Since one of the main outcome of this work is the finding of superconductivity in a model without explicit attractive interaction, it is very important to identify what are the main features that allow superconducting correlations in the ground state of the two dimensional $t-J$ model in order to understand if they are present in real materials and which other models can display a similar behavior.

Several authors [10, 11] proposed that superconductivity and phase separation should compete in the high T_c compounds and that a similar behavior is to be expected for strongly correlated electron systems, such as Hubbard and $t-J$ models.

As can be seen from the phase diagram obtained in this thesis, no phase separation occurs in the physical parameter region, even at very low doping (Fig. 4.23) and the phase separation boundary is quite far from the optimal doping region, at least for physical values of the superexchange coupling constant ($J = 0.4t$). This evidence has been achieved by computing the energy per hole [10] with several numerical methods for very large system size. It has also been shown that for $J < 0.7t$, as the size of the system is increased, the minimum in the energy per hole profile moves to lower doping (as suggested by the one side errorbars in Fig. (4.23) which are estimates of the finite size effects). In the thermodynamic limit the critical J is between $0.5t - 0.6t$.

As it has been shown in section (4.6), the Drude weight is finite even at small doping, meaning that the Mott insulator state is immediately lost and the system has a metallic character. Moreover the Drude weight decreases as the square of the doping fraction as the Mott insulating state is approached. This is consistent with the hyperscaling scenario close to a metal insulator transition proposed by Imada *et al.* [90].

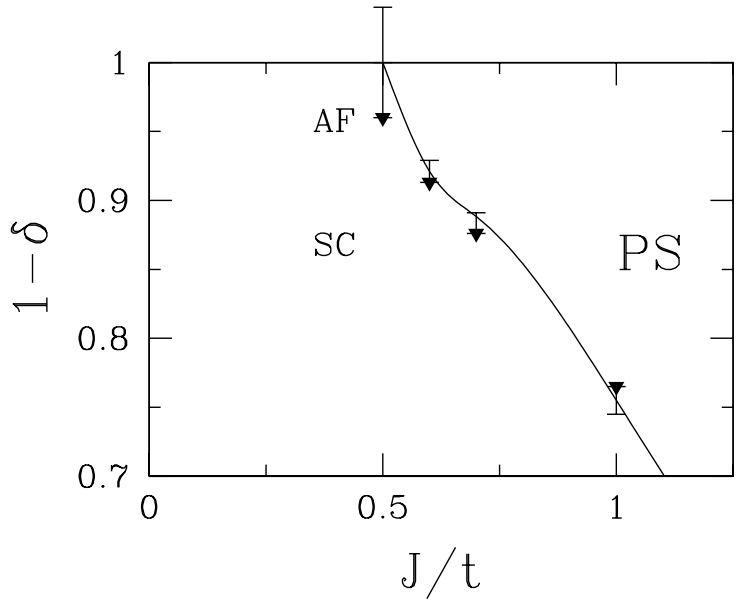

Figure 4.23: Instability of the uniform phase evaluated by GFMCSR using the Maxwell construction for the 98 site lattice. Errors are estimates of finite size effects and correspond to twice the difference between the 98 and 50 site critical doping [78]. SC label the $\delta = 0.14$ were p_d has been computed, AF label the antiferromagnetic region.

Accurate calculations of the antiferromagnetic susceptibility and of the staggered magnetization in presence of a weak magnetic field (section 4.4) have shown that, even if the magnitude of the order parameter is suppressed at small doping, antiferromagnetic correlations are strong up to $\delta \sim 0.1$.

This metallic state with strong antiferromagnetic correlations is very close to the parameter region in which superconductivity has been found. The proximity of this antiferromagnetic state enhances charge fluctuations determining a $d-$wave state well before the phase separation instability occurs.

It is important that the compressibility of the electron system is very large ($\frac{d\mu}{dn} \approx 0.54t$), almost *20 times larger* than the corresponding spinless fermion compressibility.

This anomalously large value of the compressibility clearly favor superconductivity. Indeed even in the presence of a long range Coulomb repulsion between electrons in the Copper Oxygen layers, missing in our model, but certainly present in real systems, the screening length is very short, $\left(\xi = \frac{1}{2\pi e^2}\frac{d\mu}{dn}\right)$, so that

the screening is really effective. The low dimensionality of the system plays also an important role since in three dimension the screening length is much longer ($\xi^2 = \frac{1}{4\pi e^2}\frac{d\mu}{dn}$). This strengthen the hipothesys that high temperature superconductivity is essentially a two dimensional effect, even if an explanation of the critical temperature and other strictly material dependent features, probably needs to take into account three dimensional effects related to the solid structure of the different compounds.

In section (4.5.3) the occurrence of superconductivity even in the presence of a screened Coulomb repulsion has been confirmed meaning that the pairing in this system is very robust.

The experimental discovery of stripes in a region of doping ($0.05 < \delta < 0.125$) in $\mathrm{La_{1.6-x}Nd_{0.4}Sr_xCuO_4}$ samples (chapter 1 and references therein) and the consequential suppression of superconductivity led several groups to the investigation of the possible occurrence of stripes in the two dimensional $t - J$ model.

In order to check the possible occurrence of a charge density wave order, the hole-hole correlations have been computed. Even if some features at incommensurate momenta have been found, no occurrence of charge density waves appears in our calculation at least in the physical region relevant for high temperature superconductors.

In systems with open boundary conditions, which favor stripe order, direct comparison was made with the best energy estimates obtained with density matrix renormalization group [81]. Even if on these systems the density matrix renormalization group is more accurate (the situation changes with periodic boundary conditions), the numerical techniques employed in this thesis allow to obtain an accuracy of $0.004t$ (for $J = 0.4t$) on the energy per site. Within this accuracy *no clear evidence of stripe behavior was found* and even using guiding wavefunctions with non uniform density profiles the uniform solution was recovered, in disagreement with density matrix renormalization group calculations.

This suggests, at least, that there exist low energy states very close in energy, with rather different hole density profile. This is not inconsistent with the stripe scenario, but is more plausibly explained by the anomalously large compressibility (also confirmed by density matrix renormalization group calculations[82]), found

in the t-J model. It is more likely that a small lattice distortion can easily induce stripe order, being charge excitations very close in energy, and not the strong correlation alone.

The stability of the uniform phase at low doping has been found at least for $J = 0.5t$. It is possible that before the system is completely phase separated ($J > 0.5t$) stripes may be stabilized. Indeed high temperature expansion finds the phase separation boundary at $J \approx 1.2t$ which is a too large value to be consistent with the one given in this thesis (no one of the numerical calculation [23, 62, 61] find such a high value for the critical strength for phase separation) . Nevertheless the energy per hole could display a phase separated behavior in a region where stripes occur (from $0.6 < J < 1.0$). Similarly to what happen in the one dimensional $t - J$ model [91] where the first symptoms of phase separation are a liquid of bound pairs, in two dimensions it could be an instability towards a stripe phase.

The numerical results obtained in this work lead to the remarkable conclusion that the $t-J$ model correctly reproduces the main (zero temperature) experimental findings and, as it happens in real systems, the superconducting state is reached upon doping the antiferromagnetic Mott insulator.

The antiferromagnetic long range order of the undoped system is lost at $\delta \approx 0.1$ and superconductivity is found close to optimal doping $\delta \approx 0.13$. This work suggests that antiferromagnetism and superconductivity are closely related, but a large compressibility is needed to stabilize pairing in the presence of a Coulomb repulsion.

The main outcome of this work is that the most simple scenario, appeared in the early days of superconductivity, is surprisingly confirmed by this numerical study, namely that the strong correlation *alone* may drive the system from antiferromagnetism to superconductivity.

Appendix A

Green function Monte Carlo: technical details

A.1 First momentum conservation

Given the probability $P_q(\underline{w}, \underline{x})$ at step q in the simulation evolving as shown in Eq. (3.11), the following reconfiguration

$$P'_q(\underline{w}', \underline{x}') = \int \sum_{\underline{x}} K(\underline{w}', \underline{x}'; \underline{w}, \underline{x}) P_q(\underline{w}, \underline{x}) \, [d\underline{w}] \tag{A.1}$$

$$K(\underline{w}', \underline{x}'; \underline{w}, \underline{x}) = \prod_{i=1}^{M} \left(\frac{\sum_j w_j \delta_{x'_i, x_j}}{\sum_j w_j} \right) \delta(w'_i - \frac{\sum_j w_j}{M}) \tag{A.2}$$

does not change the first momentum of the probability distribution, namely

$$X'_{1,q}(x) = X_{1,q}(x) \tag{A.3}$$

where

$$X_{k,q}(x) = \int dw_1 \int dw_2 \cdots \int dw_M \sum_{\underline{x}} \left(\frac{w_1^k \delta_{x,x_1} + w_2^k \delta_{x,x_2} + \cdots w_M^k \delta_{x,x_M}}{M} \right) P_q(\underline{w}, \underline{x}) \tag{A.4}$$

. Proof: By definition using (A.15) and (A.1)

$$X'_{1,q}(x) = \int [d\underline{w}] \int [d\underline{w}'] \sum_{\underline{x}, \underline{x}'} \left(\frac{\sum_j w'_j \delta_{x,x'_j}}{M} \right) K(\underline{w}', \underline{x}'; \underline{w}, \underline{x}) P_q(\underline{w}.\underline{x})$$

The first term in the integrand contains a sum. It is simpler to single out each term of the sum $w'_k\delta_{x,x'_k}/M$ and to integrate over all the possible variables $\underline{w'},\underline{x'}$ but w'_k and x'_k. It is then easily obtained that this contribution to X'_{1n} conventionally indicated as $[X'_{1,q}]_k$ is given by:

$$[X'_{1,q}]_k = \int [d\underline{w}] \int [dw'_k] \sum_{\underline{x},x'_k} \frac{w'_k}{M} \;\; \delta_{x,x'_k} \left(\frac{\sum_j w_j \delta_{x'_k,x_j}}{\sum_j w_j} \right) \delta(w'_k - \frac{\sum_j w_j}{M}) P_q(\underline{w},\underline{x})$$

Then by integrating simply in dw'_k and summing over x'_k in the previous integrand we easily get that $[X'_{1,q}]_k = \frac{1}{M} X_{1,q}$, independent of k. Finally by summing over k we prove the statement (3.16).

A.2 Variational proof for the Fixed Node approximation

In the most general formulation the effective fixed node hamiltonian is defined reversing the sign of the positive off-diagonal matrix elements of $\bar{H}$ and multiplying them by a constant $\gamma > 0$,namely:

$$\bar{H}^{eff}_{x',x} = \begin{cases} \bar{H}_{x',x} & \text{if} \quad \bar{H}_{x',x} \leq 0 \\ -\gamma \bar{H}_{x',x} & \text{if} \quad \bar{H}_{x',x} > 0 \end{cases} \tag{A.5}$$

as a consequence the diagonal term has an additional $sign - flip$ contribute:

$$\bar{H}^{eff}_{x,x} = \bar{H}_{x,x} + \mathcal{V}_{sf}(x) \tag{A.6}$$

$$\mathcal{V}_{sf}(x) = \sum_{\bar{H}_{x,x'}>0 \; and \; x' \neq x} \bar{H}_{x',x} \tag{A.7}$$

In order to see that the latter approximation is variational one consider the following expectation value over a variational state $|\psi\rangle$:

$$\Delta E = \langle \psi | \bar{H}^{eff} - \bar{H} | \psi \rangle \tag{A.8}$$

Following [15, 17] it can be written as

$$\Delta E = (1+\gamma) \sum_{\bar{H}_{x,x'}>0 \; and \; x \neq x'} |H_{x,x'}| \left| \psi(x) \sqrt{\left| \frac{\psi_G(x')}{\psi_G(x)} \right|} - sH(x,x') \psi(x') \sqrt{\left| \frac{\psi_G(x)}{\psi_G(x')} \right|} \right|^2 \tag{A.9}$$

denoting $sH(x', x)$ the sign of the matrix element $H_{x,x'}$. As a consequence of the variational principle and since $\Delta E \geq 0$ the ground state energy of the fixed node hamiltonian E_0^{eff} is an upper bound of the real ground state energy, namely:

$$E_0^{eff} \geq \langle \psi^{eff} | H | \psi^{eff} \rangle \geq E_0$$

Moreover from Eq. (A.9) one obtains the lower value of the energy in the standard Fixed Node approximation, $(\gamma = 0)$.

It is straightforward to verify that $\langle \psi_G | H | \psi_G \rangle = \langle \psi_G | H^{eff} | \psi_G \rangle$, and thus the GFMC procedure improves the energy of the guiding wavefunction:

$$E_0^{eff} \leq \langle \psi_G | H^{eff} | \psi_G \rangle = \langle \psi_G | H | \psi_G \rangle. \tag{A.10}$$

A.3 Proof of the bias control in the forward walking scheme

In order to implement stochastically Eq.(3.44) we need to apply the operator O_x diagonal in configuration space, in a stochastic sense and then follow the standard stochastic iteration (3.2) to the walker distribution P for N steps. To this purpose a walker from now on is identified by the triad:

$$w, \eta, x$$

where η represents the actual value of the measured operator O for the walker. Its value can change, as we will see later on in the reconfiguration process, and in general due to the forward walking $\eta \neq \langle x | O | x \rangle$. Indeed only at the beginning, $n = 0$, of the forward walking iteration $\eta_i = O_i =< x_i | O | x_i >$, for $i = 1, \cdots M$. In a probabilistic sense this is equivalent to consider the initial probability distribution:

$$P_{n=0}(\underline{w}, \underline{\eta}, \underline{x}) = P_0(w, x) \prod_{i=1,M} \delta(\eta_i - O_i) \tag{A.11}$$

where P_0 is the equilibrium distribution of the previous Markov process (3.11), which samples the ground state $\psi_0(x)$.

With this initial condition further N forward walking steps are implemented to the probability distribution P, defined with the iterations in Eq.(3.11). Then in order to determine the quantity (3.44) the following ratio is evaluated:

$$< O >= \frac{< w\eta >}{< w >} \tag{A.12}$$

where the brackets indicate the average over the distribution $\sum_x \int dw \int d\eta P(w, \eta, x)$. It is understood that in Eq.(3.11) the variables η_i remain unchanged. For instance the the evolution of $P_n(w', \eta', x')$ for the single walker will be:

$$P_{n+1}(w', \eta', x') = \sum_x p_{x', x} P_n(w'/b_x, \eta', x)/b_x \tag{A.13}$$

However in order to satisfy the bias control property described in Sec.(A.1) it is necessary to update the η variables at any reconfiguration process.

Even in this case it is easier to work with $w\eta$ momenta of order k of the distribution P for fixed configuration x:

$$X^{\eta}_{k,n}(x) = \int dw \int d\eta (w\eta)^k P_n(w, \eta, x) \tag{A.14}$$

which for $M \neq 1$ correspond to:

$$X^{\eta}_{k,n}(x) = \int d\underline{w} \int d\underline{\eta} \sum_{\underline{x}} \left(\frac{\sum_j (w_j \eta_j)^k \delta x, x_j}{M} \right) P_n(\underline{w}, \underline{\eta}, \underline{x}) \tag{A.15}$$

where, as usual underlined variables represent vectors whose components refer to the single walker index j.

With a proof exactly analogous to the one of Sec.(A.1) it is possible to show that :

- The value of the first $(w\eta)$ momentum $X^{\eta}_{1,n}(x)$, at the initial iteration of the forward walking $n = 0$, is equivalent to apply the operator O to the initial distribution $P_0(w, x)$, namely

$$X^{\eta}_{1,n=0}(x) = O_x X_{1,n=0}(x)$$

- the following reconfiguration process, which does not change the Markov chain of configurations $(\underline{w}, \underline{x})$ but modifies slightly $\underline{\eta}$, has the bias control property also for the $w\,\eta$ averages:

$$\begin{aligned} P'_n(\underline{w'}, \underline{\eta'}, \underline{x'}) &= \int\int \sum_{\underline{x}} G(\underline{w'}, \underline{\eta'}, \underline{x'}; \underline{w}, \underline{\eta}, \underline{x}) P(\underline{w}, \underline{\eta}, \underline{x})\, [d\underline{w}]\ \left[d\underline{\eta}\right] \\ G(\underline{w'}, \underline{\eta'}, \underline{x'}; \underline{w}, \underline{\eta}, \underline{x}) &= \prod_{i=1}^{M} \delta\left(\eta'_i - \frac{\sum_j w_j \eta_j \delta_{x'_i, x_j}}{\sum_j w_j \delta_{x'_i, x_j}}\right) \left(\frac{\sum_j w_j \delta_{x'_i, x_j}}{\sum_j w_j}\right) \delta(w'_i - \frac{\sum_j w_j}{M}) \end{aligned} \tag{A.16}$$

  The first factors in the Green function G, involving the $\eta' s$, represent the only difference to the previous reconfiguration process (A.16). Thus obviously the momenta $X_{k,n}$ not involving the η variables satisfy the same bias control property of the previous reconfiguration process (A.16)

As far as the $(w\eta)$ momenta are concerned is possible to prove as before the mentioned bias control property:

$$X'^{\eta}_{1,n}(x) = X^{\eta}_{1,n}(x) \tag{A.17}$$

To this purpose, analogously to the previous case, it is convenient to single out a term $j = k$ in the definition of the first $w\eta$ momentum in Eq.(A.15) , and following the same route of Sec.(A.1) integrate easily the Green function over all possible variables $\underline{w'}$,$\underline{\eta'}$ $\underline{x'}$, but the variables x'_k, η'_k and w'_k. These remaining integrations can be also performed analytically by first integrating in w_k, then in η_k and finally summing over x_k. The assertion (A.17) is therefore proved rigorously.

Appendix B

BCS mean field theory

Consider the Bardeen, Cooper and Schriffer (BCS) hamiltonian in the mean field (Hartree-Fock) approximation [74, 92, 29],

$$H_{BCS} = \sum_{k,\sigma} \epsilon_k \left(c^+_{k\sigma} c_{k\sigma} + c_{k\sigma} c^+_{k\sigma} \right) + \sum_k \Delta_k \left(c^+_{k\uparrow} c^+_{-k\downarrow} + c_{-k\downarrow} c_{k\uparrow} \right) \tag{B.1}$$

where $\epsilon_k = -2t(\cos(k_x) + \cos(k_y)) - \mu$ and μ is the chemical potential. The symmetry of the superconducting order parameter $\Delta_k = \Delta_{HF} f_k$ has been chosen to be $s-$wave or $d-$wave, namely:

$$f_k = \begin{cases} \cos(k_x) + cos(k_y) & s - \text{wave} \\ \cos(k_x) - cos(k_y) & d - \text{wave} \end{cases} \tag{B.2}$$

The quasi particles can be introduced by the Bogolubov transformations:

$$\begin{cases} \psi^+_{k\uparrow} &= u_k c^+_{-k\downarrow} + v_k c_{k\uparrow} \\ \psi^+_{-k\downarrow} &= u_k c^+_{-k\uparrow} - v_k c_{k\downarrow} \end{cases} \tag{B.3}$$

where u_k and v_k are chosen real and so that $u_k^2 + v_k^2 = 1$ (which is necessary in order for $\psi^+_{k\sigma}$ and $\psi_{k\sigma}$ to be fermionic operators). Requiring that the operator $\psi^+_{k\uparrow}$ are indeed creating quasiparticles,

$$[H, \psi^+_{k\uparrow}] = E_k \psi^+_{k\uparrow} \tag{B.4}$$

the eigenvalue of the mean field hamiltonian are obtained as

$$E_k = \pm \sqrt{\epsilon_k^2 + \Delta_k^2} \tag{B.5}$$

It is then easy to solve for u_k and v_k so that the following relations are obtained:

$$\frac{u_k}{v_k} = \frac{\Delta_k}{E_k - \epsilon_k} \tag{B.6}$$

$$u_k^2 = \frac{1}{2}\left(1 + \frac{\epsilon_k}{E_k}\right) \tag{B.7}$$

$$u_k v_k = \frac{\Delta_k}{2E_k} \tag{B.8}$$

$$\tag{B.9}$$

and $v_k^2 = 1 - u_k^2$.

The vacuum state is defined by the following equation:

$$|BCS\rangle = \prod_{k>0} \psi_{k\uparrow}\psi_{-k\downarrow}\psi_{k\downarrow}\psi_{-k\uparrow}|0\rangle \tag{B.10}$$

being $|0\rangle$ the vacuum state for the $\left\{c_{k\sigma}, c_{k\sigma}^+\right\}$ operators. By the inverse transformation of B.3,

$$|BCS\rangle = \prod_k \left(1 + w_k c_{k\uparrow}^+ c_{-k\downarrow}^+\right)|0\rangle \tag{B.11}$$

$$= \exp\left\{\sum_k w_k c_{k\uparrow}^+ c_{-k\downarrow}^+\right\}|0\rangle \tag{B.12}$$

and $w_k = u_k/v_k$.

Similarly the superconducting order parameter $\langle BCS|\Delta^+\Delta|BCS\rangle$ where $\Delta^+ = \frac{2}{L}\sum_k f_k c_{k\uparrow}^+ c_{-k\downarrow}$ can be computed using transformations B.3 so that

$$\langle BCS|\Delta^+\Delta|BCS\rangle = \frac{1}{L^2}\left[\sum_k f_k \frac{\Delta_k}{E_k}\right] + \frac{1}{L^2}\sum_k f_k^2\left(1 - \frac{\epsilon_k}{E_k}\right)^2 \tag{B.13}$$

Acknowledgements

The “Trieste adventure” had a lot of travel-mates whom I share common experiences, working hours, difficulties, laugh and joy. This work would be incomplete without their help and support.

During these years Sandro Sorella has been a continuous source of motivations, encouragement and help. The long time spent programming in a “strongly correlated” way has been constructive and funny at the same time.

Alberto Parola has been a precious guest here in Trieste, providing useful suggestions as well as laugh and happiness. Michele Fabrizio and Giuseppe Santoro gave important contributes to my work in terms of ideas and motivating discussions.

Erio Tosatti deserves a particular thank for priceless advises regarding important working and life decisions. Moreover I’m also indebted to him for the fruitful atmosphere I found in Trieste, being SISSA a very aggregative working place.

I acknowledge S. White for sending me unpublished density matrix renormalization group calculations, O. Gunnarsson and E. Koch for warm hospitality at MPI, Stuttgart.

A computational physicist must obviously deal with computers, an annoying task if people like Franz di Tolla and Carlo Cavazzoni (their help was really invaluable), Luisa Urgias and Davide Poccecai wouldn’t be so friendly and reliable. Sabrina and her smiling face helped me during these years to solve all the bureaucratic stuff that a physicist need to solve, never avoiding a friendly conversation. I am grateful to Andrea, Radikkio and all the people at the secretary office for making my life easier.

A lot of people, not directly involved in my work, have been precious friends in all these years.

Marco gave me a true friendship, here in Trieste and “on the road” in the US, which survived a few difficult moments and met a lot of smiling days. I hope it will never come to a “closing time”. Alice has been a personal confident, full of wisdom,smiles and, most important, time. Lorenzo, Antonella and the tiny Mattia have been (and will ever be) a second family for me, with their simple and warm way of talking to me and with their help. I hope life will deserve them all the happiness they need. Massimo and Luca are definitely the best “Risma” to share an office with, being laugh and jokes as well as useless discussions the main soundtrack of these years. Stefania and Cristiano have been always close to me, despite my changing moods. I always see them as two of my best friends.

A special thank is for Milena and her far-east warm e-mails.

I’m grateful to Daniele and Chiara (for the mighty “focaccia” in Nervi and for their kindness), Giovanni e Cecilia (for giving me a bed in San Diego), Valentina, Barbara and the forgotten “Parmigiano Reggiano”, Gianni (the best pizza-maker in Trieste), Leonardo, Gabriele, (and his delicious “Fiorentine”),Catia, Andrea (“viva la pappa col pomodoro”), Paul, Antonio, Dr. Bezzi, Michela, Giulia, Federico and many many more....

In the end I thank my family for continuous support and in particular my tiny ”red head” sister.

Bibliography

[1] J. G. Bednorz and K. A. Müller, Z. Phys. B **64**, 189 (1986)

[2] P. W. Anderson, Science **235**, 1196 (1987)

[3] P. W. Anderson, G. Baskaran, Z. Zou and T. Hsu, Phys. Rev. Lett. **58**, 2790 (1987)

[4] P. W. Anderson, Phys. Rev. Lett. **64**, 1839 (1990)

[5] D. J. Scalapino, E. Loh Jr. and J. E. Hirsch, Phys. Rev. B **34**, 8190 (1986)

[6] J. R. Schrieffer, X. G. Wen and S. C. Zhang, Phys. rev. Lett. **60**, 944 (1988)

[7] K. Miyake, S. Schmitt-Rink and C. M. Varma, Phys. Rev. B **34**, 6554 (1986)

[8] P. Monthoux A. V. Balatsky and D. Pines, Phys. Rev. Lett. **67**, 3448 (1991)

[9] P. Monthoux and D. Pines, Phys. Rev. B **47**, 6069 (1993)

[10] V. J. Emery, S. A. Kivelson and H. Q. Lin, Phys. Rev. Lett. **64**, 475 (1990)

[11] C. Castellani, C. Di Castro, M. Grilli, Physica Scripta, **T45**, 81 (1992)

[12] F. C. Zhang and T. M. Rice, Phys. Rev. B **37**, 3759 (1988)

[13] E. Dagotto, Rev. Mod. Phys. **66**, 763 (1994)

[14] S. R. White, Phys. Rev. B **48**, 10345 (1993)

[15] D.F.B. ten Haaf, H. J. M. van Bemmel, D.F.B. ten Haaf,J.M.J. van Leeuwen, W. van Saarlos and D. M. Ceperley, Phys. Rev. B **51**, 13039 (1995)

[16] S. Sorella, Phys. Rev. Lett. **80**, 4558 (1998)

[17] S. Sorella and L. Capriotti cond-mat/9902211

[18] L. Capriotti, A. E. Trumper and S. Sorella, Phys. Rev. Lett. **82**, 3899 (1999)

[19] M. S. L. du Croo de Jongh, "*Density Matryx Renormalization Group Variants for Spin Systems*", PhD thesis Universiteit Leiden, (1999)

[20] W. O. Putikka, M. U. Luchini and T. M. Rice, Phys. Rev. Lett. **68**, 538 (1992)

[21] C. Gros, Phys. Rev. B **38**, 931 (1988)

[22] E. S. Heeb and T. M. Rice, Europhy. Lett. **27**, 673 (1994)

[23] M. Kohno, Phys. Rev. B **55**, 1435 (1997)

[24] ,C. T. Shih, Y. C. Chen, H. Q. Lin and T. K. Lee, Phys. Rev. Lett. **98**, 1294 (1998)

[25] P. W. Anderson, Phys. Rev. **115**, 2 (1959)

[26] D. J. Van Harlingen, Rev. Mod. Phys. **67**, 515 (1995) and references therein

[27] A. Schilling, M. Cantoni, J. D. Guo and H. R. Ott, Nature **363**, 56 (1993)

[28] M. K. Crawford *et al.*, Phys. Rev. B **41**. 282 (1990)

[29] "*Introduction to Superconductivity*", M. Tinkham, Robert E. Krieger publishing company

[30] S. Hoen *et al.*, Phys. Rev. B **39**, 2269 (1989)

[31] J. P. Franck, S. Harker and J. H. Brewer, Phys. Rev. Lett. **71** 283 (1993)

[32] J. D. Axe *et al.*, Phys. Rev. Lett. **62**, 2751 (1989)

[33] J. D. Jorgensen *et al.*, Phys. Rev. B **38**, 11337 (1988)

[34] P. C. Hammel *et al.*, Phys. Rev. B **42**, 6781 (1990)

[35] M. A. Kastner *et al.*, Rev. Mod. Phys. **70**, 897 (1998)

[36] A. P. Kampf, Physics Reports **249** 219 (1994)

[37] K. Yamada *et al.*, Phys. Rev. B **57**, 6165 (1998)

[38] T. Niemoller *et al*, cond-mat 9904383

[39] J. M. Tranquada *et al.*, Nature **375**, 561 (1995)

[40] H. A. Mook *et al.*, Nature **395**, 580 (1998)

[41] A. R. Moodenbaugh *et al.*, Phys. Rev. B **38**, 4596 (1988)

[42] S. A. Kivelson, V. J. Emery, Synthetic Metals **80**, 151 (1996)

[43] J. M. Kosterliz and D. J. Thouless, J. Phys. C **6**, 1181 (1973)

[44] W. E. Pickett, Rev. Mod. Phys **61**, 433 (1989)

[45] O. K. Andersen, A. I. Liechtenstein, O. Jepsen and F. Paulsen, Stanford Superconductor Conference - March 1995, available at cond-mat 9509044

[46] M. S. Hybertsen, M. Schluter, N.E. Christensen, Phys. Rev. B **39**, 9028 (1989)

[47] M. S. Hybertsen, E.B. Stechel, M. Schluter, D.R. Jennison, Phys. Rev. B **41**, 11068 (1990)

[48] A. K. McMahan, J.F. Annett, R. M. Martin, Phys. Rev. B **42**, 6268 (1990)

[49] A. K. McMahan, R. M. Martin, S. Satpathy, Phys. Rev. B **38**, 6650 (1988)

[50] H. Eskes and G.A. Sawatzky, Phys. Rev. B **44**, 9656 (1991)

[51] F. Mila, Phys. Rev. B **38**, 11358 (1988)

[52] E.B. Stechel and D.R. Jennison, Phys. Rev. B **38**, 4632 (1988)

[53] A. Auerbach, "*Interacting electrons and quantum magnetism*", Springer, 1994

[54] H. Eskes and J. H. Jefferson, Phys. Rev. B **48**, 9788 (1993)

[55] E. Lieb and D. Mattis, J. Math. Phys. (NY) **3**, 749 (1962)

[56] J. D. Reger and A. P. Young, Phys. Rev. B **37**, 5978 (1988)

[57] E. Manousakis Rev. Mod. Phys. **63**, 1 (1991)

[58] K. J. Runge, Phys. Rev. B **45**, 7229 (1992); **45**, 12 292 (1992)

[59] A. W. Sandvik, Phys. Rev. B **56**, 11678 (1997)

[60] M. Calandra Buonaura and S. Sorella, Phys. Rev. B **57**, 11446 (1998)

[61] C. S. Hellberg and E. Manousakis, Phys. Rev. Lett. **78**, 4609 (1997)

[62] C. T. Shih, Y. C. Chen and T. K. Lee, Phys. Rev. B **57**, 627 (1998)

[63] E. Dagotto *et al.*, Phys. Rev. B **45**, 10741 (1992)

[64] D. Poilblanc, Phys. Rev. B **48**, 3368 (1993)

[65] T. Giamarchi and C. Lhuiller, Phys. Rev. B **43**, 12943 (1991)

[66] S. Zhang, J. Carlson and J. E. Gubernatis, Phys. Rev. Lett. **74**, 3652 (1995)

[67] S. Zhang, J. Carlson and J. E. Gubernatis, Phys. Rev. B, **55**, 7464 (1997)

[68] H. Yokoyama and H. Shiba, J. Phys. Soc. Japan **57**, 2482 (1988)

[69] N. Trivedi and D. M. Ceperley, Phys. Rev. B **41**, 4552 (1990)

[70] A. D. Sokal in *Monte Carlo Methods in Statistical Mechanics: Foundations and New Algorithm*, Cours de Troisieme Cycle de la Physique en Suisse Romande.

[71] D. M. Ceperley and M. H. Kalos, in *Monte Carlo Method in Statistical Physics*, edited by K. Binder (Springer-Verlag, Heidelberg, 1992)

[72] J. H. Fetherington, Phys. Rev. A **30**,2713 (1984)

[73] F. Franjic and S. Sorella Prog. Theor. Phys. **97**, 399 (1997)

[74] "*Theory of Superconductivity*", J.R. Schrieffer, Addison Wesley

[75] C. S. Hellberg and E. Manousakis, Phys. Rev. B, **52**, 4639 (1995)

[76] Y. Nagaoka, Phys. Rev. **147**, 392 (1966)

[77] D. Poilblanc, J. of Low Temp. Phys. **99**, 481 (1995)

[78] M. Calandra, F. Becca and S. Sorella, Phys. Rev. Lett. **81**,5185 (1998)

[79] S. R. White and D. J. Scalapino, Phys. Rev. Lett. **80**,1272 (1998), Phys. Rev. Lett. **81**, 3227 (1998)

[80] W.O. Putikka, R. L. Glenister, R. R. P. Singh, H. Tsunetsugu , Phys. Rev. Lett. **73**, 170 (1994).

[81] S. R. White, private communication.

[82] S. R. White and D. J. Scalapino, cond-mat/9907375

[83] S. Fahy and D. R. Hamann, Phys. Rev. B, **43**, 765 (1991)

[84] B. S. Shastry J. Phys. A; Math General **30** L635 (1997)

[85] E. Brezin, J. Zinn-Justin, Nucl. Phys. B257 (1985),867

[86] A. W. Sandvik, cond-mat/9904218

[87] N. H. March and M. P. Tosi, "*Coulomb Liquids*", Academic Press (1984)

[88] D. J. Scalapino, S. R. White, S. Zhang, Phys. Rev. Lett. **68**, 2830 (1992), Phys. Rev. B **47**, 7995 (1993)

[89] E. Peierls, Z. Phys. **80**, 763 (1933)

[90] M. Imada, A. Fujimori, Y. Tokura, Rev. Mod. Phys. **70**, 1039 (1998)

[91] M. Ogata *et al.*, Phys. Rev. Lett. **66**, 2388 (1991)

[92] "*Superconductivity of Metals and Alloys*", P. G. de Gennes, Addison Wensley